8-27-2009

Statistical mechanics of transport in disordered lattices and reaction-diffusion systems

Ziya Kalay

Follow this and additional works at: https://digitalrepository.unm.edu/phyc_etds
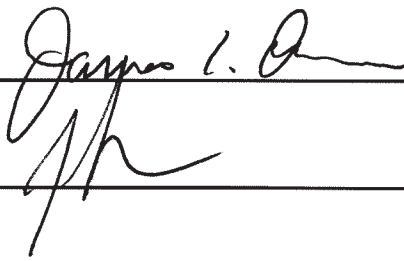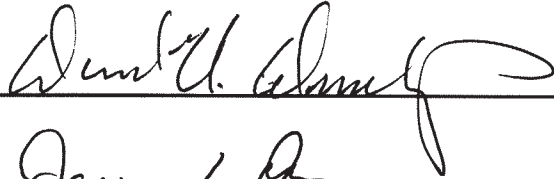
Ziya Kalay
_____
Candidate

Physics and Astronomy
_____
Department

This dissertation is approved, and it is acceptable in quality
and form for publication:

Approved by the Dissertation Committee:

_____ , Chairperson

_____

_____

_____

_____

_____

_____

_____

Statistical mechanics of transport in disordered lattices and reaction-diffusion systems

by

Ziya Kalay

B.Sc. Physics, Orta Doğu Teknik Üniversitesi, Ankara/Turkey, 2005

DISSERTATION

Submitted in Partial Fulfillment of the

Requirements for the Degree of

Doctor of Philosophy,

Physics

The University of New Mexico

Albuquerque, New Mexico

August, 2009

Dedication

To my parents.

anneme ve babama, eşek sıpasından..

Acknowledgments

During the long journey that ended with the completion of this doctoral dissertation, I was supported by many. Here, I would like to take a moment to express my gratitude to those who helped me in many different ways.

First of all, I would like to thank my thesis advisor Nitant for everything he taught me, and for all the opportunities he provided for me. Working with him on a large number of physics problems broadened my horizon, and made me acquire new skills. It was always a pleasure to talk with him about anything in life, as his curiosity and enthusiasm extends well beyond the bounds of physics. I also am grateful to him for being patient and supportive during the difficult parts of this journey. I wish he will someday find the old Turkish coin I had given him and with it perform his magic tricks, which, regrettably, he never taught me how to do...

As a graduate student, I learned so much from my teachers here and elsewhere. I especially would like to thank Profs. Dave Dunlap, Paul Parris, and Ivan Deutsch for having been excellent instructors in the classes I took from them. Although I complained plenty about the vast amounts of homework assignments given in classes, even in a published newspaper article, I think they were beneficial for me. I also would like to thank Eli Ben-Naim, who was my supervisor while working at the Los Alamos National Laboratory as a summer student. Another person who taught me a great deal along the way is Luca Giuggioli. It was always a pleasure to work with him.

Being a part of the Consortium of the Americas for Interdisciplinary Science was an enriching experience for me. The Consortium provided me and other graduate students with a stimulating and active research environment all the time. I am especially thankful to Victor Dossetti, Francisco Sevilla and Yiu-Man Wong, along with many other visitors to the Consortium, for stimulating discussions. Also, it was a pleasure for me to work with the fellow graduate students, Mukesh Tiwari, David MacInnis, Luis Felipe Gonzalez, Sabrina Araujo, Kathrin Spendier, Alden Astwood and Julian Antolin. Finally, I always appreciated the help of the administrative assistants Adriana Recalde and Lela Castillo, and I would like to thank them for being such wonderful people.

During the last four years in the land of enchantment, I have made many friends. I consider myself lucky to have met Carlos Riofrio, Heather Partner, Daniel Mirell, Steven Tremblay, Vaibhav Madhok, Rob Cook, Ben Baragiola, Daniel Riofrio and many others. In particular, I am grateful to Carlos and Heather for all the good time we had and for supporting me when I needed friends most. I am sure that we are going to meet again in the future.

In addition to being a graduate student in the physics department, I also participated in the Program in Interdisciplinary Biological and Biomedical Sciences at the University of New Mexico. It was a privilege for me to get to know everyone in this program, especially Profs. James Brown and Felisa Smith, administrative assistants Shannon McCoy-Hayes, Justin Stewart, and Fornessa Randal, and the graduate students Paul Hooper, Eric Erhardt, Sushmita Roy, Jordan Okie, Wenyun Zuo, Helen Davis, Lai Xu and George Bezerra.

I also would like to express my gratitude to the physics department staff, especially to the academic advisor Alisa Gibson for doing a marvelous job and to the department chair Prof. Bernd Bassalleck for being so helpful.

Lastly, I am indebted to my parents without whose support this work could not have been completed, and I would like to dedicate this dissertation to them.

Statistical mechanics of transport in disordered lattices and reaction-diffusion systems

by

Ziya Kalay

ABSTRACT OF DISSERTATION

Submitted in Partial Fulfillment of the

Requirements for the Degree of

Doctor of Philosophy,

Physics

The University of New Mexico

Albuquerque, New Mexico

August, 2009

Statistical mechanics of transport in disordered lattices and reaction-diffusion systems

by

Ziya Kalay

B.Sc. Physics, Orta Doğu Teknik Üniversitesi, Ankara/Turkey, 2005

Ph.D., Physics, University of New Mexico, 2009

Abstract

This thesis is the report of a study of several different problems in statistical physics. The first two are about random walks in a disordered lattice, with applications to a biological system, the third is about reaction-diffusion systems, particularly the phenomena of front propagation and pattern formation, and the last is about a special kind of evolving complex networks, the addition-deletion network. The motivation for the first of the two random walk investigations is provided by the diffusion of molecules in cell membranes. A mathematical model is constructed in order to predict molecular diffusion phenomena relating to the so-called compartmentalized view of the cell membrane. The theoretical results are compared with experimental observations available in the literature. The second random walk part in the thesis contains contributions to the analysis of transport in disordered systems via effective medium theory. Calculation of time-dependent transport quantities are presented along with discussion of effects of finite system size, significance of long-range memory functions, and consequences of correlated disorder. The investigation of reaction-diffusion systems that deals with front propagation is concerned with providing a method

of studying transient dynamics in such systems whereas the study of pattern formation focuses on determining necessary conditions for such patterns to arise in situations wherein sub- and super-diffusion are present in addition to simple diffusion. In the network study, results are reported on cluster size distribution in addition-deletion networks, on the basis of both numerical and analytic investigations.

Contents

Contents

Contents

Contents

List of Figures

List of Figures

List of Tables

Chapter 1

Introduction

1.1   Opening remarks

This thesis is on problems both in fundamental aspects, and applications of statistical physics. At a conceptual level, it is mainly divided into two parts. The first that consists of Chapters 2 and 3 is about transport in disordered lattices with applications to biology and the second that is formed by Chapter 4 is on some properties of reaction-diffusion systems, that are described by diffusion equations with nonlinear interaction terms. The last chapter is about an investigation in network theory, which has established a place for itself in the statistical physics literature during the last decade or so.

It is worthwhile to note that the two main parts of this thesis are on *dis*ordered and *non*linear systems. As opposed to ordered and linear problems, relatively less tools are available to study disordered and nonlinear problems. When we study systems that are described by linear equations, we have access to a whole lot of tools including integral transformations that make life easy. In addition to this, it is possible to use the principle of superposition in solving linear equations and take full advantage of the Green's function formalism to make progress. When we consider systems that evolve according to nonlinear

equations, superposition principle does not hold and we cannot use a large number of tools available for solving linear equations. The situation is similar in disordered systems. Solving a problem that involves an ordered structure can usually be conveniently done by taking advantage of the symmetries in the problem. Integral transforms such as the Fourier transform are very useful in doing these. However, when the structure in the system is disordered, it is usually not possible to find any symmetry that would allow us to proceed in this way. Therefore, exploring systems with nonlinearities or disorder and finding generally applicable results can be cumbersome. Nevertheless, nonlinear terms and disordered structures lead to behavior that is enormously richer than that observed in linear systems, making them more interesting to study.

There are four chapters in this thesis whose contents are briefly summarized in the next section. The necessary background regarding the subjects discussed in the thesis is given in the first section of each chapter individually, rather than here in the introduction.

1.2   Overview of the thesis

The first Chapter of this thesis is about a problem that is of interest to both physics and biology. It is about constructing a mathematical model for molecular motion in cell membranes, based on a relatively recent perception of the cell membranes [1]. Motivated by the results of high resolution single molecule tracking experiments, Kusumi and collaborators [1] proposed two new models for the plasma membrane that can account for some phenomena that the Fluid Mosaic Model [2] cannot. According to these new models, there is a mesh-like structure beneath the surface of the plasma membrane which can directly or indirectly interfere with, and hinder the diffusion of molecules that diffuse in the membrane. Based on these new ideas, we constructed a mathematical model that can predict time dependent transport quantities such as the diffusion coefficient and the mean square displacement. To our knowledge, there were two other mathematical models in the liter-

ature that are similar to ours in the spirit [3, 4], which we mention in passing in Chapter 2. The model we propose differs from one of its earlier counterparts in the way that it provides explicit and simple expressions for the exact diffusion coefficient and the mean square displacement. We compare the predictions of the model against the results of some single molecule tracking experiments and find good agreement between them. We then generalize the model to account for the effects of disordered structures that are always present in real cell membranes. We believe that this generalization which considers the disordered nature of the system we are interested in is an important one, which was not done previously in an explicit way.

The mathematical model that we present in Chapter 2 is also relevant in some physics problems. In fact, the calculation we present in inspired by an unpublished work of Kenkre on the transport of excitons in molecular crystals [5]. Therefore, the calculations that we present there also apply for many solid state physics problems involving exciton transport.

Earlier we mentioned that this thesis makes contributions to statistical physics both fundamentally and in an applied way. Chapter 3 is where we present the contributions to the theoretical development of statistical mechanics. The topic we are interested in Chapter 3 is effective medium theory of transport in disordered lattices, and its extensions. Effective medium theory, or effective medium approximation, has been used in many different contexts [6, 7, 8, 9, 10] in physics, ranging from the calculation of the effective resistivity of a random resistor network [11] to random walks in disordered lattices [12, 13, 14, 10] to obtain approximate expressions for ensemble averaged quantities. Most of the previous work in this subject is limited to studying the long-time values of the observables of interest. In our analysis, one of the main goals is to extend and verify the applicability of the effective medium theory in predicting the quantities of interest for all times, as suggested by Kenkre [15] in the context of stress distribution in granular materials. We do this by treating the problem of random walk in a one dimensional (1-D) lattice whose sites are connected to each other with transfer rates that are random variables with our extended

use of the effective medium theory. In addition to discussing the calculation of time dependent observables, we also explore the effects of correlated random transfer rates, finite system size, and a few more, as given in [16]. It is also worth mentioning that we include a clear prescription of how to use the effective medium theory, by starting from the basic principles.

In Chapter 4, we are interested in two different aspects of reaction-diffusion systems. Reaction-diffusion systems have been extensively studies, mainly due to their applicability to a large number of problems in physics, chemistry, biology, and other research areas. They provide a convenient framework for studying systems in which the constituents are entities that flow in real or in some phase space, and interact with one another and themselves. A few early, but remarkable, works on reaction-diffusion systems are due to Fisher [17] on the spread on advantageous genes in a population along with Kolmogorov, Petrovskii, and Piskunov [18], Turing on pattern formation in biological systems explained in his seminal article titled "The chemical basis of morphogenesis" [19], and Belousov [20] and Zhabotinskii [21] on a class of chemical reactions with many reacting species that can show oscillatory behavior, now termed "Belousov-Zhabotinskii" reactions.

Although reaction-diffusion systems are very useful in modeling various phenomena, the equations they involve are rarely exactly solvable for the time evolution of the quantities in the system. In the first part of Chapter 4, we report results on a study that is interested in the transient behavior in some reaction diffusion systems and thus, is an attempt at understanding the time evolution in a reaction-diffusion system. After stating the exact solutions of the reaction-diffusion equations considered for long times, we discuss our way of analyzing the problem. The method we use in trying to discover the properties of the transients in the system relies on our knowledge of these exact solutions. Conceptually, our analysis consists of comparing the numerical solution of the problem with the exact solution can calculate the difference between them at all times. In this way, we hope to gain same insight into how the system relaxes to its asymptotic solution.

In the second part of Chapter 4, we concentrate on a quite different problem: pattern formation in reaction-diffusion systems. The work we present there is inspired by the relatively recent work of Fuentes, Kuperman, and Kenkre [22] on pattern formation in a particular reaction-diffusion system with spatially non-local interactions. Pattern formation in reaction-diffusion systems has been extensively studied. Most of these studies consider the formation of patterns in reaction-diffusion systems involving multiple reacting species. Our study differs from them in this respect, as it involves only one species that interact with itself, and diffuse in a bounded space with periodic boundary conditions. As early as in the work of Turing [19], it was shown that the rate of diffusion plays an important role in determining the properties of the patterns produced. An interesting question to ask is: how does the characteristic properties of transport, like its being diffusive, sub- or super-diffusive, effect the formation of patterns? Motivated by this question, we use a generalized reaction-diffusion equation, much like a generalized master equation [5] with a memory function, to be able to consider types of transport other that diffusion. We proceed by generalizing the approach of Fuentes et al. [22], and exploring the conditions for pattern formation as a function of transport properties.

The last chapter is about a special kind of evolving networks, the addition-deletion network [23, 24, 25, 26, 27]. For over 10 years, the study of complex networks has also been considered a topic of statistical physics, and many advancements has been made [28, 29, 30, 31]. Most of the early findings concerning the properties of complex networks are due to mathematicians. The branch of mathematics that is interested in studying network structure is called graph theory. Perhaps the first written work on the theory of graphs is known as the Königsberg problem, and was studied by the Swiss mathematician Euler [32]. One of the most remarkable advances in the theory of graphs is due to the Hungarian mathematicians Erdős and Rényi [33], who started a probabilistic study of graphs. Today Erdős and Rényi are considered as the founders of the random graph theory. The addition-deletion network that we are interested in studying in this thesis is also a form of random graph. It is constructed by starting with a single network element, and subsequently adding

or removing network elements in a random fashion. Because we are removing elements in addition to adding them, the network will be partitioned into disconnected components. And it is the size distribution of these components that we are interested in calculating in Chapter 5.

The last chapter is reserved for a brief statement of the results obtained in this thesis, and for some final thoughts of the author.

Chapter 2

A mathematical model for molecular motion in cell membranes

2.1 Introduction

The cell membrane plays essential roles in the life of all organisms. The most fundamental of these is isolating the organelles, which constitute the basic machinery of life, from the noisy environment. Besides this crucial function, a few of the other important processes that it takes part in are: cell shaping and movement [34], cell division [35], transduction of signals that are vital for the organism at many levels [36], and selective transportation of molecules in and out of the cell [37]. Some of these tasks are performed by membrane molecules, such as proteins, that diffuse in the membrane. Therefore, investigating the motion of membrane molecules in detail is important in understanding how cell membranes function. In this chapter, we will present transport calculations for molecular diffusion in cell membranes inspired by new membrane models proposed by Kusumi and collaborators [1] and an earlier theoretical treatment of diffusion in the presence of permeable barriers given by Powles and others [3]. Most of the results we present in this chapter of this thesis

are published in two articles by Kenkre, Giuggioli and Kalay [38] and Kalay, Parris, and Kenkre [39].

Before discussing our calculations, we will briefly summarize how cell membrane models evolved. Several models were proposed starting in the early 20th century. In 1925, Gorter and Grendel [40] suggested that a bilayer of lipids can form a membrane that is similar to the ones found in live cells. Phospholipids, which are one of the most common types of lipids in the membrane, can spontaneously come together and form a bilayer under most circumstances. In an aqueous medium, hydrophobic parts of the phospholipids point inside the bilayer whereas their hydrophilic parts point out into the surroundings. This model does not make any reference to proteins that are now known to exist in the membrane. Later in 1935, Davson and Danielli [41] used the lipid bilayer as their starting point and incorporated membrane proteins into the picture. In their description, membrane proteins are attached to the hydrophilic parts of the lipid molecules, which are on the outer surfaces of the bilayer. But later it has become apparent that proteins can also be found in the membrane as its integral components. Finally in 1972, Singer and Nicholson [2] came up with the famous fluid mosaic model of the cell membrane. According to the fluid mosaic model, proteins are inserted into the lipid bilayer and can be found throughout the membrane and not just on its outer surfaces. Therefore, the collection of lipid molecules are thought to form a two dimensional (2-D) fluid in which membrane proteins move around and take part in numerous membrane functions.

The fluid mosaic model can account for many phenomena associated with the membrane. However, starting in 1980's, results of single molecule tracking experiments with very high temporal resolution gave rise to new puzzles. It was found that molecules diffuse 5 to 50 times slower in live cell membranes than in artificially reconstituted membranes [42, 43, 44, 45, 46, 47, 48, 1] (see Table 2.1). In addition to this, an even more surprising result was that larger molecules diffuse at much slower rates than one would expect them to in a 2-D fluid [49]. Saffman and Delbrück showed that the translational diffusion coeffi-
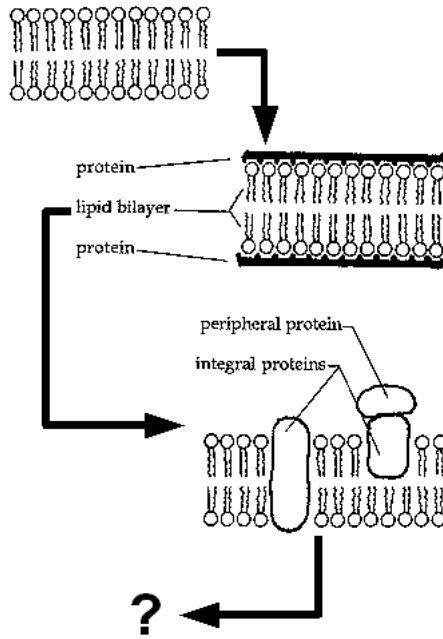
Figure 2.1: A schematic illustration of the evolution of membrane models. First Gorter and Grendel's lipid bilayer, then Davson and Danielli model with peripheral proteins, and then the Fluid Mosaic model with integral proteins due to Singer and Nicholson. The Fluid Mosaic model accounts for many phenomena, but our description of the membrane is still evolving. Images are from: http://www1.umn.edu/ships/9-2/membrane.htm

cient of a cylindrical object with radius r, diffusing in a bilayer with its axis perpendicular to the surface is given by [50]

$$D = \frac{k_B T}{4\pi\mu h}\left(\ln\frac{\mu h}{\mu' r} - \gamma\right),\tag{2.1}$$

where h is the thickness of the bilayer which is also equal to the length of the cylindrical object, γ is Euler's constant, $k_B T$ is the thermal energy, μ and μ' are the viscosity of the bilayer and the environment respectively. One of the most important implications of this relation is that D drops off with the radius of the diffusant in a very slow fashion. Experimentally it was found that larger molecules diffuse at rates that are significantly lower than what Eq. (2.1) gives [49, 1]. These observations indicate that it may not be correct to consider the membrane molecules as objects that diffuse in a viscous and

homogeneous fluid.

Probe-Protein	Cell type or artificial membrane lipid	Effective diffusion coefficient $\left[\mu m^2\right]$ & reference
Fl-AchR	DMPC	2.4±0.8 [51]
Rh-AchR	Rat Myotube	0.016±0.003 [52]
Fl-Thy-1	DOPC:SM, 1:1 ratio	0.58±0.04 [53]
Gold-Thy-1	C3H 10T1/2	0.081±0.007 [54]

Table 2.1: Diffusion coefficients of some membrane proteins as measured in live cell membranes and in artificial membranes. Excerpt from Table 1 of ref. [1]. DMPC (1,2-dimyristoyl-sn-glycero-3-phosphocholine) and SM (sphingomyelin) are lipids used in the artifical membranes and C3H 10T1/2 (mouse embryo fibroblast) and Rat Myotube are the live cell types. Fl- and Rho-AchR are fluorescein and tetramethylrhodamine labeled bungarotoxin bound to acetylcholine receptor, respectively and Fl- and gold- Thy-1 correspond to Thy-1 labelled with fluorescein-isothiocyanate and colloidal gold particles.

By conducting single molecule tracking experiments with very high time resolution, such as on the scale of 25 μs, Kusumi and collaborators observed [1] that at very short times, the diffusion coefficient of membrane proteins and lipids in live cell membranes is very close to what it would be, were they diffusing in an artificial lipid membrane. However, long-time diffusion coefficients are found to be significantly lower than those for short-times. It is impossible to observe this effect without the use of high speed imaging techniques as the frame length at usual video speeds ($\sim$ 33ms) is already long enough for the diffusion coefficient to reach its final value. To explain the slowdown effects observed in the motion of molecules in the membrane, two new models, namely "Membrane Skeleton Fence Model" and "Anchored-Protein Picket Model" have been proposed by the Kusumi lab [55, 1]. According to the Membrane Skeleton Fence model, motion of large membrane molecules like proteins are hampered because of the interaction between their cytoplasmic parts and the surface of the cytoskeleton, which lies just below the lipid bilayer and is basically a meshwork of actin filaments. See Fig. 2.2 for a schematic illustration. Therefore, the membrane proteins that interact with the actin meshwork effectively
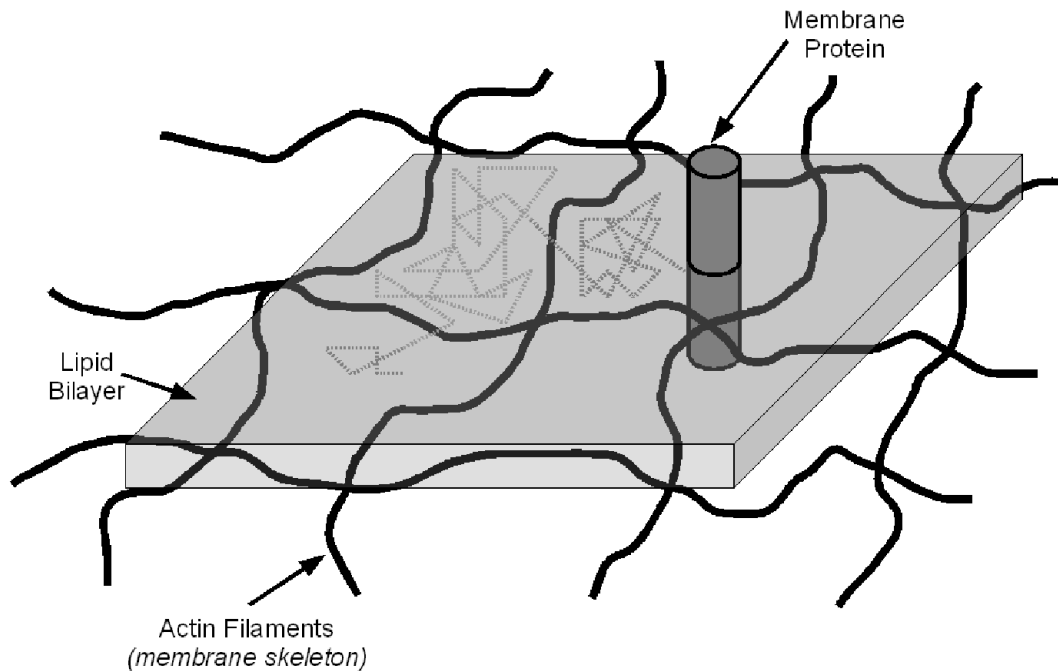
Figure 2.2: The Membrane Skeleton-Fence model.

move in a compartmentalized space, where the compartment sizes range from 30 to 240 *nm* [1, 55, 56]. The observed temporary confinement of these proteins strongly supports this model (see the review [1], and references therein). What is even more interesting is that lipids, which do not have any cytoplasmic part, and thus cannot interact with the membrane skeleton, are also observed to be temporarily confined like proteins, in domains of similar size [57]. In the Anchored Protein-Picket model, it is argued that some of the membrane proteins are attached to the membrane skeleton either temporarily or permanently so that they present themselves as immobile obstacles to diffusing lipids and other molecules in the cell membrane, as illustrated in Fig. 2.3. In this case, strength of the confinement effect on lipids would be proportional to the fraction of the compartment boundaries that are covered with immobile proteins[1].

---

[1]Unfortunately, it is not possible to measure directly what fraction of the boundaries are occupied by proteins. However, one can do simulations of lipid motion for various values of this fraction and find its value for which the results fit experimental findings the best [57].
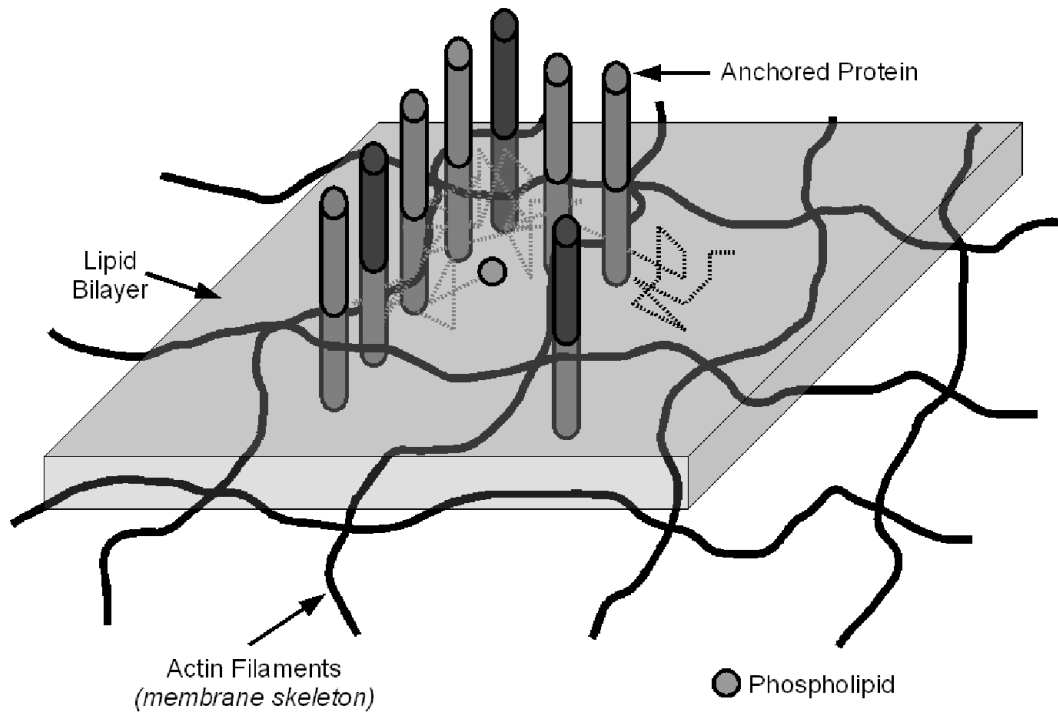
Figure 2.3: The Anchored Protein-Picket model.

Many different experiments [1] provide further evidence for the existence of compart-ments. Here, we will mention a couple of these in passing. Experiments in which a latex bead in the plasma membrane dragged by the use of optical tweezers showed that this in-duces a drift in the motion of nearby molecules [45]. This supports the hypothesis that a mesh-like structure exists below the cell surface. Another, more direct, evidence for the existence of the membrane skeleton is provided by the electron microscope images of the cytoplasmic part of the cell surface [58]. In these images, it is possible to see the network of actin filaments forming the compartment boundaries.

The rest of this chapter is mainly divided into two parts. The first part consists of Sections 2.2-2.6 and is about the fundamentals of our calculations, expressed for ordered systems. The second part is given in Sec. 2.7, and it is concerned with generalizing our results for the first part to include disorder. In Sec. 2.2, we present the details of our

mathematical model concerning the random walk problem in discrete space. In Sec. 2.3, we take the continuum limit of our results to be able to make contact with experimentally observable quantities. Sections 2.4 and 2.5 are about describing how to convert the expressions we obtained in the previous sections to functions of time using explicit Laplace inversions, partly analytical and partly numerical, and then using them to compare our theory with published experimental observations. Before moving on to Sec. 2.7 in which a generalization of our calculations is given, some practical results are presented in Sec. 2.6. Final remarks are made in Sec. 2.8 that mark the end of this chapter.

The three main research contributions of this thesis chapter are: obtaining exact formulas concerning transport quantities for a random walk in the presence of permeable barriers as functions of time, using explicit Laplace inversion schemes, part analytical and part numerical, showing that the predictions based on these formulas agree well with experimental results, and generalizing the calculations to be able to account for the presence of imperfections in the system.

2.2   Our mathematical model

In this section we introduce the mathematical model for molecular diffusion in plasma membranes, presented by Kenkre, Giuggioli, and Kalay in ref. [38]. Based on the Membrane-Skeleton Fence model, we think of the membrane as a 2-D space which is partitioned into domains of the same size with permeable barriers. Obviously, this is an idealization of the live cell membranes which would naturally have varying compartment sizes and barrier strengths. Later in this chapter, we will explore the effects of disorder in barrier strengths and locations in detail. In our model, we think of the diffusing molecules as random walkers moving in the partitioned space we described above. As the domains we consider in this idealized picture are squares with equal size, motion of the random walker in x and y directions will be independent from each other (provided that the bar-

riers lie parallel to the *x* and *y* axes). Therefore, under these assumptions, we only need to model the motion of the random walker in 1-D. To do this, we will consider a random walk in a 1-D chain, i.e. in discrete space, with periodically placed barriers, and then take the continuum limit of the results to obtain experimentally observable transport quantities. This calculation is inspired by the unpublished work of Kenkre on Frenkel exciton transport [5] in deutered molecular crystals.

To our knowledge, there have been two exactly solvable models for diffusion in the presence of permeable barriers, presented by Powles, Mallett, Rickayzen, and Evans [3], and Dudko, Berezhkovskii, and Weiss [4]. We were aware of the results given by Powles, but we came to know about the work of Dudko after our article was published. Although Powles and collaborators give exact results for the probability of finding the random walker at a certain position and time, their expressions are very complicated and difficult to evaluate, even numerically. In addition to this, explicit expressions for the exact mean square displacement of diffusion coefficient, which are quantities of great relevance in experiments, are not found among their results. Therefore, one of the motivations for our analysis is obtaining simpler and more useful expressions for experimentally accessible quantities that can be easily computed.

We start by considering a 1-D chain whose links have the same transfer rate F. Then we modify the transfer rate of every $H + 1^{\text{th}}$ link, so that it becomes f. If $f < F$, the links with transfer rate f will act like barriers to diffusion as the random walker seldom moves through them. Because every $H + 1^{\text{th}}$ link is a barrier, the chain we construct in this way is partitioned into compartments that have $H + 1$ sites each. See Fig. 2.4 for an illustration of this structure. Obviously, the molecules whose motion we set out to model do not move in discrete space. The reason we consider random walks in discrete space is that, in solving this problem, we will take advantage of the tools that are applicable to discrete lattices. Also, as we will see later, the generalization of this problem to include varying barrier heights is straightforward in discrete space, through the use of effective medium theory.
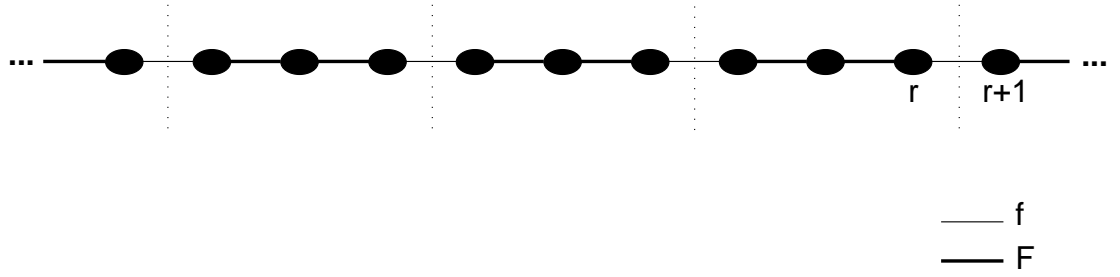
Figure 2.4: Schematic illustration of a piece of the 1-D chain with periodically placed links of different transfer rate. Transfer rate within a compartment is F whereas the rate of moving from one compartment to the next is f. Here $H = 2$, so that there are $H + 1 = 3$ sites in each compartment. The dotted vertical lines indicate compartment boundaries.

Let $P_m(t)$ be the probability of finding the random walker at the mth site of the chain at time t. Assuming that transitions occur only between neighboring sites, $P_m(t)$ obeys

$$\frac{dP_m(t)}{dt} = F\left[P_{m+1}(t) + P_{m-1}(t) - 2P_m(t)\right],$$

if the site m is not on the boundary of a compartment,

$$\frac{dP_r(t)}{dt} = f\left[P_{r+1}(t) - P_r(t)\right] + F\left[P_{r-1}(t) - P_r(t)\right],$$

if m is the rightmost site in a compartment, and

$$\frac{dP_{r+1}(t)}{dt} = f\left[P_r(t) - P_{r+1}(t)\right] + F\left[P_{r+2}(t) - P_{r+1}(t)\right],$$

if m is the leftmost site in a compartment as illustrated in Fig. 2.4. As there are $H + 1$ sites in one compartment, the index r takes on the values $H/2 + (H + 1)\ell$ where ℓ is any integer. Using Kronecker δ's, $\delta_{ij} = 1$ for $i = j$ and 0 otherwise, the three equations above can be put together in a compact form

$$\frac{dP_m(t)}{dt} - F\left[P_{m+1}(t) + P_{m-1}(t) - 2P_m(t)\right] = -\Delta \sum_r{}' \left[P_{r+1}(t) - P_r(t)\right]\left(\delta_{m,r} - \delta_{m,r+1}\right),$$

(2.2)

where $\Delta = F - f$ and the primed summation is over barrier locations. Eq. (2.2) is not newly introduced. Equations of this form have been used to describe the dynamics of excitons in

molecular crystals [5]. Since Eq. (2.2) is linear in $P_m(t)$, it is possible to convert it to an algebraic equation by an appropriate integral transform. Let $\eta_m(t)$ be the solution of Eq. (2.2) for $\Delta = 0$, i.e. when there are no barriers, given by

$$\eta_m(t) = \sum_n \psi_{m-n}(t) P_n(0),$$

where $\psi_m(t)$ is the probability propagator for a 1-D chain with uniform transfer rates F. Taking the Laplace transform of Eq. (2.2), and using the fact that $\eta_m(t)$ is solution of its homogeneous part, we write

$$\widetilde{P}_m(\epsilon) = \widetilde{\eta}_m(\epsilon) - \Delta \sum_r{}' \widetilde{p}_r(\epsilon) \left[\widetilde{\psi}_{m-r}(\epsilon) - \widetilde{\psi}_{m-r-1}(\epsilon) \right], \tag{2.3}$$

where $\widetilde{p}_r = \widetilde{P}_{r+1}(\epsilon) - \widetilde{P}_r(\epsilon)$. In order to make progress, we can try to obtain a closed equation in $\widetilde{p}_r$. To do this, we substitute $m = s + 1$ and $m = s$ in Eq. (2.3), where s is a site to the left of a barrier, to get the following equations

$$\widetilde{P}_{s+1}(\epsilon) = \widetilde{\eta}_{s+1}(\epsilon) - \Delta \sum_r{}' \widetilde{p}_r(\epsilon) \left[\widetilde{\Psi}_{s-r+1}(\epsilon) - \widetilde{\Psi}_{s-r}(\epsilon) \right],$$

$$\widetilde{P}_s(\epsilon) = \widetilde{\eta}_s(\epsilon) - \Delta \sum_r{}' \widetilde{p}_r(\epsilon) \left[\widetilde{\Psi}_{s-r}(\epsilon) - \widetilde{\Psi}_{s-r-1}(\epsilon) \right].$$

Subtracting $\widetilde{P}_s(\epsilon)$ from $\widetilde{P}_{s+1}(\epsilon)$, we obtain

$$\widetilde{p}_s(\epsilon) = \widetilde{\zeta}_s(\epsilon) - \Delta \sum_r{}' \widetilde{p}_r(\epsilon) \widetilde{\Psi}_{s-r}(\epsilon), \tag{2.4}$$

where we defined

$$\widetilde{\zeta}_s(\epsilon) = \widetilde{\eta}_{s+1}(\epsilon) - \widetilde{\eta}_s(\epsilon),$$
$$\widetilde{\Psi}_r(\epsilon) = \widetilde{\psi}_{r+1}(\epsilon) + \widetilde{\psi}_{r-1}(\epsilon) - 2\widetilde{\psi}_r(\epsilon).$$

Note that $\widetilde{\psi}_m(t)$'s obey the Laplace transform of the homogeneous part of Eq. (2.2)

$$\epsilon \widetilde{\psi}_m(\epsilon) - \psi_m(0) = F \left[\widetilde{\psi}_{m+1}(\epsilon) + \widetilde{\psi}_{m-1}(\epsilon) - 2\widetilde{\psi}_m(\epsilon) \right],$$

so that we can write

$$\widetilde{\Psi}_r(\epsilon) = \frac{1}{F}\left[\epsilon\widetilde{\psi}_r(\epsilon) - \delta_{r,0}\right],$$

where we used the fact that $\psi_m(0) = 1$, as $\psi_{m-n}(t)$ is the probability of finding the random walker at site m if it started at site n. Note that solving Eq. (2.4) for $\widetilde{p}_s(\epsilon)$ requires solving a set of N simultaneous linear equations, where N is the number of barriers. If we are considering a finite system, it may be plausible to solve these equations for $\widetilde{p}_s(\epsilon)$. When there are infinitely many barriers, as in our case, we need to find an alternative solution. One way is to sum Eq. (2.4) over s

$$\sum_s \widetilde{p}_s(\epsilon) = \sum_s \widetilde{\zeta}_s(\epsilon) - \Delta\sum_s \widetilde{\mu}_s(\epsilon)\widetilde{p}_s(\epsilon), \tag{2.5}$$

where

$$\widetilde{\mu}_s(\epsilon) = \sum_r{}' \widetilde{\Psi}_{s-r}(\epsilon),$$

and calculate $\widetilde{\mu}_s(\epsilon)$ for specific cases. Note that if $\widetilde{\mu}_s(\epsilon)$ is independent of s, then Eq. (2.5) leads to

$$\sum_s \widetilde{p}_s(\epsilon) = \frac{1}{1 + \Delta\widetilde{\mu}(\epsilon)}\sum_s \widetilde{\zeta}_s(\epsilon),$$

which means that we can replace $\widetilde{p}_s(\epsilon)$ with $\widetilde{\zeta}_s(\epsilon)/(1 + \Delta\widetilde{\mu}(\epsilon))$, under sums over s, if the summation is over all values of s. Therefore, the expression for $\widetilde{P}_m(\epsilon)$ given by Eq. (2.3) would become a solution after this replacement. It turns out that when the barriers are placed periodically $\widetilde{\mu}_s(\epsilon)$ is independent of s, as shown below[2]. In this case, we need to evaluate the sum

$$\widetilde{\mu}_s = \sum_r{}' \widetilde{\Psi}_{s-r} = \frac{1}{F}\sum_r{}' \left(\epsilon\widetilde{\psi}_{s-r} - \delta_{s-r,0}\right).$$

---

[2]It is worth mentioning that $\widetilde{\mu}_s(\epsilon)$ is also independent of s if the barriers are placed randomly.

Note that $r = H/2 + (H+1)\ell$ and ℓ runs over all integers. This means that $s - r = (H+1)n$, where n can be any integer just as ℓ is. Therefore, the summation is equivalent to

$$\widetilde{\mu} = \frac{1}{F} \sum_{n=-\infty}^{+\infty} \left(\epsilon \widetilde{\psi}_{(H+1)n} - \delta_{n,0} \right). \tag{2.6}$$

The Laplace transform of the propagator $\widetilde{\psi}_m(t)$ is explicitly given by

$$\widetilde{\psi}_m(\epsilon) = \frac{(2F)^{|m|}}{\sqrt{\epsilon(\epsilon + 4F)} \left(\epsilon + 2F + \sqrt{\epsilon\,(\epsilon + 4F)} \right)^{|m|}}. \tag{2.7}$$

If we define $\cosh \xi = 1 + \epsilon/2F$, then the propagator can be written as

$$\widetilde{\psi}_m(\epsilon) = \frac{e^{-\xi|m|}}{2F \sinh \xi}. \tag{2.8}$$

Substituting this in Eq. (2.6), we get

$$\widetilde{\mu} = \frac{1}{F} \left[\frac{\epsilon}{2F \sinh \xi} \sum_{n=-\infty}^{+\infty} e^{-\xi(H+1)|n|} - 1 \right] \tag{2.9}$$

$$= \frac{1}{F} \left[\frac{\tanh\left(\xi/2\right)}{\tanh\left(\xi\,(H+1)\,/2\right)} - 1 \right]. \tag{2.10}$$

Now we can use Eq. (2.3) to express the solution for $\widetilde{P}_m(\epsilon)$ in terms of the initial conditions (hidden in $\widetilde{\eta}_r(\epsilon)$), the propagators of $\widetilde{\psi}_m(\epsilon)$, and the $\widetilde{\mu}$ function as

$$\widetilde{P}_m(\epsilon) = \widetilde{\eta}_m(\epsilon) - \left(\frac{\Delta}{1 + \Delta\widetilde{\mu}(\epsilon)} \right) \sideset{}{'}\sum_{r} \left[\widetilde{\eta}_{r+1}(\epsilon) - \widetilde{\eta}_r(\epsilon) \right] \left[\widetilde{\psi}_{m-r}(\epsilon) - \widetilde{\psi}_{m-r-1}(\epsilon) \right]. \tag{2.11}$$

If the random walker initially occupies the pth site of the chain, i.e. $P_n(0) = \delta_{n,p}$, we have

$$\widetilde{\eta}_m(\epsilon) = \widetilde{\psi}_{m-p}(\epsilon).$$

Note that choosing such an initial condition does not cause a loss in generality as we can express any initial condition as a superposition of $\delta_{n,p}$'s in this linear problem. As all compartments are equivalent, we will take the initially occupied site to be within the middle compartment that contains the 0th site. Therefore, $p \in [-H/2, H/2]$.

The transport quantities that we are interested in calculating are the time-dependent mean square displacement (MSD), and diffusion coefficient. The dimensionless mean square displacement for a random walker that starts at the pth site is defined as

$$\text{MSD}_p(t) = \left\langle (m - p)^2 \right\rangle = \sum_m (m - p)^2 P_m(t).$$

Using this definition and the result given in Eq. (2.11), we can express the Laplace transform of the MSD as

$$\widetilde{\text{MSD}}_p(\epsilon) = \sum_m (m - p)^2 \widetilde{\psi}_{m-p}(\epsilon) - \Delta \sum_r{}' \widetilde{p}_r(\epsilon) \sum_m (m - p)^2 \left[\widetilde{\psi}_{m-r}(\epsilon) - \widetilde{\psi}_{m-r-1}(\epsilon) \right],$$

$$(2.12)$$

where

$$\sum_r \widetilde{p}_r(\epsilon) = \frac{1}{1 + \Delta \widetilde{\mu}(\epsilon)} \sum_r \left[\widetilde{\psi}_{r-p}(\epsilon) - \widetilde{\psi}_{r+1-p}(\epsilon) \right].$$

The first term in the right hand side of Eq. (2.12) is simply the MSD in the absence of barriers. We will denote it by $\widetilde{\text{MSD}}_p^0(\epsilon)$. Note that we can express the square $(m - p)^2$ as $(m - p)^2 = m^2 - 2p(m - p) - p^2 =$, which proves useful in showing the following results. From Eq. (2.7), it is clear that the first moment of the propagators is zero, as $\widetilde{\psi}_m(\epsilon) = \widetilde{\psi}_{-m}(\epsilon)$. Using this result together with $\sum_m \widetilde{\psi}_m(\epsilon) = 1/\epsilon$, we can show that

$$\sum_m (m - p)^2 \left[\widetilde{\psi}_{m-r}(\epsilon) - \widetilde{\psi}_{m-r-1}(\epsilon) \right] = -\frac{2r - 2p + 1}{\epsilon}.$$

Therefore, the Laplace transform of the MSD becomes

$$\widetilde{\text{MSD}}_p(\epsilon) = \widetilde{\text{MSD}}_p^0(\epsilon) - \frac{1}{\epsilon} \left(\frac{\Delta}{1 + \Delta \widetilde{\mu}(\epsilon)} \right) \sum_r{}' (2r - 2p + 1) \left[\widetilde{\psi}_{r-p}(\epsilon) - \widetilde{\psi}_{r+1-p}(\epsilon) \right].$$

It is well known that in the absence of barriers, $\text{MSD}_p^0(t) = 2Ft$ so that $\widetilde{\text{MSD}}_p^0(\epsilon) = 2F/\epsilon^2$. Note that $\text{MSD}_p^0(t)$ is the second integral of the function $2F\delta(t)$. Therefore, we can express $\text{MSD}_p(t)$ as the second integral of $2F\phi_p(t)$, where $\phi_p(t) = \delta(t) - g_p(t)$ and $g_p(t)$ is a function whose Laplace transform is

$$\widetilde{g}_p(\epsilon) = \frac{\Delta}{F} \frac{\epsilon}{1 + \Delta \widetilde{\mu}} \sum_r{}' \left(r - p + \frac{1}{2} \right) \left(\widetilde{\psi}_{r-p} - \widetilde{\psi}_{r+1-p} \right). \qquad (2.13)$$

19

The summations involved in this equation can be evaluated by using Eq. (2.8), to give

$$\sum_{r}{}' \left(\widetilde{\psi}_{r-p} - \widetilde{\psi}_{r+1-p} \right) = \frac{\sinh(\xi/2)}{F \sinh(\xi)} \frac{\sinh(\xi p)}{\sinh(\xi(H+1)/2)},$$

$$\sum_{r}{}' r \left(\widetilde{\psi}_{r-p} - \widetilde{\psi}_{r+1-p} \right) = \frac{H+1}{2F \sinh \xi} \frac{\sinh(\xi/2) \cosh\left(\frac{\xi(H+1-2p)}{2} \right)}{\sinh^2 \left(\frac{\xi(H+1)}{2} \right)}.$$

Substituting these in Eq. (2.13) and going through some tedious but simple algebra, the function $\widetilde{g}_p(\epsilon)$ can be put in the following form

$$\widetilde{g}_p(\epsilon) = \frac{\Delta}{F} \frac{1}{P(\epsilon) + (\epsilon/2F + 2f/F) Q(\epsilon)}$$
$$\times \left[(H+1) \frac{P(\epsilon) + (\epsilon/2F) Q(\epsilon)}{P(\epsilon) + (2 + \epsilon/2F) Q(\epsilon)} \cosh(\xi p) - 2p \sinh(\xi p) \tanh(\xi/2) \right]. \quad (2.14)$$

where $P(\epsilon) = \cosh(\xi H/2)$ and $Q(\epsilon) = \sinh(\xi H/2)/\sinh \xi$. Once H is fixed, it is straightforward to calculate $\widetilde{g}_p(\epsilon)$. In order to give the reader an idea of how the inverse Laplace transform of $\widetilde{g}_p(\epsilon)$ behaves as a function of time, we will present $g_p(t)$ for a couple of H values below. For compartments consisting of 3 sites so that $H = 2$, $P(\epsilon) = 1 + \epsilon/2F$, $Q(\epsilon) = 1$ and

$$g_{2,0}(t) = 3F \left[e^{-3Ft} - \frac{f}{F} e^{-\left(1 + \frac{f}{F}\right)Ft} \right],$$

$$g_{2,\pm 1}(t) = \Delta \left(\frac{3F}{2} \frac{e^{-3Ft}}{f - F} - \frac{(F^2 - Ff/2 + f^2)e^{-(1+2\frac{f}{F})Ft}}{F(f-F)} + \frac{\delta(t)}{2F} \right),$$

where the first and second subscripts of $g(t)$ correspond to the value of H and initial position of the random walker, respectively. When there are 5 sites per compartment, $H = 4$, we have $P(\epsilon) = 1 + 2\epsilon/F + \epsilon^2/2F^2$, $Q(\epsilon) = 2 + \epsilon/F$ and

$$g_{4,0}(t) = 10F \left[e^{-\frac{5Ft}{2}} \frac{\sinh\left(\sqrt{5}Ft/2 \right)}{\sqrt{5}} - \frac{f}{F} e^{-\left(\frac{3}{2} + \frac{f}{F}\right)Ft} \frac{\sinh\left(\sqrt{5 - 4\frac{f}{F} + 4\left(\frac{f}{F}\right)^2} Ft/2 \right)}{\sqrt{5 - 4\frac{f}{F} + 4\left(\frac{f}{F}\right)^2}} \right].$$

$$(2.15)$$

For this case, the expressions corresponding to the initial conditions with $p = 1, 2$ and 3 are lengthy, and thus not displayed here.

In many experiments, the knowledge about initial conditions is absent, so that it is appropriate to average over all initial positions p, within a compartment. The average of $\widetilde{g}_p(\epsilon)$ over p is defined as

$$\widetilde{g}(\epsilon) = \frac{1}{H+1} \sum_{p=-H/2}^{H/2} \widetilde{g}_p(\epsilon), \tag{2.16}$$

and is explicitly given by

$$\widetilde{g}(\epsilon) = \frac{\Delta}{F(H+1)} \frac{P(\epsilon) + (\epsilon/2F + 2) Q(\epsilon)}{P(\epsilon) + (\epsilon/2F + 2f/F) Q(\epsilon)}. \tag{2.17}$$

From now on, the absence of the subscript p in all quantities will imply an average over initial conditions in the sense of Eq. (2.16).

Before moving on, a few limiting properties of $g_p(t)$ are worth mentioning. If the starting site is not adjacent to a compartment boundary, at short times the random walker will diffuse as if there are no barriers, and its MSD will go as $2Ft$. This means that $\lim_{t\to 0} g_p(t) = \lim_{\epsilon\to\infty} \epsilon \widetilde{g}_p(\epsilon)$ must vanish provided that the site p is not adjacent to a boundary. As for the long time limit, we would expect $\lim_{t\to\infty} g_p(t)$ to vanish, as its integral, which is related to the diffusion coefficient, must be finite. Lastly, the asymptotic diffusion coefficient should be independent from the initial conditions, as it is determined by the structure of the chain, which depends on the values of f and F. Using Eq. (2.14) and limit theorems of the Laplace transform [59], it can be shown that $g_p(t)$ satisfies all of these asymptotic properties.

If we define the time dependent hopping rate, which is the analogue of the diffusion coefficient in discrete space, as $F_p(t) = (1/2)d(\text{MSD}_p(t))/dt$, then transport quantities that we are interested in are conveniently given as

$$\text{MSD}_p(t) = 2F \int_0^t ds \int_0^s ds' \phi_p(s'), \tag{2.18}$$

$$F_p(t) = 2F \int_0^t ds \phi_p(s), \tag{2.19}$$

in time domain and

$$\widetilde{\widehat{\mathrm{MSD}}}_p(\epsilon) = 2F\frac{\widetilde{\phi}_p(\epsilon)}{\epsilon^2},$$

$$\widetilde{F}_p(\epsilon) = 2F\frac{\widetilde{\phi}_p(\epsilon)}{\epsilon},$$

in Laplace domain. The function $\phi(t)$ acts like the memory of a generalized master equation [5] considering the way it is connected with the MSD and F. Using the Laplace transform of $F_p(t)$, we can easily calculate the hopping rate at asymptotically long times, which we will call the effective hopping rate, and denote it by F_{eff}. It is well known that the integral of a function $h(t)$ from 0 to ∞ is related to its Laplace transform through [59]

$$\int_0^\infty ds\, h(s) = \lim_{\epsilon\to 0}\widetilde{h}(\epsilon).$$

Hence the effective hopping rate is given by

$$F_{\mathrm{eff}} = F\int_0^\infty ds\, \phi_p(s) = F\lim_{\epsilon\to 0}\widetilde{\phi}_p(\epsilon) = f\frac{H+1}{1+(f/F)H}. \tag{2.20}$$

Note that F_{eff} is independent from p as expected. Let us take a closer look at Eq. (2.20) and its marginal values. If $f = F$, then all the links in the chain have the same transfer rate F, and consequently $F_{\mathrm{eff}} = F$. If we consider the situation in which the barriers are infinitely high, so that it is not possible for the random walker to cross them, $f = 0$ and F_{eff} vanishes according to Eq. (2.20). This is what one would expect, as the random walker is confined within a compartment, so that its MSD will saturate and the rate at which the MSD changes should become zero. If the barrier heights are large, but not infinite so that there is a small rate for leaving one compartment for another, F_{eff} is predominantly determined by the ratio $(f/F)H$. If $(f/F)H$ is negligible, we have $F_{\mathrm{eff}} \approx f(H+1)$. Another interesting case of a completely different nature is $f > F$. This means that the random walker's hopping rate is enhanced rather than suppressed, periodically throughout the chain. One would expect that this would cause an increase in F_{eff}, and it indeed does. For $f \gg F$, Eq. (2.20) becomes

$$F_{\mathrm{eff}} \approx F\left(1 + 1/H\right).$$

Note that the enhancement in F_{eff} due to f being larger than F is limited to a factor of $3/2$, and decreases with H.

In order to verify these results, we compare the MSD given by exact calculations to that found by Monte Carlo simulations for $H = 4$. In this case it is straightforward to calculate $g_p(t)$, see Eq. (2.15) for $g_{4,0}(t)$, for $p = 0, \pm 1, \pm 2$ and obtain $\text{MSD}_p(t)$. The Monte Carlo simulation of the random walk is performed similarly as in [60], where a random walk on a network structure is considered. Initially, we place the random walker at one of the sites in the middle compartment. At each subsequent step of the simulation, which corresponds to an increment Δt in time, the random walker moves between neighboring sites. The probability it will take a step either to the left or right is given by $h_i \Delta t$, where h_i is a transfer rate between sites and the subscript i indicates direction. This implies that with probability $1 - (h_{\text{left}} + h_{\text{right}})\Delta t$, the random walker will not move during that step. The increment Δt should be chosen to be a small enough number such that the probabilities $h_i \Delta t$ and $1 - (h_{\text{left}} + h_{\text{right}})\Delta t$ are between 0 and 1. In order to obtain the $\text{MSD}_p(t)$, we calculate the value of $(m - p)^2$ for 20000 trajectories, each generated in the way described above. The comparison between exact calculations and simulation results are shown in Fig. 2.5 for different initial conditions.

2.3   The continuum limit

Our aim is to predict the time dependence of transport quantities like the MSD of molecules diffusing in the cell membrane. The results that are shown so far capture the effects of compartments on diffusion, but they apply for entities that move in discrete space. Therefore, we somehow need to find the counterparts of those results that are valid in continuous space. In this section we will show how to achieve this by taking the appropriate limits of the results obtained earlier.
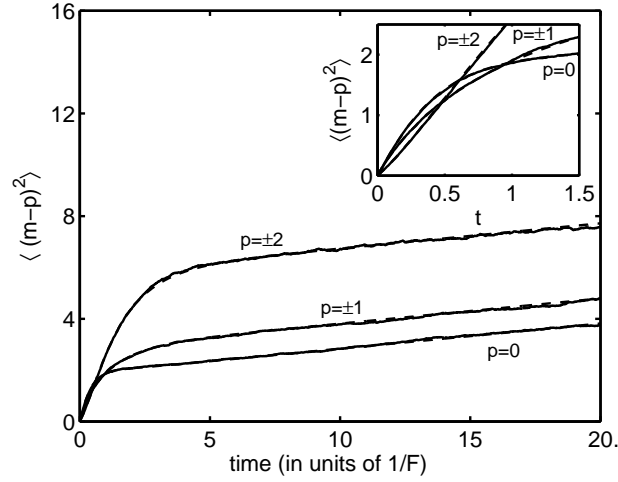
Figure 2.5: Comparison of exact results with Monte Carlo simulations for the mean square displacement of the random walker. Parameters are $f = 0.01$, $F = 2$ $H = 4$. Solid curves show the result of the simulations, averaged over 20000 trajectories, whereas the dashed curves are analytical results. The agreement between the two is almost perfect. The inset shows the behavior at short times.

Let a be the spacing between two adjacent sites in the chain, as shown in Fig. 2.6. Then the size of a compartment can be expressed as $a(H + 1)$. Note that if the number of sites goes to infinity while their spacing a goes to zero, the discrete chain of sites can be thought as a continuous 1-D space. In continuum, we will denote the size of a compartment by L,

$$\lim_{\substack{H \to \infty \\ a \to 0}} a(H + 1) = L. \tag{2.21}$$

Naturally, the initial condition will be given by

$$\lim_{a \to 0} pa = x_0. \tag{2.22}$$

Next, we will show how f and F change in the continuum limit. Without the presence of barriers, the diffusion equation in 1-D is

$$\frac{\partial \mathscr{P}(x, t)}{\partial t} = D \frac{\partial^2 \mathscr{P}(x, t)}{\partial x^2},$$

where D is the diffusion coefficient with dimensions $[\text{length}]^2 [\text{time}]^{-1}$, and $\mathscr{P}(x, t)$ is the probability *density*. By discretizing the second derivative with respect to x, the diffusion
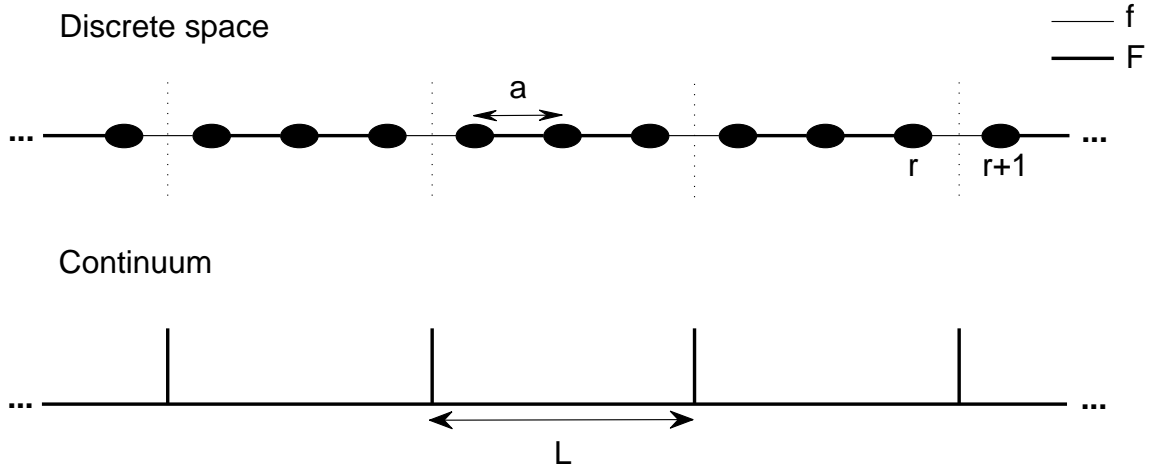
Figure 2.6: An illustration of the discrete chain and the continuum with periodically placed barriers (shown by vertical dotted lines in discrete space and solid lines in continuum). In discrete space, each site is separated from its neighbor by a distance a. In taking the continuum limit, we take $a \to 0$, and the number of sites in a compartment to ∞, such that $(H + 1)a \to L$ becomes the compartment size.

equation can also be written as

$$\frac{\partial P(x_m, t)}{\partial t} = D \lim_{a \to 0} \frac{P(x_{m+1}, t) + P(x_{m-1}, t) - 2P(x_m, t)}{a^2}, \qquad (2.23)$$

where we also multiplied both sides by a to convert the probability density $\mathscr{P}(x, t)$, to the probability $P(x, t) = a\mathscr{P}(x, t)$. Note the similarity between Eq. (2.23) and the left hand side of Eq. (2.2). Hence, one of the steps in taking the continuum limit of Eq. (2.2) involves multiplying and dividing the second term on the left hand side with a^2, and letting $a \to 0$. This implies that the diffusion coefficient is related to the transfer rate (or hopping rate) F by

$$\lim_{a \to 0} Fa^2 = D. \qquad (2.24)$$

Now that we know the limiting properties of F and H as $a \to 0$, we can use Eq. (2.20) to find out what happens to f in the continuum limit. As $\lim_{a \to 0} Fa^2 = D$, $F_{\text{eff}}a^2$ given by Eq. (2.20) should become the effective diffusion coefficient, D_{eff}. As a result, if $F_{\text{eff}}a^2$ stays

finite when $a \to 0$, Eqs. (2.20, 2.21, 2.24) imply that f should satisfy,

$$\lim_{a \to 0} f a = \mathcal{D},$$

where $\mathcal{D}$ is a quantity with dimensions $[\text{length}][\text{time}]^{-1}$, and is proportional to the permeability of barriers, as we will see later. Consequently, the analogue of Eq. (2.20) in continuum is

$$D_{\text{eff}} = \frac{D}{1 + \frac{D}{\mathcal{D}L}}, \tag{2.25}$$

that is the asymptotic value of $D(t)$. This expression is equivalent to that obtained by Powles and collaborators [3], with $\mathcal{D}/D$ being the permeability of each barrier, denoted by $\mathcal{P}$.

Having established the basics of taking the continuum limit, we now will give the expressions for the function g in continuous space. Multiplying and dividing the terms in Eqs. (2.14) and (2.17) by powers of a, letting $a \to 0$ and using the limits in Eqs. (2.21, 2.22, 2.24, 2.25), we obtain

$$\widetilde{g}^c_{x_0}(s) = \frac{s^2}{s \cosh s + \frac{D_{\text{eff}}}{D - D_{\text{eff}}} \sinh s} \left[\coth s \cosh\left(\frac{2x_0}{L}s\right) - \frac{2x_0}{L} \sinh\left(\frac{2x_0}{L}s\right) \right], \tag{2.26}$$

and

$$\widetilde{g}^c(s) = \frac{\sinh s}{s \cosh s + \frac{D_{\text{eff}}}{D - D_{\text{eff}}} \sinh s}, \tag{2.27}$$

where $\widetilde{g}^c_{x_0}(s)$ and $\widetilde{g}^c(s)$ are the continuum limits of $\widetilde{g}_p(\epsilon)$ and its average over initial conditions, $\widetilde{g}(\epsilon)$. In order to simplify the notation, we defined the quantity $s = (L/2)\sqrt{\epsilon/D}$, which is proportional to the Laplace variable ϵ. We are now in a position to give expressions for the MSD and D in terms of the g's. The MSD in continuum is defined as

$$\text{MSD}_{x_0}(t) = \left\langle (x - x_0)^2 \right\rangle = \int_{-\infty}^{\infty} dx (x - x_0)^2 \mathcal{P}(x, t).$$

The MSD and D are related to the memory $\phi_{x_0}^c(t) = \delta(t) - g_{x_0}^c(t)$ by

$$\text{MSD}_{x_0}(t) = 2D \int_0^t ds \int_0^s ds' \phi_{x_0}^c(s'), \tag{2.28}$$

$$D_{x_0}(t) = 2D \int_0^t ds \phi_{x_0}^c(s), \tag{2.29}$$

in time domain and

$$\widetilde{\text{MSD}}_{x_0}(\epsilon) = 2D \frac{\widetilde{\phi}_{x_0}^c(\epsilon)}{\epsilon^2}, \tag{2.30}$$

$$\widetilde{D}_{x_0}(\epsilon) = 2D \frac{\widetilde{\phi}_{x_0}^c(\epsilon)}{\epsilon}, \tag{2.31}$$

in Laplace domain. From now on, we will drop the superscript c, as we concentrate on comparing the predictions with experiments, in which only the continuum limit of the expressions is relevant.

2.4 Inverting the Laplace transforms

To this point, all expressions for the MSD and D were given in the Laplace domain, in terms of the Laplace transform of $\phi(t)$. In order to be able to compare these results with experimental data, one needs to take their inverse Laplace transforms to express them as functions of time. In this section, our aim is to describe how to obtain the transport quantities in time domain by showing the details of taking the inverse Laplace transform $\widetilde{\text{MSD}}_{x_0}(\epsilon)$, given by Eq. (2.30).

We would like to calculate

$$\mathcal{L}^{-1}\left\{\widetilde{\text{MSD}}_{x_0}(\epsilon)\right\} = \text{MSD}_{x_0}(t),$$

where $\mathcal{L}^{-1}$ denotes the inverse Laplace transformation operator and represents the Bromwich contour integral

$$\mathcal{L}^{-1}\left\{\widetilde{f}(\epsilon)\right\} = f(t) = \frac{1}{2\pi i} \int_{\gamma-i\infty}^{\gamma+i\infty} d\epsilon e^{\epsilon t} \widetilde{f}(\epsilon), \tag{2.32}$$

and γ is a real number larger than the real parts of all singularities of $\widetilde{f}(\epsilon)$. Therefore, we are interested in evaluating

$$\text{MSD}_{x_0}(t) = 2Dt - 2D \oint_C d\epsilon \frac{\widetilde{g}_{x_0}(\epsilon)}{\epsilon^2} e^{\epsilon t}, \tag{2.33}$$

where $\oint_C$ represents a contour integral with C being any deformation of the contour defined in Eq. (2.32) that encloses all singularities of $\widetilde{g}(\epsilon)$. See, for instance, ref. [61] on the freedom in choosing the contour in the Bromwich integral. Note that in Eq. (2.33), $\widetilde{g}_{x_0}$ is taken as a function of ϵ, but as Eq. (2.26) shows, it can more conveniently be written as a function of $s = (L/2)\sqrt{\epsilon/D}$. Therefore, it is convenient to change the integration variable from ϵ to s. Furthermore, we will use the following notation in order to simplify the expressions

$$\gamma = D_{\text{eff}}/(D - D_{\text{eff}}), \tag{2.34}$$

$$\alpha = 2x_0/L, \tag{2.35}$$

$$\tau = 4Dt/L^2. \tag{2.36}$$

After changing the integration variable and doing some algebra, Eq. (2.33) becomes

$$\text{MSD}_{x_0}(\tau) = \frac{L^2}{2}(\tau - (\sigma_1(\tau) - \gamma\sigma_2(\tau) - \alpha\sigma_3(\tau))),$$

where

$$\sigma_1(\tau) = \frac{1}{2\pi i}\oint_C ds \frac{\cosh(\alpha s)e^{s^2\tau}}{s^2 \sinh s},$$
$$\sigma_2(\tau) = \frac{1}{2\pi i}\oint_C ds \frac{\cosh(\alpha s)e^{s^2\tau}}{s^2(s\cosh s + \gamma\sinh s)},$$
$$\sigma_3(\tau) = \frac{1}{2\pi i}\oint_C ds \frac{\sinh(\alpha s)e^{s^2\tau}}{s(s\cosh s + \gamma\sinh s)}. \tag{2.37}$$

Therefore, $\sigma_1, \sigma_2, \sigma_3$ will be equal to the sum of the residues of the integrands in Eqs.

(2.37). Let

$$w_1(s, \tau) = \frac{\cosh(\alpha s)e^{s^2\tau}}{s^2 \sinh s},$$

$$w_2(s, \tau) = \frac{\cosh(\alpha s)e^{s^2\tau}}{s^2(s \cosh s + \gamma \sinh s)},$$

$$w_3(s, \tau) = \frac{\sinh(\alpha s)e^{s^2\tau}}{s(s \cosh s + \gamma \sinh s)}.$$

Then,

$$\text{MSD}_{x_0}(\tau) = \frac{L^2}{2}\left(\tau - \left(\sum_{s_n} Res\{w_1, s_n\} - \gamma \sum_{s_n} Res\{w_2, s_n\} - \alpha \sum_{s_n} Res\{w_3, s_n\}\right)\right),$$

where s_n's are the poles of w_1, w_2, and w_3. For w_2 and w_3, s_n's are the solutions of $-s = \gamma \tanh s$, and for w_1, they satisfy $\sinh s = 0$. At $s = 0$, w_1 and w_2 have poles of order 3 and w_3 has a pole of order 2. The residues at $s_n = 0$ for each case are

$$Res\{w_1, 0\} = \tau + \alpha^2/2 - 1/6,$$

$$Res\{w_2, 0\} = (6\tau(\gamma + 1) + 3\alpha^2(\gamma + 1) - (\gamma + 3))/(6(\gamma + 1)^2),$$

$$Res\{w_3, 0\} = \alpha/(\gamma + 1).$$

Note that each of the functions w_1, w_2 and w_3 possess infinitely many poles in addition to the pole at $s=0$. By expanding $\sinh s$ and $s \cosh s + \gamma \sinh s$ in Taylor series, we see that all other poles are simple poles, as the first derivative of these expressions do not vanish at $s = s_n$. By solving $\sinh s = 0$, it is found that the nonzero poles of w_1 are located at $s=im\pi$ where $m = \pm 1, \pm 2, \pm 3....$ For w_2 and w_3, exact locations of the poles cannot be found because it is not possible to find the roots of the transcendental equation $s \cosh s + \gamma \sinh s$

analytically. Therefore,

$$\sigma_1(\tau) = \tau + \alpha^2/2 - 1/6 + \sum_{s_n} \lim_{s \to s_n} \frac{\cosh(\alpha s)e^{s^2\tau}}{s^2 \cosh s}, \tag{2.38}$$

$$\sigma_2(\tau) = \frac{6\tau(\gamma + 1) + 3\alpha^2(\gamma + 1) - (\gamma + 3)}{6(\gamma + 1)^2}$$

$$+ \sum_{s_n} \lim_{s \to s_n} \frac{\cosh(\alpha s)e^{s^2\tau}}{s^2(s \sinh s + (1 + \gamma)\cosh s)}, \tag{2.39}$$

$$\sigma_3(\tau) = \frac{\alpha}{(\gamma + 1)} + \sum_{s_n} \lim_{s \to s_n} \frac{\sinh(\alpha s)e^{s^2\tau}}{s(s \sinh s + (1 + \gamma)\cosh s)}, \tag{2.40}$$

where $s_n \neq 0$ in the summations. Because the roots of $\sinh(s) = 0$ can be found analytically, $\sigma_1(\tau)$ can also be expressed as

$$\sigma_1(\tau) = \sum_{\substack{m=-\infty, \\ m\neq 0}}^{\infty} (-1)^{m+1} \frac{\cos(\alpha m\pi)e^{-m^2\pi^2\tau}}{m^2\pi^2}, \tag{2.41}$$

which is related to the integral of elliptic theta functions integrated over τ.

In order to evaluate $\sigma_2(\tau)$ and $\sigma_3(\tau)$, we need to find the roots s_n numerically with high precision, and perform the sums in Eqs. (2.39) and (2.40). In doing this, we use the bisection method to find the first few thousands of the roots of $\sigma_2(\tau)$ with an accuracy of 10^{-13}. The sums involved in Eqs. (2.39) and (2.40) converge quickly, as s_n's in the term $e^{s^2\tau}$ are purely imaginary numbers. Furthermore, $\lim_{s \to s_n} \cosh(\alpha s)$ and $\lim_{s \to s_n} \sinh(\alpha s)$ lie in $[-1, 1]$ and the magnitude of $\lim_{s \to s_n}((1 + \gamma)\cosh s + s \sinh s)$ tends to ∞ with increasing $\text{Im}(s_n)$. Therefore, unless $\tau \approx 0$, summing over just a few terms provides one with results that are significantly precise.

Using the procedure we described above, one can find expressions for many other time dependent transport quantities. A collection of results is given in Sec. 2.6 of this chapter.

In Fig. 2.7 we show behavior of the dimensionless quantities MSD/L^2 and $D/D(0)$ as a function of τ, where the latter is defined as

$$\frac{D(t)}{D} = \frac{1}{2D}\frac{d}{dt}\text{MSD}(t) = \frac{2}{L^2}\frac{d}{d\tau}\text{MSD}(\tau). \tag{2.42}$$
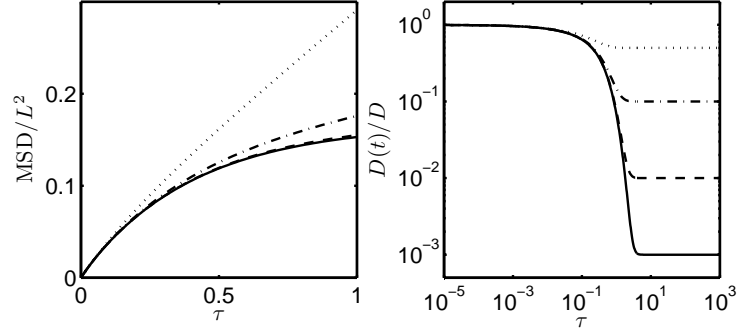
Figure 2.7: The mean square displacement (left) and the diffusion coefficient (right) as a function of dimensionless time τ, normalized by L^2 and D, respectively. Each of the plotted quantities are obtained by averaging over all initial conditions. The solid, dashed, and dash-dotted curves in both plots correspond to D_{eff}/D being equal to 0.001, 0.01, and 0.1.

The quantities plotted in Fig. 2.7 are averaged over initial conditions. In order to demonstrate the effect of initial conditions, we show that half the derivative of the MSD_p in discrete space, which is the time dependent transfer rate given by Eq. (2.19), as a function of time in Fig. 2.8. We chose to display the results for the discrete case because of a couple of reasons. Firstly, as the number of sites in a compartment is finite in this case, we can cover all possible initial states of the system. Secondly, we observed no qualitative difference between considering discrete space and continuum. The results shown in Fig. 2.8 pertain to a chain with 11 sites per compartment. Because of the symmetry in the problem, initial conditions that are merely the mirror images of each other will produce the same results. Therefore, there are 6 different values of p that we need to consider: $p = 0, \pm1, \pm2, \pm3, \pm4$, and ±5. Among these cases, Fig. 2.8 shows $p = 0$, starting at the center of the compartment, $p = \pm4$ and ±5, starting at the site that is 1 site away from the boundary and next to the boundary, respectively. Additionally, we also display the result for averaging over all p within a compartment. Note that except when averaged over the initial conditions, the behavior of $d(\text{MSD})/dt$ is non-monotonic. In order to understand

31

the significance of these features, let us first remember how the time dependent transfer rate, $F(t)$, is defined. $F(t)$ is given by

$$F(t) = \sum_m (m - p)^2 \frac{dP_m}{dt}, \tag{2.43}$$

where $P_m(t)$ obeys the master equation

$$\frac{dP_m}{dt} = F_{\text{left}} (P_{m-1} - P_m) + F_{\text{right}} (P_{m+1} - P_m).$$

Here, F_{left}, F_{right} are the transfer rates of the links to the left and right of the site m, respectively. At very short times only the pth site is occupied so that the only contribution to the $F(t)$ is made by the nonzero terms

$$\left. \frac{dP_{p+1}}{dt} \right|_{t=0} = F_{\text{left}},$$
$$\left. \frac{dP_{p-1}}{dt} \right|_{t=0} = F_{\text{right}},$$

where we used $P_n(0) = \delta_{p,0}$. Note that dP_p/dt is also nonzero, but it is weighed by $(m - p)^2$ which vanishes. According to these equations, we have

$$F(0) = F_{\text{left}} + F_{\text{right}}. \tag{2.44}$$

If p is not next to a compartment boundary, then $F_{\text{left}} = F_{\text{right}} = F$, so that $F(0) = 2F$. However, if p is on the boundary, then F_{left} and F_{right} will have different values with their sum being $(F + f)/2$. Therefore, if the random walker is initially placed at the boundary of a compartment, it will diffuse with the rate $(F + f)$ which is less than F. Fig. 2.8 clearly shows this behavior. Having explained the relation between the $F(0)$ and the initial conditions, we now focus on the other features of $F(t)$. Note that when the random walker starts at the center of the compartment, $F(t)$ goes below its asymptotic value F_{eff} for some time and then rises to reach F_{eff}. This effect can easily be understood by taking another look at Eq. (2.43). As we have seen above, the value of dP_m/dt is lower when m is a site adjacent to a compartment boundary compared to what it is when m is away from the boundaries. Therefore, as the probability of occupation of the sites adjacent to the boundaries increases,

we expect the value of $F(t)$ to decrease. As time goes by, the random walker will cross the boundary and step into an unexplored compartment. This has two consequences: the probability of occupation of the sites that are adjacent to the boundary will decrease while the probability of occupation of the sites that are away from the boundary will increase. As a result, after reaching a minimum, $F(t)$ will start increasing until the probability of finding the random walker around the next barrier becomes significant. As the probability distribution broadens, this effect will be repeatedly observed with rapidly diminishing magnitude, as $F(t)$ reaches its asymptotic value F_{eff}. The non-monotonic behavior of $F(t)$ for all other initial conditions can also be explained in these terms.
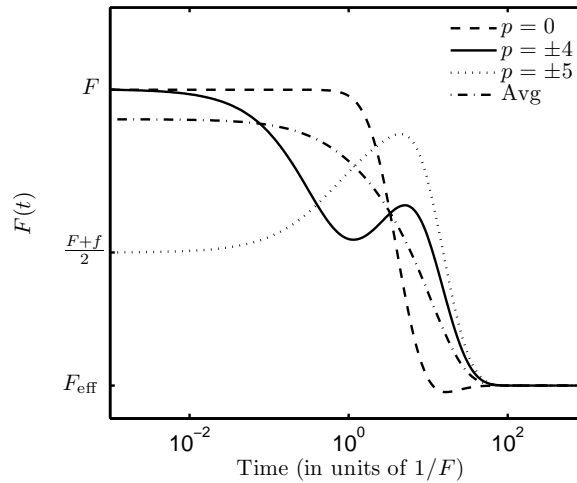
Figure 2.8: Time dependent transfer rate $F(t)$, which can be thought as the analogue of $D(t)$ in discrete space, for different values of the initial condition parameter p. In this case $H = 10$ so that there are 11 sites in each compartment, and $f/F = 0.01$. $p = 0, \pm 4$, and ± 5 correspond to the random walker starting at the center of the compartment, 1 site away from the compartment boundary and next to the boundary, respectively. The dash-dotted line shows $F(t)$ obtained by averaging over all initial placements p. Note that unless one averages over all initial conditions, $F(t)$ evolves non-monotonically while it reaches its asymptotic value F_{eff}.

As a final remark, we will briefly discuss putting $\widetilde{\text{MSD}}_{x_0}(s)$ in an alternative form.

Writing out Eq. (2.30) by expanding $\widetilde{\phi}^c_{x_0}(\epsilon)$, we get

$$\widetilde{\mathrm{MSD}}_{x_0}(s) = \frac{L^4}{8D}\left(\frac{1}{s^4} - \frac{1}{s^3 \cosh s}\Omega(s; x_0, L)\right)$$
$$+ \frac{L^4}{8D}\frac{D_{\mathrm{eff}}}{D - D_{\mathrm{eff}}}\frac{1}{s^3}\frac{\tanh s}{\left(\cosh s + \frac{D_{\mathrm{eff}}}{D - D_{\mathrm{eff}}}\sinh s\right)}\Omega(s; x_0, L), \tag{2.45}$$

where

$$\Omega(s; x_0, L) = \coth s \cosh\left(\frac{2x_0}{L}s\right) - \frac{2x_0}{L}\sinh\left(\frac{2x_0}{L}s\right).$$

Note that when $D_{\mathrm{eff}} = 0$ so that the random walker is completely confined, the second term in Eq. (2.45) vanishes. It is interesting to note that the MSD in the presence of permeable barriers can be written as a sum of the MSD for complete confinement and an additional term. This is reminiscent of a perturbation expansion which is commonly used in tackling many problems in physics. See ref. [38] for an extended discussion. The inverse Laplace transform of the first term in Eq. (2.45) can be taken analytically, to give

$$\mathrm{MSD}^{D_{\mathrm{eff}}=0}_{x_0}(t) = \frac{L^2}{2}\left(\frac{1}{3} - 32\sum_{n=0}^{\infty}\frac{e^{-\frac{\pi^2}{4}(2n+1)^2\left(\frac{4D}{L^2}t\right)}}{\pi^4(2n+1)^4}\right),$$

by using methods similar to those described in detail above.

2.5 Comparison with experiment

In this section, we put the theoretical results obtained so far to use, by showing how they compare against observations of molecules in cell membranes. We consider two different sets of experimentally found MSD versus time data, obtained by using single molecule tracking technique. One of them is shown in Fig. 4b (left) of Suzuki and others [62], and pertains to the motion of a membrane protein. The other data set is about the motion of phospholipids that are much smaller than proteins, obtained by Fujiwara and others and is displayed in Fig. 2b of ref. [57]. Both of the experimental results given in these

references are obtained by single molecule tracking techniques where the molecule of interest is tagged with a colloidal gold particle so that it can be seen. The time resolution in these experiments is $25\mu s$, which is high enough to capture the short time behavior of the diffusion coefficient when the molecules are diffusing freely in a compartment. Note that in this context, by short times we mean t less than the expected value of $L^2/2D$, which is the characteristic time scale in this problem. In order to compare our results with experimental findings, we digitized plots of MSD versus time published in the articles mentioned above.

In each of the following cases, we first extract the x and y components of the MSD from experimental data. Then we separately fit them to the theoretical expression for MSD(t), given by Eq. (2.62) in Sec. 2.6. The parameters we use in the fit are as follows. D: the diffusion coefficient without the presence of compartments, or equivalently, the short time diffusion coefficient, D_{eff}: asymptotic value of the diffusion coefficient which also is the diffusion coefficient one would find if the observations are carried out with a low time resolution, and finally L: the compartment size. Our specific aim is to find out how experimental data compares with the theoretical predictions for typical values of L.

In ref. [62], the authors observed the diffusion of a gold-tagged G-protein coupled μ-opioid receptor in the plasma membrane of normal rat kidney cells. It was found that the motion of this complex is not simply Brownian, as its $D(t)$ is varies greatly over the duration of the observation. After performing the fit in the way we described above, we find that that the linear compartment size L should lie between 250 nm and 470 nm. This range of values for L is compatible with the distribution of compartment sizes given in Fig. 4d of ref. [62] and with other general results in the literature [1]. We would like to emphasize that the data set that was available us to use was for a single trajectory rather than an ensemble average over many. Therefore, it is difficult to either be accurate in the prediction of L, or give statistics about the error involved.

The second set of data we considered consists of the MSD as a function of time of a

phospholipid molecule (1,2-dioleoyl-sn-glycero-3-phosphoethanolamine), again as a single trajectory, and is given in ref. [57]. In this case we plot the theoretical prediction for the MSD against the x and y components of the experimental data. The extreme values of the diffusion coefficient, D and D_{eff} are found by performing a linear fit to the slope of the experimental data at appropriate time intervals. The results are turned out to be the same as those given in ref. [57] without much surprise, and can be found in the caption of Fig. 2.9. In Fig. 2.9 experimental data and three theoretical curves each corresponding to a different value of L, are plotted. The theoretical results correspond to Eq. (2.62) which is the MSD as a function of time, averaged over all initial conditions. We found that the agreement between theory and experiment is remarkably good for $L \approx 230$, which is the value of the average compartment size deduced in ref. [57]. For significantly smaller or larger compartment sizes, the theoretical predictions substantially deviate from the experimental results, as shown in Fig. 2.9.

Since the data correspond to a single trajectory, it can contain information about the initial position of the molecule relative to the compartment boundaries. Motivated by this, $\text{MSD}_{x_0}(t)$ as given by Eq. (2.52) is plotted with the same experimental data in Fig. 2.10, for different values of x_0. The value of L is taken to be 230 nm, and D and D_{eff} is kept the same.

2.6   A summary of useful results

In this section we present a collection of additional expressions for various transport quantities, as functions of time. All of the results presented in this section are derived by going through the procedure for inverting the Laplace transform of $\widetilde{g}_{x_0}(\epsilon)$, as described in full detail in Sec. 2.4.
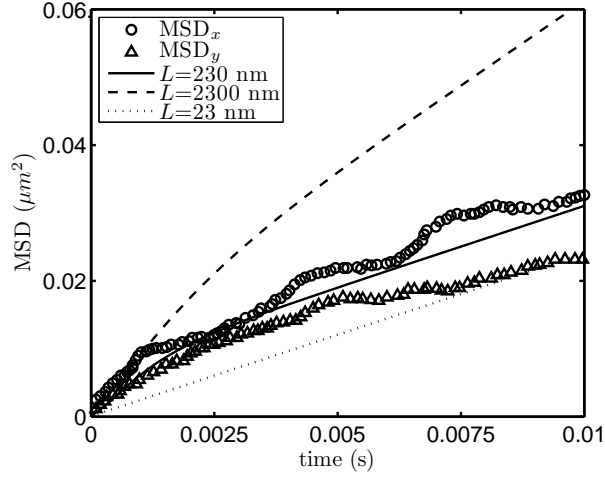
Figure 2.9: Theoretical predictions for different values of the compartment size L versus experimental results concerning the diffusion of phospholipids, reported in ref. [57]. This plot emphasizes that the agreement between theory and experiment is best when L is close to the value deduced in ref. [57], which is $L = 230$ nm. Therefore, the theoretical prediction makes sense, even when it is compared to a single trajectory. Circles and triangles correspond to x and y components of the experimentally obtained MSD versus time data. The parameter values used to plot the theoretical curves are $L = 23$ nm (dotted), $L = 230$ nm (solid), $L = 2300$ nm (dashed), with $D=4.6$ $\mu m^2 s^{-1}$ and $D_{\text{eff}}=1.2$ $\mu m^2 s^{-1}$ the same for all cases. Note that except when $L = 230$ nm, theory and experiment do not agree.

2.6.1 Expressions for MSD and D

$$\text{MSD}_{x_0}(\tau) = \frac{L^2}{2}\Bigg(c_1 + c_2\tau + \sum_{\substack{m=-\infty, \\ m\neq 0}}^{\infty} (-1)^m \frac{\cos(\alpha\pi m)e^{-\pi^2\tau m^2}}{\pi^2 m^2}$$

$$+ \sum_n \lim_{s\to s_n} e^{s^2\tau} \frac{\cosh(\alpha s)}{s^2 \cosh(s)}\left[\frac{\frac{D_{\text{eff}}}{D-D_{\text{eff}}} + \alpha s \tanh(\alpha s)}{\frac{D}{D-D_{\text{eff}}} + s \tanh(s)}\right]\Bigg) \qquad (2.46)$$

where

$$c_1 = \frac{1}{\gamma + 1}\left(\frac{1}{6} + \frac{\alpha^2}{2} - \frac{\gamma}{3(\gamma+1)}\right) = \left(1 - \frac{D_{\text{eff}}}{D}\right)\left(\frac{1}{6} + \frac{\alpha^2}{2} - \frac{1}{3}\frac{D_{\text{eff}}}{D}\right)$$

$$c_2 = \frac{\gamma}{\gamma+1} = \frac{D_{\text{eff}}}{D}, \qquad\qquad\qquad\qquad\qquad\qquad\qquad\qquad (2.47)$$
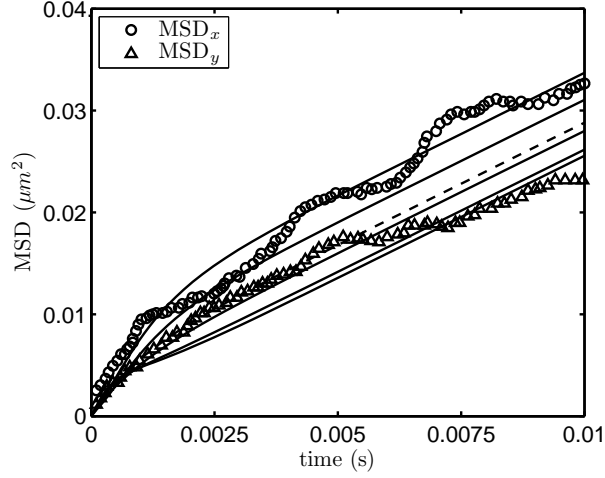
Figure 2.10: Comparison of theoretical predictions given by Eq. (2.52) with experimental data in ref. [57], for various initial conditions x_0. For the solid lines representing the theory, the initial position is: $x_0=0$, $L/8$, $L/4$, $3L/8$ and $7L/16$, from top to bottom. Again, the circles and triangles correspond to experimental data. Parameter values are the same as those in Fig. 2.9 except that here, L has the fixed value 230 nm.

γ, τ, and α are defined by Eq. (2.36), and s_n represents the solutions of $s = -\gamma \tanh(s)$ other than $s = 0$. For convenience, we make the following definition:

$$\Omega_1(D_{\text{eff}}/D) = \sum_n \lim_{s \to s_n} e^{s^2 \tau} \frac{\cosh(\alpha s)}{s^2 \cosh(s)} \left[\frac{\frac{D_{\text{eff}}}{D - D_{\text{eff}}} + \alpha s \tanh(\alpha s)}{\frac{D}{D - D_{\text{eff}}} + s \tanh(s)} \right] \tag{2.48}$$

When $D_{\text{eff}} = D$, $s_n = in\pi$, $n = \pm 1, \pm 2, \pm 3...$ and

$$\Omega_1(1) = \sum_{\substack{m=-\infty, \\ m \neq 0}}^{\infty} (-1)^m \frac{\cos(\alpha \pi m) e^{-\pi^2 m^2 \tau}}{\pi^2 m^2} \tag{2.49}$$

so that the MSD becomes

$$\text{MSD}_{x_0}^{D_{\text{eff}}=D}(\tau) = \frac{L^2}{2}\tau, \tag{2.50}$$

as expected. In complete confinement, $D_{\text{eff}} = 0$, $s_n = i(2n + 1)\pi/2$, $n = 0, \pm 1, \pm 2, \pm 3...$ and we have

$$\Omega_1(0) = 4\alpha/\pi^2 \sum_{m=-\infty}^{\infty} (-1)^{m+1} \frac{\sin((2m + 1)\alpha\pi/2) e^{-\pi^2(2m+1)^2/4\tau}}{(2m + 1)^2}, \tag{2.51}$$

38

giving,

$$\text{MSD}_{x_0}^{D_{\text{eff}}=0}(\tau) = \frac{L^2}{2}\left(\frac{1+3\alpha^2}{6} + \sum_{\substack{m=-\infty,\\m\neq0}}^{\infty}(-1)^m\frac{\cos(\alpha\pi m)e^{-\pi^2\tau m^2}}{\pi^2 m^2}\right.$$

$$\left. + \alpha\sum_{m=-\infty}^{\infty}\frac{(-1)^{m+1}\sin\left((2m+1)\frac{\alpha\pi}{2}\right)e^{-(2m+1)^2\frac{\pi^2}{4}\tau}}{(2m+1)^2\frac{\pi^2}{4}}\right). \tag{2.52}$$

Similarly, we can write expressions for the dimensionless diffusion coefficient

$$\frac{D_{x_0}(\tau)}{D} = \frac{2}{L^2}\frac{d}{d\tau}\text{MSD}_{x_0}(\tau). \tag{2.53}$$

For arbitrary D_{eff}/D we have

$$\frac{D_{x_0}(\tau)}{D} = c_2 - \sum_{\substack{m=-\infty,\\m\neq0}}^{\infty}(-1)^m\cos(\alpha\pi m)e^{-\pi^2\tau m^2}$$

$$+ \sum_n \lim_{s\to s_n}e^{s^2\tau}\frac{\cosh(\alpha s)}{\cosh(s)}\left[\frac{\frac{D_{\text{eff}}}{D-D_{\text{eff}}}+\alpha s\tanh(\alpha s)}{\frac{D}{D-D_{\text{eff}}}+s\tanh(s)}\right], \tag{2.54}$$

The first sum in the expression above can be expressed in terms of Jacobi Theta Functions:

$$\sum_{\substack{m=-\infty,\\m\neq0}}^{\infty}(-1)^m\cos(\alpha\pi m)e^{-\pi^2\tau m^2} = \vartheta_4\left(\frac{\alpha\pi}{2}\bigg|i\pi\tau\right) - 1 \tag{2.55}$$

where $\vartheta_4(u|\tau')$ is the Theta function of the fourth kind as given in Eq. (8.180.1) of ref. [63], so that we can write

$$\frac{D_{x_0}(\tau)}{D} = \left(\frac{D_{\text{eff}}}{D}+1\right) - \vartheta_4\left(\frac{\alpha\pi}{2}\bigg|i\pi\tau\right) + \sum_n\lim_{s\to s_n}e^{s^2\tau}\frac{\cosh(\alpha s)}{\cosh(s)}\left[\frac{\frac{D_{\text{eff}}}{D-D_{\text{eff}}}+\alpha s\tanh(\alpha s)}{\frac{D}{D-D_{\text{eff}}}+s\tanh(s)}\right]. \tag{2.56}$$

Let us define

$$\Omega_2(D_{\text{eff}}/D) = \sum_n\lim_{s\to s_n}e^{s^2\tau}\frac{\cosh(\alpha s)}{\cosh(s)}\left[\frac{\frac{D_{\text{eff}}}{D-D_{\text{eff}}}+\alpha s\tanh(\alpha s)}{\frac{D}{D-D_{\text{eff}}}+s\tanh(s)}\right] \tag{2.57}$$

For $D_{\text{eff}} = D$, $s_n = in\pi$, $n = \pm1,\pm2,\pm3...$ and $\Omega_2(1) = \vartheta_4\left(\frac{\alpha\pi}{2}\big|i\pi\tau\right) - 1$ so that:

$$\left(\frac{D_{x_0}(\tau)}{D}\right)_{D_{\text{eff}}=D} = 1. \tag{2.58}$$

For $D_{\text{eff}} = 0$, $s_n = i(2n + 1)\pi/2$, $n = 0, \pm1, \pm2, \pm3...$ and $\Omega_2(0) = \alpha\vartheta_1\left(\frac{\alpha\pi}{2}\Big|i\pi\tau\right)$ where $\vartheta_1(u|\tau')$ is the Theta function of the first kind as given in Eq. (8.180.2) of ref. [63]. Therefore, we have

$$\left(\frac{D_{x_0}(\tau)}{D}\right)_{D_{\text{eff}}=0} = 1 - \vartheta_4\left(\frac{\alpha\pi}{2}\Big|i\pi\tau\right) + \alpha\vartheta_1\left(\frac{\alpha\pi}{2}\Big|i\pi\tau\right). \tag{2.59}$$

2.6.2 Quantities that are averaged over initial conditions

In this section we consider the $\text{MSD}_{x_0}(\tau)$ and $D_{x_0}(\tau)$ that are averaged over all initial conditions such that

$$\text{MSD}(\tau) = \frac{1}{2}\int_{-1}^{1} d\alpha \text{MSD}_{x_0}(\tau), \tag{2.60}$$

and

$$\frac{D(\tau)}{D} = \frac{1}{2}\int_{-1}^{1} d\alpha\frac{D_{x_0}(\tau)}{D}. \tag{2.61}$$

Therefore, we have

$$\text{MSD}(\tau) = \frac{L^2}{2}\left(c_1' + c_2\tau + \sum_n \lim_{s\to s_n}\frac{e^{s^2\tau}}{s^3}\left[\frac{s + \left(\frac{D_{\text{eff}}}{D-D_{\text{eff}}} - 1\right)\tanh(s)}{\frac{D}{D-D_{\text{eff}}} + s\tanh(s)}\right]\right), \tag{2.62}$$

where $c_1' = \frac{1}{3}\left(1 - \frac{D_{\text{eff}}}{D}\right)^2$. For $D_{\text{eff}} = 0$,

$$\text{MSD}_{x_0}^{D_{\text{eff}}=0}(t) = \frac{L^2}{2}\left[\frac{1}{3} - 32\sum_{n=0}^{\infty}\frac{e^{-\frac{\pi^2}{4}(2n+1)^2\left(\frac{4D}{L^2}t\right)}}{\pi^4(2n + 1)^4}\right], \tag{2.63}$$

Similarly, for $D(\tau)/D$

$$\frac{D(\tau)}{D} = \frac{D_{\text{eff}}}{D} + \sum_n \lim_{s\to s_n}\frac{e^{s^2\tau}}{s}\left[\frac{s + \left(\frac{D_{\text{eff}}}{D-D_{\text{eff}}} - 1\right)\tanh(s)}{\frac{D}{D-D_{\text{eff}}} + s\tanh(s)}\right] \tag{2.64}$$

and when $D_{\text{eff}} = 0$

$$\left(\frac{D(\tau)}{D}\right)_{D_{\text{eff}}=0} = \sum_{m=-\infty}^{\infty}\frac{e^{-(2m+1)^2\frac{\pi^2}{4}\tau}}{\frac{(2m+1)^2\pi^2}{4}}. \tag{2.65}$$

2.6.3 Expression for the memory

As we stated in several occasions, the MSD and D can also be expressed as integrals of a memory function $\phi(t)$.

$$\text{MSD}(t) = 2D \int_0^t ds \int_0^s ds' \phi(s')$$

$$\phi(t) = \frac{d}{dt}\left(\frac{D(t)}{D}\right). \tag{2.66}$$

Using the expressions we gave above, the memory can be written as

$$\phi(\tau) = -\frac{d}{d\tau}\left[\vartheta_4\left(\frac{\alpha\pi}{2}\bigg|i\pi\tau\right)\right] + \sum_n \lim_{s\to s_n} s^2 e^{s^2\tau} \frac{\cosh(\alpha s)}{\cosh(s)} \left[\frac{\frac{D_{\text{eff}}}{D-D_{\text{eff}}} + \alpha s \tanh(\alpha s)}{\frac{D}{D-D_{\text{eff}}} + s \tanh(s)}\right] \tag{2.67}$$

2.7 Effects of disorder

The mathematical model we presented so far describes an ideal membrane in which all compartment boundaries have the same properties and the compartment size is uniform. In naturally occurring membranes, barrier heights associated with each boundary and compartment sizes tend to vary, as shown by the electron microscopy images of the cell surface obtained by Morone and others [58]. Hence, we think it is important to extend our mathematical model to take into account the effects of disorder in barrier heights and compartment sizes.

In this section, we present a generalization of our model by employing an effective medium theory. Most of the discussions and results presented here have also been published in the work of Kalay, Parris, and Kenkre [39]. Effective medium theories (or effective medium approximations) have been successfully used to calculate ensemble averaged quantities in many disordered systems. For a review on this subject and an extensive list of references see Chapter 3 of this thesis. Here we will state the results that are obtained by using an effective medium theory without much detail, as an extensive discussion is given in Chapter 3.
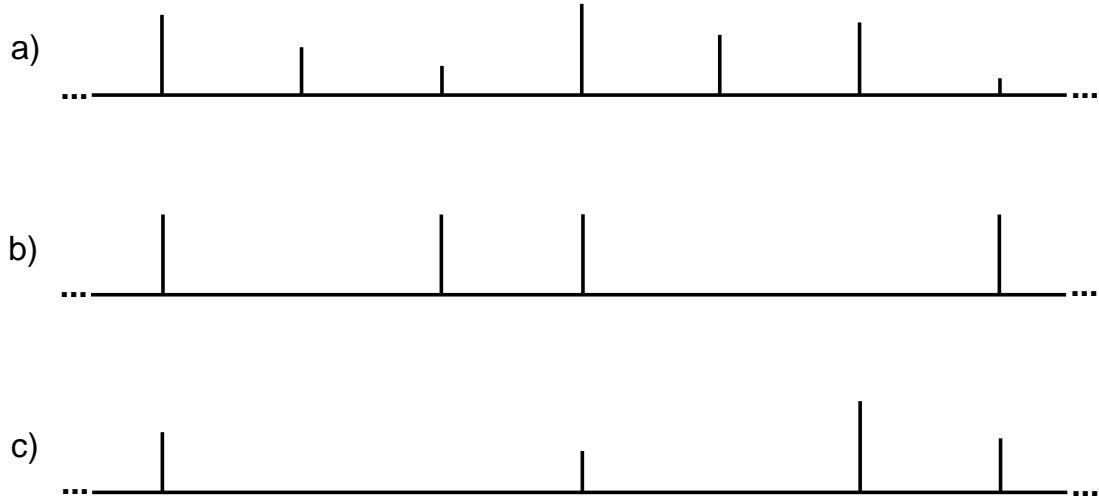
Figure 2.11: Illustration of different types of disorder we would like to incorporate in our mathematical model presented in the previous section. Case a, b, and c correspond to disorder in barrier heights, in barrier locations and both in barrier height and locations.

First, we will consider the situation in which the compartment sizes are uniform, but the barrier heights are taken to be random variables. We will generalize the model first in the discrete space, and then take the continuum limit in exactly the same way as in the previous sections. In this case, the analogue of Eq. (2.2) is

$$\frac{dP_m}{dt} = F\left[P_{m+1} + P_{m-1} - 2P_m\right] - \sum_r{}^{'} (F - f_r)\left[P_{r+1} - P_r\right]\left(\delta_{m,r} - \delta_{m,r+1}\right), \qquad (2.68)$$

where f_r stands for the transfer rate of the barrier to the right of the rth site. We suppose that f_r's are independently distributed random variables, each drawn from a probability distribution $\rho(f)$. In principle Eq. (2.68) can be solved for a particular realization of the f_r's by means of diagonalizing matrices. However, this is a cumbersome task that is impractical, especially for large systems. Our aim is to calculate transport quantities that are averaged over the disorder, which we will do with the help of an effective medium approximation.

In our context, the essence of the effective medium theory is transforming a Master equation with disordered transfer rates to a generalized master equation with translation-

ally invariant transfer rates. Therefore, the disorder in space is effectively replaced by nonlocal time evolution that is characterized by the memory of the generalized master equation. In Eq. (2.68), the only transfer rates that are random variables are those that connect the sites around each barrier. Hence, making the effective medium approximation will correspond to modifying Eq. (2.68) around each barrier, which results in

$$\frac{dP_m(t)}{dt} = F\left[P_{m+1}(t) + P_{m-1}(t) - 2P_m(t)\right]$$

$$- \int_0^t dt'\left[F\delta(t-t') - \mathcal{F}(t-t')\right]\sum_r{}'\left[P_{r+1}(t') - P_r(t')\right](\delta_{m,r} - \delta_{m,r+1}), \quad (2.69)$$

where $\mathcal{F}(t)$ is the memory of this generalized master equation around each barrier. We then proceed to solve for $\mathcal{F}(t)$, or its relevant limiting values, using our knowledge of the disorder characterized by $\rho(f)$. The Laplace transform of the probability propagator for Eq. (2.69) is given by

$$\widetilde{\chi}_{m,n} = \widetilde{\psi}_{m-n} - \frac{F - \widetilde{\mathcal{F}}}{1 + (F - \widetilde{\mathcal{F}})\widetilde{\mu}}\sum_r{}'(\widetilde{\psi}_{r-n+1} - \widetilde{\psi}_{r-n})(\widetilde{\psi}_{m-r} - \widetilde{\psi}_{m-r-1}), \quad (2.70)$$

which is simply Eq. (2.11) with $P_m(0) = \delta_{n,0}$ and $f \to \mathcal{F}$. In order to find $\widetilde{\mathcal{F}}$, we will impose a self consistency condition, whose details are explained in Chapter 3. Suppose that we replace the link between the sites s and $s + 1$, where s is a site to the left of one of the barriers, by one with transfer rate f. Then the propagator for this modified chain becomes

$$\widetilde{\chi}_{m,n} + \frac{(f - \widetilde{\mathcal{F}})}{1 + (f - \widetilde{\mathcal{F}})\widetilde{\beta}}(\widetilde{\chi}_{m,s} - \widetilde{\chi}_{m,s+1})(\widetilde{\chi}_{s+1,n} - \widetilde{\chi}_{s,n}), \quad (2.71)$$

where

$$\widetilde{\beta} = -\widetilde{\chi}_{s+1,s} + \widetilde{\chi}_{s+1,s+1} + \widetilde{\chi}_{s,s} - \widetilde{\chi}_{s,s+1}.$$

As f is supposed to be distributed according to $\rho(f)$, if we average Eq. (2.71) over all values of f weighted by $\rho(f)$, it should reduce to the propagator given in Eq. (2.70) regardless of the values of m and s. That is to say,

$$\int df \rho(f)\frac{f - \widetilde{\mathcal{F}}}{1 + (f - \widetilde{\mathcal{F}})\widetilde{\beta}} = 0. \quad (2.72)$$

This is what we referred to as the self consistency condition. Solving Eq. (2.72) for $\widetilde{\mathcal{F}}$ can be cumbersome in general. However, we will be interested in solving for the integral of $\mathcal{F}$ over all times, for which the expressions simplify substantially.

Note that the integral of $\mathcal{F}$ from 0 to ∞ will be the effective transfer rate of a barrier, defined by

$$f_{\text{eff}} = \int_0^\infty ds \mathcal{F}(s) = \widetilde{\mathcal{F}}(0).$$

This can be seen from Eq. (2.19) with $\mathcal{F}(t)$ being the memory $\phi(t)$. This means that, if we are interested in the value of observables at asymptotically large times, each barrier will act like it has the effective transfer rate f_{eff}. The quantity $\widetilde{\mathcal{F}}(0)$ can be easily calculated from Eq. (2.72),

$$\frac{1}{f_{\text{eff}}} = \frac{1}{\widetilde{\mathcal{F}}(0)} = \int df \frac{\rho(f)}{f},$$

where we used

$$\lim_{\epsilon \to 0} \widetilde{\beta}(\epsilon) = \frac{1}{\widetilde{\mathcal{F}}(0)}.$$

Substituting f_{eff} for f in Eq. (2.20), we get the effective hopping rate as a function of the distribution $\rho(f)$

$$F_{\text{eff}} = \frac{\frac{H+1}{H}}{\frac{1}{F} + \frac{1}{H} \int df \frac{\rho(f)}{f}}. \tag{2.73}$$

Eq. (2.73) is the main result of this section as it provides us with a relation between the effective transfer rate and the properties of the disorder. In continuum, Eq. (2.73) becomes the effective diffusion coefficient,

$$\lim_{a \to 0} F_{\text{eff}} a^2 = D_{\text{eff}} = \frac{D}{1 + \frac{D}{L} \int d\mathcal{D}_f \frac{\rho(\mathcal{D}_f)}{\mathcal{D}_f}}, \tag{2.74}$$

$$\mathcal{D}_f = \lim_{a \to 0} f a, \tag{2.75}$$

where we used Eqs. (2.21) and (2.24). In the next subsection, we will give results corresponding to a few different choices for $\rho(f)$.

2.7.1 Results for specific cases

We will begin with considering one of simplest choices for $\rho(f)$ which is the sum of two δ-distributions

$$\rho(f) = \alpha\delta(f - f_1) + (1 - \alpha)\delta(f - f_2). \tag{2.76}$$

Substituting this in Eq. (2.73), we get

$$F_{\text{eff}} = \frac{H + 1}{\frac{H}{F} + \frac{(1-\alpha)f_1 + \alpha f_2}{f_1 f_2}}.$$

Note that if either f_1 or f_2 is zero, F_{eff} vanishes. This makes sense, because when there is a possibility of having impenetrable barriers, the random walker will be confined and its diffusion coefficient will eventually vanish.

In this simple case, it is possible to solve for the memory $\widetilde{\mathcal{F}}(\epsilon)$ for all values of ϵ, exactly. For a general $\rho(f)$, Eq. (2.72) can be put in the following form

$$\frac{1}{\Gamma} = \int df \frac{\rho(f)}{f + (\Gamma - \widetilde{\mathcal{F}})}, \tag{2.77}$$

where

$$\Gamma = -\frac{(1 + \widetilde{\mu}F) - \widetilde{\mathcal{F}}\widetilde{\mu}}{\zeta + \theta((1 + \widetilde{\mu}F) - \widetilde{\mathcal{F}}\widetilde{\mu})},$$

and

$$\theta = \frac{\coth(\xi/2) - 1}{F} - \zeta,$$

$$\zeta = \frac{1}{\widetilde{\mu}F^2}(1 - 2\coth(\xi/2) + \coth^2(\xi/2)\coth\xi(H + 1)).$$

In arriving Eq. (2.77), we made use of the following expression for $\widetilde{\beta}$ in terms of the propagators $\widetilde{\psi}_0$ and $\widetilde{\psi}_1$

$$\widetilde{\beta} = 2(\widetilde{\psi}_1 - \widetilde{\psi}_0) - \frac{f - \widetilde{\mathcal{F}}}{F^2(1 + (f - \widetilde{\mathcal{F}})\widetilde{\mu})}\left(1 - 2\epsilon\widetilde{\psi}_0 + \epsilon^2\sum_r' \widetilde{\psi}_{s-r}^2\right),$$

where

$$\sum_r{}' \widetilde{\psi}_{s-r}^2 = \frac{\coth \xi (H+1)}{4F^2 \sinh^2 \xi}.$$

Setting $\rho(f)$ in Eq. (2.77) equal to the sum of two δ-distributions as given in Eq. (2.76) and doing some algebra, we obtain a cubic equation for $\widetilde{\mathcal{F}}$

$$\widetilde{\mathcal{F}}^3 + b\widetilde{\mathcal{F}}^2 + c\widetilde{\mathcal{F}} + d = 0, \tag{2.78}$$

where

$$b = -(f_1 + f_2 - 1/\theta) - \eta/\theta\widetilde{\mu},$$

$$c = f_1 f_2 - [\widetilde{\mu}(f_2 + \alpha(f_1 - f_2)) + (1 + \widetilde{\mu}F) - \eta(f_1 + f_2)]/\theta\widetilde{\mu},$$

$$d = [\eta f_1 f_2 - (f_2 + \alpha(f_1 - f_2))(1 + \widetilde{\mu}F)]/\theta\widetilde{\mu},$$

$$\eta = \zeta + \theta(1 + \widetilde{\mu}F).$$

Using the well known cubic formula, Eq. (2.78) can be solved for $\widetilde{\mathcal{F}}$ as a function of ϵ. The physically relevant solution is displayed in Fig. 2.12 for a particular choice of f_1, f_2, H, and α given in the figure caption. Note that $\widetilde{\mathcal{F}}$ has the following limiting properties

$$\lim_{\epsilon \to 0} \widetilde{\mathcal{F}} = \frac{f_1 f_2}{(1-\alpha)f_1 + \alpha f_2}, \tag{2.79}$$

$$\lim_{\epsilon \to \infty} \widetilde{\mathcal{F}} = \alpha f_1 + (1-\alpha)f_2. \tag{2.80}$$

In the rest of this subsection, we will consider three different distributions $\rho(f)$, or $\rho(\mathscr{D}_f)$ in continuum, and calculate the corresponding effective diffusion coefficient. The first of these distributions is what we will call a uniform distribution, which is equal to a constant in an interval $[l, u]$ and zero elsewhere, the second is a Rayleigh distribution, and the last is a Rice distribution. For each of these cases, we will present the results in the continuum limit, as we are interested in quantities that pertain to molecules diffusing in continuum.
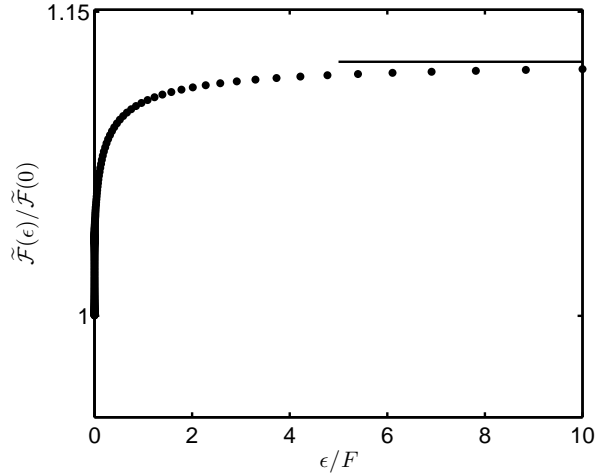
Figure 2.12: The memory function $\widetilde{\mathcal{F}}(\epsilon)$, which satisfies Eq. (2.78), normalized to its initial value as a function of ϵ. Here ϵ is taken to be a real although it is a complex number by definition. Sometimes the inverse Laplace transform of a function can be taken by evaluating it only at real values of the Laplace variable. See Chapter 3 for an example. The $\rho(f)$ that gives rise to this memory function is a sum of δ-distributions: $\rho(f) = \alpha\delta(f - f_1) + (1 - \alpha)\delta(f - f_2)$ where $f_1 = 0.1F$, $f_2 = 0.2F$, $\alpha = 0.5$, and the compartment size, $H + 1$, is equal to 11. The solid horizontal line corresponds to the asymptotic value of $\widetilde{\mathcal{F}}(\epsilon)/\widetilde{\mathcal{F}}(0)$, which is given by the ratio of Eq. (2.80) to Eq. (2.79).

Uniform distribution

In this case, $\rho(\mathscr{D}_f)$ is defined by

$$
\rho(\mathscr{D}_f) = \begin{cases} \frac{1}{u-l} & l < \mathscr{D}_f < u \\ 0 & \text{otherwise} \end{cases}
$$

Then, Eq. (2.75) gives

$$
\frac{D_{\text{eff}}}{D} = \left[1 + \frac{D\ln(u/l)}{L(u-l)}\right]^{-1}. \tag{2.81}
$$

Note that $\mathscr{D}_f$ has the dimensions of [length][time]$^{-1}$ and if $l = u = D/L$, then $D_{\text{eff}} = D$.

Rayleigh distribution

The Rayleigh distribution is a biased Gaussian distribution, defined in the following way

$$\rho(\mathcal{D}_f) = \frac{\mathcal{D}_f e^{-\mathcal{D}_f^2/2\sigma^2}}{\sigma^2},$$

and its the mean and variance are given by $\sigma \sqrt{\pi/2}$, $\sigma^2 \left(\frac{4-\pi}{2}\right)$ respectively. Note that $\rho(\mathcal{D}_f)$ vanishes identically at $\mathcal{D}_f = 0$. Substituting the Rayleigh distribution in Eq. (2.75), we get

$$\frac{D_{\text{eff}}}{D} = \left[1 + \frac{D \sqrt{\pi/2}}{L\sigma} \right]^{-1}. \tag{2.82}$$

Rice distribution

Lastly, we will consider a distribution which is referred to as the Rice distribution,

$$\rho(\mathcal{D}_f) = \frac{\mathcal{D}_f}{\sigma^2} e^{-\frac{(\mathcal{D}_f^2 + v^2)}{2\sigma^2}} I_0 \left(\mathcal{D}_f \frac{v}{\sigma^2} \right).$$

The main reasons for choosing this distribution is that unlike the Rayleigh distribution, the value at which it peaks does not depend on its variance, and it vanishes identically at $\mathcal{D}_f = 0$. It has two parameters, σ and v that determine its mean

$$\sigma \sqrt{\pi/2} L_{1/2} \left(-v^2/2\sigma^2 \right),$$

and variance

$$\sigma^2 + v^2 - \pi\sigma^2/2 L_{1/2}^2 \left(-v^2/2\sigma^2 \right),$$

where

$$L_{1/2}(x) = e^{x/2} \left[(1-x)I_0(-x/2) - x I_1(-x/2) \right]$$

is the Laguerre Polynomial of fractional order and $I_m(x)$ are modified Bessel Functions of the first kind. For this case D_{eff}/D becomes

$$\frac{D_{\text{eff}}}{D} = \left[1 + \frac{D \sqrt{\pi/2}}{L\sigma} e^{-v^2/4\sigma^2} I_0(v^2/4\sigma^2) \right]^{-1}. \tag{2.83}$$

In Fig. 2.13, we display plots of Rayleigh and Rice distributions for various parameter values. Note that although the Rice distribution is asymmetric in $\mathscr{D}_f$, it can be made substantially symmetric by choosing its parameters appropriately.

As pointed out in ref. [39], the effective diffusion constant depends on the ratio of D to the product of L and a value of $\mathscr{D}_f$ that depends on the particular distribution $\rho\left(\mathscr{D}_f\right)$.
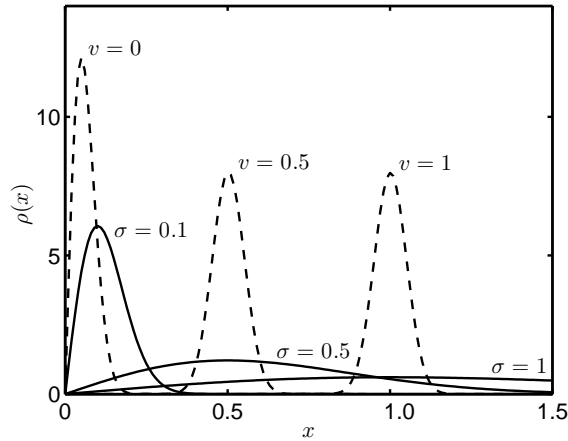
Figure 2.13: Rayleigh(solid) and Rice(dashed) distributions as a function of $x = \mathscr{D}_f$. For the Rice distribution, σ=0.05 in all cases. All of these distributions satisfy the normalization condition $\int_0^\infty dx \rho(x) = 1$.

2.7.2 Treatment of a case with disorder in compartment size

So far we gave results for the diffusion coefficient in the presence of equally sized compartments with either homogeneous or varying barrier heights. As we stated earlier, one of our aims is to generalize our mathematical model to include disorder also in compartment sizes. In this subsection, we describe how to achieve this in a particular way by taking advantage of the results that are already given.

Treating the compartment sizes, or equivalently the barrier locations, as random variables turns out to be a little bit more complicated than doing the same with barrier heights.

In the previous subsection, we saw that one can choose any probability distribution $\rho(\mathcal{D}_f)$ for the distribution of barrier heights and easily calculate D_{eff}. An important point that we did not emphasize in that situation is that the random variables that correspond to barrier heights were uncorrelated. When one uses an effective medium theory, the random variables being uncorrelated makes the problem much easier to solve. See the last section of chapter 3 for a detailed discussion on this. If the compartment size is distributed according to the probability distribution $P(q)$, then the locations of the barriers will mostly likely be correlated random variables. Therefore, in this case it is not so simple to obtain a relation between D_{eff} and $P(q)$ because of the difficulties involved in solving the problem with correlated random variables. Below, we will present a way of going around this difficulty by choosing the barrier locations to be uncorrelated random variables to begin with, and then calculating the corresponding compartment size distribution $P(q)$. This way we will be able to use the results we already obtained to treat a particular kind of disorder in compartment sizes. The shortcoming of this method is that the form of $P(q)$ obtained in this way is very restricted.

Consider the following distribution for barrier heights

$$\rho(f) = \alpha\delta(f - g) + (1 - \alpha)\delta(f - F). \tag{2.84}$$

This means that the transfer rate across a barrier is either g or F with corresponding probabilities α and $1 - \alpha$. Choosing the distribution of barrier heights in this way corresponds to starting with a chain that has periodic barriers of the same height g, as in ref. [38], and removing each barrier with probability $1 - \alpha$. Note that a barrier with transfer rate F acts just like another link within one compartment. Therefore, some of the compartments are now merged as the barrier between them is removed. The chain obtained in this way will have compartment sizes that are always in multiples of $(H + 1)a$, as compartments of different size will arise as a result of merging events. Here a is the lattice spacing as before. Our next task is to find the distribution of compartment size, which is a random variable whose statistics depend on the probability α in Eq. (2.84). Below we will show

how this can be done by using some simple arguments.

We start with considering N points in a discreet linear space. Each point is assigned a number s_i which is either 1 or 0. The points in this space will correspond to links that were barriers in our original problem. A point i with $s_i = 1$ and 0 will represent a barrier with transfer rate F and g, respectively. Hence points with $s_i = 1$ indicate that the compartments that the ith barrier was separating is now merged. According to Eq. (2.84), 0's will occur with probability α and 1's with $1 - \alpha$. We let σ be the number of elements in a contiguous sequence of 1's such that the distance between two consecutive barriers is given by $(\sigma + 1)(H + 1)a$. Note that $\sigma = 0$ corresponds to the distance between two consecutive barriers taking on its minimum value $(H+1)a$. In the light of these arguments, we find

$$\mathcal{N}(\sigma) = \delta_{\sigma,0} \sum_{j=1}^{N-1} (1 - s_j)(1 - s_{j+1})$$

$$+ (1 - \delta_{\sigma,0}) \sum_{j=1}^{N-\sigma-1} (1 - s_j) \left(\prod_{i=0}^{\sigma-1} s_{j+i+1} \right)(1 - s_{j+\sigma+1}), \tag{2.85}$$

where $\mathcal{N}(\sigma)$ is the number distribution of σ in a particular realization of the chain, i.e. for a specific choice of each of the s_i's. The first and second terms in Eq. (2.85) correspond to the number of occurrence of compartments of sizes $(H + 1)a$ and $(\sigma + 1)(H + 1)a$ respectively. As we take s_i's to be uncorrelated random variables, we can write:

$$\langle s_i \rangle = 1 - \alpha,$$

where the angular brackets mean an ensemble average over all realizations of s_i's. The ensemble averaged number distribution is given by

$$\langle \mathcal{N}(\sigma) \rangle = (N - \sigma - 1)\alpha^2(1 - \alpha)^\sigma, \tag{2.86}$$

and therefore the probability distribution for σ is equal to the ratio

$$\langle P(\sigma) \rangle = \frac{\langle \mathcal{N}(\sigma) \rangle}{\sum_{\sigma=0}^{N-1} \langle \mathcal{N}(\sigma) \rangle}.$$

As we are interested in infinite chains, we take the limit $N \to \infty$ and the probability distribution for σ becomes

$$\langle P_{N \to \infty}(\sigma) \rangle = \alpha(1-\alpha)^{\sigma}. \tag{2.87}$$

As σ is proportional to the size of a compartment, the ensemble averaged compartment size distribution is given by

$$P(q, \alpha) = \alpha(1-\alpha)^{\frac{q}{H+1}-1},$$

where $q = (\sigma + 1)(H + 1)$ is the dimensionless compartment size. The mean and variance of $P(\sigma, \alpha)$ are

$$\overline{q} = \frac{H+1}{\alpha}, \tag{2.88}$$

$$(\Delta q)^2 = \overline{(q^2)} - \overline{(q)}^2 = (H+1)^2 \frac{1-\alpha}{\alpha^2}. \tag{2.89}$$
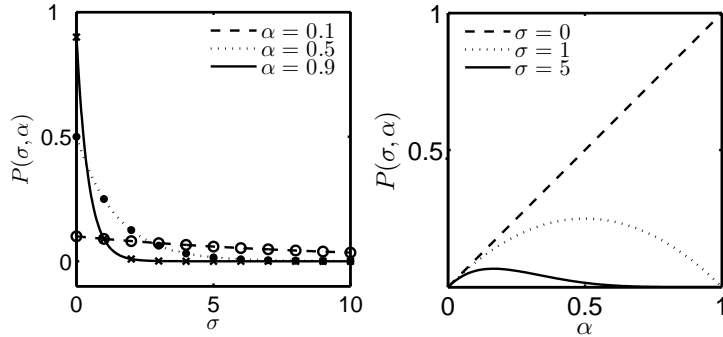
Figure 2.14: The distribution of compartment sizes, $P(\sigma, \alpha)$, as a function of σ (left) and α (right). By definition, σ is an integer, however the curves plotted in the left are for illustrtive purposes and obtained from Eq. (2.7.2) by treating σ as a continuous variable.

Fig. 2.14 shows a plots of the compartment size distribution as a function of σ and α. Note that $P(\sigma, \alpha)$ has a maximum at $\sigma = 0$, and decreases exponentially with σ, as shown on the plot on the left. This is a consequence of s_i's being uncorrelated. In order to

obtain more general $P(\sigma, \alpha)$ that peak at a nonvanishing value of σ, one needs to introduce correlations between the s_i's. The plot on the right shows $P(\sigma, \alpha)$ as a function of α. The values $\alpha = 0$ and 1 correspond to no barriers and periodically placed barriers (with period $H + 1$), respectively.

Now we are in a position to give an expression for F_{eff} and D_{eff}, for the particular case of nonuniformity in compartment sizes described above. Substituting Eq. (2.84) in Eq. (2.73), we obtain

$$F_{\text{eff}} = \frac{\overline{q}}{1/f + (\overline{q} - 1)/F}, \tag{2.90}$$

where $\overline{q}$ is defined in Eq. (2.88), f and F are the transfer rate across a barrier and within a compartment, respectively. Taking the continuum limit of Eq. (2.90) gives the effective diffusion coefficient

$$\frac{D_{\text{eff}}}{D} = \left[1 + \frac{D}{Q\mathscr{D}_f} \right]^{-1}, \tag{2.91}$$

where $Q = \overline{q}a$ is the mean compartment size in continuum.

It is possible to extend this result for cases in which both the barrier heights and compartment sizes are independently distributed random variables. Consider the distribution

$$\rho(f) = (1 - \alpha)\delta(f - F) + \eta(f, \alpha), \tag{2.92}$$

where $\eta(f, \alpha)$ is a distribution normalized to α, and $\eta(0, \alpha) = 0$. Based on the discussions above, using the distribution in Eq. (2.92) corresponds to starting with a chain that has periodically placed barriers, removing a fraction $(1 - \alpha)$ of them and sampling the transfer rates of the rest of them from the distribution $\eta(f, \alpha)$. It is worthwhile to note that the statistics of compartment size distribution do not change even if the barrier heights are not the same, provided that the random variables involved are uncorrelated. Hence, F_{eff} and its continuum limit D_{eff} are given by

$$F_{\text{eff}} = \frac{\frac{H+1}{H}}{\frac{1}{F}\left(\frac{H+1-\alpha}{H}\right) + \frac{1}{H}\int df \frac{\eta(f,\alpha)}{f}}, \tag{2.93}$$

and

$$\frac{D_{\text{eff}}}{D} = \left[1 + \frac{D}{L}\int d\mathscr{D}_f \frac{\eta(\mathscr{D}_f, \alpha)}{\mathscr{D}_f}\right]^{-1}. \tag{2.94}$$

The distribution $\eta(\mathscr{D}_f, \alpha)$ is normalized to α, such that $\int_0^\infty dx \eta(x, \alpha) = \alpha$. This implies that $\eta(x, 0) = 0$ as η is defined to be positive for all values of the independent variable x. Therefore, when $\alpha = 0$, we recover the results for diffusion without the presence of barriers, such that $F_{\text{eff}} = F$ and $D_{\text{eff}} = D$.

2.7.3 Comparison of theory with numerical solutions

In this subsection, we will compare numerically found values for a transport quantity against the those we obtained theoretically. The transport quantity we choose is the time dependent transfer rate $F(t)$ defined in Eq. (2.19), and is the analog of the diffusion coefficient in discrete space. Comparing the theory and numerical results in discrete space also has the advantage of avoiding discretization errors. In obtaining the numerical solutions, we first solve the Master equation for the chain with disordered barrier heights, Eq. (2.68), for many realizations of the random variables f_r and calculate $F(t)$ for each case. Then we average over all of these to obtain the final results. Typically we average over 10000 different $F(t)$ curves each corresponding to a particular realization of the disorder. The main plot in Fig. 2.15 shows numerically calculated $F(t)/F$ as a function of t for three Rice distributions with parameters ($v = 0.1$, $s = 0.02$), ($v = 0.2$, $s = 0.06$) and ($v = 0.4$, $s = 0.02$) that are represented by the dashed, solid, and dash-dotted curves respectively. The horizontal dotted line corresponds to the theoretically predicted value of F_{eff}, given by Eq. (2.73), for each case. There is excellent agreement between theory and numerics at long times. The inset shows the shape of the probability distribution $\rho(f)$ corresponding to each case, keeping the same linestyle code. We also get similar results for different $\rho(f)$'s, but here we only display results for the Rice distribution. The apparent dip in $F(t)/F$ at intermediate times is due to the particular initial condition chosen in numerically solving

the Master equation. The initial condition for all of these cases is such that the random walker occupies the central site in the starting compartment. Therefore, it is natural to expect this feature in $F(t)$, as explained with detail in Sec. 2.4.
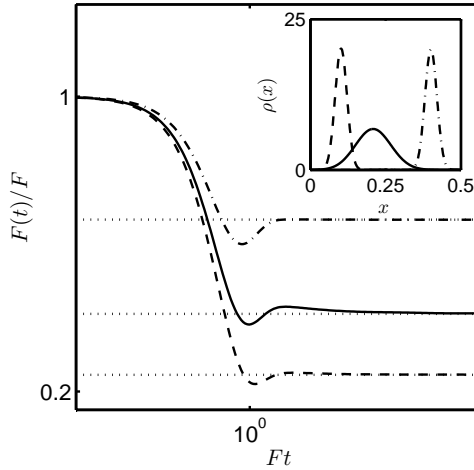
Figure 2.15: Comparison of theoretical results obtained by using the effective medium theory and the numerical solutions of the Master equation (2.68), for the time-dependent transfer rate $F(t)$. The barrier heights are sampled from three Rice distributions with parameters ($v = 0.1$, $s = 0.02$), ($v = 0.2$, $s = 0.06$) and ($v = 0.4$, $s = 0.02$) and the corresponding $F(t)/F$ versus t plots are represented by the dashed, solid, and dash-dotted curves, respectively. Horizontal lines show the value of F_{eff} for each case. The agreement between theoretical predictions and numerical solutions is excellent at sufficiently long times. The plots in the inset display the behavior of ρ for each curve in the main figure, using the same linestyle code. For further details, see text.

2.8 Concluding remarks

In this chapter we described our mathematical model for the motion of molecules in cell membranes also published in refs. [38, 39]. Our model can predict the transport properties of molecules diffusing in the cell membrane in the presence of compartmentalization effects due to the membrane skeleton, as explained in the introduction with considerable detail. In Secs. 2.2-2.6, we presented our results for the ordered case, in which one as-

sumes that the compartment sizes and barrier heights are uniform. Similar results for this case are also found in the literature in the works of Powles, Mallett, Rickayzen, and Evans [3], and Dudko, Berezhkovskii, and Weiss [4]. Our analysis resulted in considerably simple expressions for the time-dependent transport properties and are summarized in Sec. 2.6. The Laplace transforms of the formulas we obtain for these transport properties are exact. In order to express them as functions of time, we employ analytical and numerical methods of taking the inverse Laplace transform, which were explained in detail in Sec. 2.4. In Sec. 2.5 we compared the predictions of our theory with experimental data, and showed that they agree well. An important feature of our analysis is that the effects of the initial position of the molecule on the diffusion coefficient and mean square displacement are clearly explained. In the past, the effects of initial conditions were virtually inaccessible because of the large experimental errors, but the recent advancements in single molecule tracking techniques may make it possible for us to observe them.

In the second part, which consists of Sec. 2.7, we described how to generalize our model to account for the structural disorder in the system. Encouraged by the success of our simple mathematical model for the ordered case, we generalized it to take into account the disorder in compartment sizes and barrier heights that is present in live cell membranes. We used an effective medium approximation to calculate an effective diffusion constant for diffusion in the presence of barriers, that have variable heights, and placed disorderly in space. We believe that this achievement is one of the most important contributions of our work as the previous models that describe diffusion in the presence of permeable barriers did not consider the effects of disorder explicitly.

Chapter 3

Contributions to the effective medium theory of transport in disordered lattices

3.1 Introduction

In this chapter we are interested in investigating the properties of random walk in disordered lattices by using the effective medium theory. Effective medium theories have been widely used to estimate the values of ensemble averaged quantities in many disordered systems. Recently Kenkre, Kalay, and Parris [16] have made essential contributions to this field, and some of their findings are part of this thesis. This chapter gives a background on the fundamental aspects of the effective medium theory and presents those new contributions.

Understanding the motion of particles in disordered media is important in the investigation of many natural phenomena. Examples include electron transfer in organic crystals [64, 65] (also important for understanding photosynthesis), conductivity in metals and semiconductors [66, 67, 68, 5], motion of molecules in cell membranes [42, 69, 70, 1], and virtually any problem that involves the consideration of particle motion in a random

landscape [10].

In discrete space, the most general structure that one can consider is a graph. A graph consists of a finite number of nodes, or infinitely many nodes, that may be connected to each other with links in many different ways. Consider a random walker that hops between connected nodes in a graph. Let F_{mn} denote the rate at which it hops in continuous time from node n to node m. In other words, F_{mn} is the transfer rate associated with the link connecting those nodes. Then the probability of finding the random walker at the mth node of the graph at time t will obey the Master equation

$$\frac{dP_m}{dt} = \sum_n \left[F_{nm}P_n(t) - F_{nm}P_m(t) \right]. \tag{3.1}$$

For details on the master equation description of random walks, see for instance Bedeaux et al. [71], Oppenheim et al. [72], Kenkre [5], van Kampen [73], Hughes [10] and references therein. Another noteworthy resource is the extensive review on the use of master equation techniques in the description of energy transfer given by Kenkre [74]. We will be specifically interested in random walks that take place in a 1-D chain, in which the random walker can only hop between nodes that are nearest neighbors. As the graph we are considering is a 1-D chain, the nodes can be thought as sites in space at which the random walker can be found. In this respect, we will use the word site instead of node from now on. The transfer rates F_{mn} are nonzero only for $n = m + 1$ or $n = m - 1$. Furthermore, we will take them to be symmetric so that $F_{mn} = F_{nm}$ which leads to unbiased random walk. In this case Eq. (3.1) reduces to

$$\frac{dP_m}{dt} = F_m \left[P_{m-1} - P_m \right] + F_{m+1} \left[P_{m+1} - P_m \right], \tag{3.2}$$

where F_n denotes the transfer rate between sites n and $n-1$ so that $F_n = F_{n,n-1} = F_{n-1,n}$. As stated in the beginning of this section, we are interested in random walks in a disordered chain. Throughout this section, by a disordered chain we mean that F_n's are random variables that are drawn from a probability density function $\rho(F_1, F_2, F_3, \dots)$ in the general case and simply $\rho(F)$ if F_n's are independently distributed. In the literature, the type of

disorder we are considering here is sometimes referred to as bond disorder, as the links (or bonds) that connect each site in the chain with its neighbor have nonuniform transfer rates. Our aim is to predict the evolution of transport quantities, such as the diffusion coefficient, in a disordered chain where the disorder in transfer rates is characterized by the probability density ρ. This problem has been addressed by many in the past, see for instance Parris [12, 13, 14]. Although Eq. (3.2) gives the evolution of probabilities in its full detail for a particular realization of the random variables F_n, it definitely is not possible to solve it exactly and express P_m's explicitly. In order to proceed, we would like to write down an equation for the evolution of ensemble averaged probabilities, P_m^{ens}. One way of defining P_m^{ens} is to argue that it is equal to the average of all solutions P_m of Eq. (3.2) over all possible realizations of the random chain. Note that a realization of the random chain with N sites is characterized by $N-1$ values of the transfer rates, sampled from the probability density function ρ.

The properties of diffusion in a lattice with random transfer rates is extensively studied in the past by using methods other than the effective medium theory. In a 1-D lattice, it is possible to obtain exact results for the asymptotic value of the diffusion coefficient if the transfer rates at different locations are uncorrelated. Some of these exact results and limit theorems are given by Alexander et al. [68], Zwanzig [75], and Kawazu and Kesten [76]. In the review by Alexander et al. [68], exact results are compared to the predictions of the effective medium theory for asymptotic times. Here, we would like to mention a couple of other works that are related to studying random walk in a disordered lattice by using Master equations. The first is due to Derrida and Luck [77], and they consider diffusion in a lattice with random and asymmetric transfer rates using a perturbation theory approach and obtain expressions for the weak disorder expansion of the velocity, the diffusion co-efficient, and the conductivity. The second study is by Machta [78], who obtained the asymptotic diffusion coefficient in the disordered lattice by using a real space renormal-ization group method. In his investigation, Machta [78] also shows that the presence of disorder leads to a generalized master equation and calculates some of the properties of

the memory function associated with it.

Here, we are interested in making an effective medium approximation which consists of replacing the Master equation (3.2) with a generalized master equation

$$\frac{dP_m^{\text{ens}}}{dt} = \int_0^t ds \mathcal{F}(t-s) \left[P_{m+1}^{\text{ens}}(s) + P_{m-1}^{\text{ens}}(s) - 2P_m^{\text{ens}}(s) \right]. \tag{3.3}$$

From now on, we will drop the superscript ens of P's that appear in effective medium equations. Note that Eq. (3.3) has two important features. Firstly, it is translationaly invariant, as the memory functions $\mathcal{F}(t)$ do not depend on position. Secondly, it is nonlocal in time, which means that the probability $P_m(t)$ at time t depends on its values at all earlier times $0 < s < t$. The details of how one gets from Eq. (3.2) to Eq. (3.3) will be given shortly in a broader context.

The effective medium approximation that consists of replacing Eq. (3.2) by Eq. (3.3) is not new, and was employed as early as in 1935 by Bruggeman [6] in calculating the dielectric constant of a mixture of dielectrical materials. Since then the theory has been further developed an applied to many different problems. One of the earlier successful applications is due to Kirkpatrick [11] who used an effective medium approximation to calculate the effective conductivity of a random resistor network. Many other significant contributions were made by Odagaki [7], Lax [8], Haus and Kehr [9], just to name a few. For an extensive list of earlier references and a brief discussion of the subject see Hughes [10].

In almost all of these studies, the focus of interest has been the asymptotic values of transport quantities, such as the asymptotic diffusion coefficient which is given by the integral of $\mathcal{F}(t)$ over all t in Eq. (3.3). Therefore, very little amount of work has been done about predicting the time dependence of transport quantities by using the effective medium approximation. Some exceptions to these are the works of Odagaki and Lax [7], Dyre and Schroder [79], and Haus and Kehr [80, 81, 9] on ac conductivity, Parris [12, 82] on studying anisotropic disordered systems, and Kenkre [15] on stress distribution in granular

materials.

As we stated above, the effective medium approximation can be viewed as a procedure in which one replaces a Master equation with inhomogeneous transfer rates by a generalized master equation that has space-independent memory functions. This obviously involves a substantial simplification of the problem, and is appropriate provided that we are interested in ensemble averaged quantities, especially in their asymptotic values. During the earlier development of the effective medium theory, the significance of considering a generalized master equation instead of a Master equation had not been stressed. The early works of Kenkre [5, 83, 84] show that the solutions of generalized master equations can display a lot more features than those of the Master equation, because of the freedom introduced by the memory function. Therefore, generalized master equations have the potential for modeling a wider range phenomena than Master equations, including, for example, coherent transport of excitons [5]. As emphasized in ref. [16], *"What is really necessary in the sense of calculations comes to ... the finding of an explicit and practical prescription that would allow one to go from information about the disorder in the real system to the memories (or pausing time distribution functions) in the replacement problem"*. One such attempt is in an early work, where Scher and Lax [85] attempted to give a method to calculate the waiting time distribution, which is a quantity related to the memory function [83] in Eq. (3.3), using the information in the disorder. In this spirit, our aim is to use a recipe which gives out the memory functions corresponding to a particular kind of disorder, characterized by the distribution ρ. A clear recipe of this kind is given by Kenkre [15] in the context of granular materials.

This chapter is organized as follows: In Sec. 3.2 we present one of the well known ways of showing how the generalized master equation arises. Then, in Sec. 3.3, we give the prescription that we use in solving for the memory functions in the effective medium descriptions. The next three sections are devoted to calculating the time dependence of the memory, finding the memories for some specific distributions $\rho(f)$, and comparison of the

predictions of the effective medium theory with numerical findings, respectively. In Sec. 3.7, we explore the significance of long-range, or higher order, memory functions with respect to the nearest neighbor memory function, which is followed by a discussion on the effects of finite system size in Sec. 3.8. In Sec. 3.9, we present results for the cases in which the disorder is correlated so that links at different locations have transfer rates that are not independently distributed anymore. Finally, we give some concluding remarks in Sec. 3.10.

3.2 How does the generalized master equation arise?

The Master equation, describes an evolution in which the current state of the system is determined entirely by its previous state. The type of processes that lead to this kind of evolution are classified as Markov processes. In many situations, the state of the system in the future depends on part of its history and its evolution would poorly be described by a master equation. For instance, if transport in a system is coherent to some degree, history dependent evolution will arise [5, 83]. In these situations, one may use a generalized master equation that would respect the *memory effect*. At this point, it is important to understand how generalized master equations emerge, by using only first principles. Generalized master equations naturally arise while switching between microscopic and macroscopic descriptions of a system. The memory appears simply because of concentrating on the evolutions of a part of the system and ignoring the rest as we will see shortly. The generalized master equation comes about naturally based on the underlying microscopic dynamics, and only under certain conditions reduces to the master equation. In order to show how these conclusions are drawn, we will follow Zwanzig [86] and make use of the projection operator technique that he originated along with Nakajima [87]. Projection operator techniques have been successfully used in many problems in statistical mechanics not only involving the transition from microscopic dynamics to macroscopic dynamics

which provides an understanding of the origin of irreversibility [88], but also for practical problems [89, 90, 91]. For a generalization of this technique, see Kenkre [83] and Kenkre and Knox [84]. Let u be the density of states of a system. Then u will evolve according to the Liouville equation,

$$\frac{\partial u}{\partial t} = -iLu = \{H, u\}$$

where $\{\cdot, \cdot\}$ stand for Poisson brackets and H is the Hamiltonian. This equation governs the evolution of the microscopic states of the system. The quantum mechanical analog of the Liouville equation is the Von Neumann equation and is given by

$$i\hbar\frac{\partial u}{\partial t} = [H, u],$$

where $[\cdot, \cdot]$ is the commutator and u now stands for the density matrix of the system. For the purpose of this discussion, it does not make a difference to consider classical or quantum mechanical evolution. Here, we consider the quantum mechanical situation for notational brevity. Suppose that we are only interested in the evolution of a part of the system. Let us denote this subset of the whole system by u' and the rest by u'', so that $u = u' + u''$. The projection operators are defined as

$$\mathcal{P}u = u',$$

$$(1 - \mathcal{P})u = u''.$$

We can apply the operators $\mathcal{P}$ and $(1 - \mathcal{P})$ to both sides of the Liouville equation and use $u = u' + u''$ and obtain

$$\frac{\partial u'}{\partial t} = -i\mathcal{P}Lu' - i\mathcal{P}Lu'',$$
$$\frac{\partial u''}{\partial t} = -i(1 - \mathcal{P})Lu'' - i(1 - \mathcal{P})Lu'.$$

We can formally solve for u'' and substitute it in the differential equation for u', giving

$$\frac{\partial u'}{\partial t} = -i\mathcal{P}Lu' - i\mathcal{P}Le^{-it(1-\mathcal{P})L}u''(0) - \int_0^t ds\, \mathcal{P}Le^{-i(t-s)(1-\mathcal{P})L}(1-\mathcal{P})Lu'(s) \qquad (3.4)$$

Note that Eq. (3.4) does not depend on u'' except at its initial value. If $u''(0) = 0$, then Eq. (3.4) would be closed in u' and we can solve for it with whatever method is available. The conditions under which $u''(0) = 0$ would depend on the nature of the particular problem. For instance it may correspond to an initial phase randomization in the quantum mechanical system being considered [92, 93]. If we take $\mathcal{P}$ as an operator that returns the diagonal part of the matrix that it acts on, the first term in the right hand side of Eq. (3.4) vanishes as Lu' is an off diagonal matrix. One can easily see this by calculating the matrix elements of $Lu' = Hu' - u'H$. From now on, we will take $u''(0) = 0$. This also corresponds to arguing that the subset of the system that we are interested in actually is the whole system to begin with. Off-diagonal elements can naturally develop in time, but we will keep looking at the diagonal part only. Then we are left with

$$\frac{\partial u'}{\partial t} = -\int_0^t ds K(t-s) u'(s),$$
(3.5)

where

$$K(t-s) = PL e^{-i(t-s)(1-\mathcal{P})L} (1-\mathcal{P}) L,$$

which is the generalized master equation, as the diagonal elements of u' are the probabilities of finding the system in a particular macroscopic state. In order to make further progress, we need to make approximations or consider a specific system. Note that Eq. (3.5) is a system of equations for the probability of finding the system in the mth state, as $P_m = u'_{mm}$. One can put Eq. (3.5) in a gain-loss form so that it takes on the more familiar look of a generalized master equation. To do this, one can take the diagonal matrix elements of both sides of Eq. (3.5)

$$\langle m| \frac{\partial u'}{\partial t} |m\rangle = \frac{dP_m}{dt} = -\int_0^t ds \langle m|K(t-s) u'|m\rangle.$$

where we use the Dirac notation, and then express the matrix elements $\langle m|K(t-s) u'|m\rangle$ in terms of the probabilities $P_n(t)$.

Now we turn our attention to how the projection technique can be employed to study transport in a disordered lattice. The discussion of the standard procedure mainly follows

that in [9]. Suppose that A is a matrix of random transition rates. Then the probabilities of finding the random walker at the lattice sites are given by the master equation

$$\frac{dP}{dt} + AP = 0, \tag{3.6}$$

where $P = P(P_1, P_2, P_3, \ldots)$. We are not concerned with random walk in a particular random lattice but in the one that is obtained by ensemble averaging over all possible realizations of the random transition rates. Suppose that the projection operator $\mathcal{P}$ takes the ensemble average over transition rates when it acts on the matrix A. We start with Eq. (3.6) and apply the operators $\mathcal{P}$ and $(1 - \mathcal{P})$ like we did above and obtain

$$\frac{d\,[\mathcal{P}P]}{dt} = -\mathcal{P}A\,[\mathcal{P}P] + \mathcal{P}A \int_0^t ds e^{-(1-\mathcal{P})A(t-s)} (1 - \mathcal{P})\,A\,[\mathcal{P}P]. \tag{3.7}$$

In order to get this result, we assumed that we start with a P which is already ensemble averaged over all of its possible realizations, so that $(1 - \mathcal{P})\,P(0) = 0$. From now on, we will put angular brackets around ensemble averaged quantities, e.g. $\mathcal{P}P = \langle P \rangle$, $\mathcal{P}A = \langle A \rangle$. Taking the Laplace transform of Eq. (3.7) and rearranging terms,

$$\epsilon \widetilde{P} - P(0) = \widetilde{B}\widetilde{P},$$

$$\widetilde{B}(\epsilon) = -\langle A \rangle + \langle A\,[\epsilon + (1 - \mathcal{P})\,A]^{-1}\,[A - \langle A \rangle]\rangle.$$

Note that the matrix $\widetilde{B}$ describes a translationaly invariant system unlike A. Inverting the Laplace transform, we get

$$\frac{dP}{dt} = \int_0^t ds B\,(t - s)\,P(s). \tag{3.8}$$

Let

$$B_{mm}(t) = -\sum_n \mathcal{F}_{nm}(t),$$

$$B_{mn}(t) = \mathcal{F}_{mn}(t).$$

Then we can express Eq. (3.8) as

$$\frac{dP_m(t)}{dt} = \int_0^t ds \sum_n [\mathcal{F}_{mn}\,(t - s)\,P_n(s) - \mathcal{F}_{nm}\,(t - s)\,P_m(s)], \tag{3.9}$$

which is a generalized master equation in the more familiar gain-loss form. This shows that probabilities that are ensemble averaged over different realizations of the disorder obey a generalized master equation with space-independent memory functions. Therefore, in this approach, the problem reduces to expressing the memory functions $\mathcal{F}_{mn}(s)$ in terms of the distribution of random transfer rates.

3.3 The effective medium recipe

Probability of finding the random walker at the mth site in the effective medium approximation is given by

$$\frac{dP_m}{dt} = \int_0^t ds \mathcal{F}(t-s) \left[P_{m+1}(s) + P_{m-1}(s) - 2P_m(s)\right]. \tag{3.10}$$

The quantity $P_m(t)$ should be interpreted as the probability of finding the random walker at site m of the ensemble averaged chain, which is translationaly invariant in space. Our aim is to solve for the memory $\mathcal{F}(t)$ given a transfer rate distribution $\rho(f)$ which characterizes the disorder in the system. In order to achieve this, we will make use of a self consistency condition also emplyed by many others (see ref. [10] and references therein). Suppose that we replace the memory function between sites r and $r+1$ with $f\delta(t-s)$. This simply means placing a link between r and $r+1$ whose transfer rate is f. With this replacement, the equation for $P_m(t)$ becomes

$$\begin{aligned}
\frac{dP_m}{dt} &= \int_0^t ds \mathcal{F}(t-s) \left[P_{m+1}(s) + P_{m-1}(s) - 2P_m(s)\right] \\
&+ \delta_{m,r+1} \left(\int_0^t ds \mathcal{F}(t-s) \left[P_{r+1}(s) - P_r(s)\right] - f\left(P_{r+1}(t) - P_r(t)\right) \right) \\
&+ \delta_{m,r} \left(\int_0^t ds \mathcal{F}(t-s) \left[P_r(s) - P_{r+1}(s)\right] - f\left(P_r(t) - P_{r+1}(t)\right) \right).
\end{aligned} \tag{3.11}$$

Let $\eta_m(t)$ be the solution of Eq. (3.10). It can explicitly be written as

$$\eta_m(t) = \sum_n \psi_{m-n}(t) P_n(0).$$

Evidently $\sum_n \psi_{m-n}(t)$ is the Green's function for Eq. (3.11). Therefore, its solution can formally be expressed as

$$
\begin{aligned}
P_m(t) = \eta_m(t) + \Bigg\{ \int_0^t ds \sum_n \psi_{m-n}(t-s) \\
\times \Bigg[\delta_{n,r+1}\Big(\int_0^t ds \mathcal{F}(t-s)[P_{r+1}(s) - P_r(s)] - f(P_{r+1}(t) - P_r(t)) \Big) \\
+ \delta_{n,r}\Big(\int_0^t ds \mathcal{F}(t-s)[P_r(s) - P_{r+1}(s)] - f(P_r(t) - P_{r+1}(t)) \Big) \Bigg] \Bigg\}.
\end{aligned}
$$

(3.12)

Taking the Laplace transform of Eq. (3.12) and doing algebraic manipulations, we obtain

$$
\widetilde{P}_m(\epsilon) = \widetilde{\eta}_m(\epsilon) + \Delta \frac{\widetilde{\eta}_{r+1}(\epsilon) - \widetilde{\eta}_r(\epsilon)}{1 + 2\Delta\left(\widetilde{\psi}_1(\epsilon) - \widetilde{\psi}_0(\epsilon)\right)} \left(\widetilde{\psi}_{m-r-1}(\epsilon) - \widetilde{\psi}_{m-r}(\epsilon)\right),
$$

(3.13)

where $\Delta = \widetilde{\mathcal{F}}(\epsilon) - f$, tildes denote Laplace transformed quantities and ϵ is the Laplace variable. Here comes the key point in this discussion. The second term in Eq. (3.13) stems from the fact that we replaced one of the links in the effective medium chain by one with transfer rate f. Therefore, we introduced a defect into to the otherwise translationaly invariant chain. If we average both sides of Eq. (3.13) over f using the distribution $\rho(f)$, then this term should vanish, because this procedure restores the translational invariance by averaging over all possible values of f, and for a translationaly invariant chain we know that $\widetilde{P}_m(\epsilon)$ is simply equal to $\widetilde{\eta}_m(\epsilon)$. Therefore, we have

$$
\langle \widetilde{P}_m(\epsilon) \rangle = \langle \widetilde{\eta}_m(\epsilon) \rangle + \left\langle \Delta \frac{\widetilde{\eta}_{r+1}(\epsilon) - \widetilde{\eta}_r(\epsilon)}{1 + 2\Delta\left(\widetilde{\psi}_1(\epsilon) - \widetilde{\psi}_0(\epsilon)\right)} \left(\widetilde{\psi}_{m-r-1}(\epsilon) - \widetilde{\psi}_{m-r}(\epsilon)\right) \right\rangle,
$$

$$
\widetilde{P}_m(\epsilon) = \widetilde{\eta}_m(\epsilon),
$$

$$
\left\langle \Delta \frac{\widetilde{\eta}_{r+1}(\epsilon) - \widetilde{\eta}_r(\epsilon)}{1 + 2\Delta\left(\widetilde{\psi}_1(\epsilon) - \widetilde{\psi}_0(\epsilon)\right)} \left(\widetilde{\psi}_{m-r-1}(\epsilon) - \widetilde{\psi}_{m-r}(\epsilon)\right) \right\rangle = 0,
$$

(3.14)

where

$$
\langle \cdot \rangle = \int_0^\infty df \rho(f)[\cdot].
$$

Chapter 3. Contributions to the effective medium theory of transport in disordered lattices

Note that averaging does not affect $\widetilde{P}_m(\epsilon)$ or $\widetilde{\eta}_m(\epsilon)$ as they are quantities that pertain to the ensemble averaged, effective medium chain. The expression given by Eq. (3.14) is a self consistency condition, as averaging over transfer rates of the links with respect to $\rho(f)$ should give rise to the memory functions $\widetilde{\mathcal{F}}(\epsilon)$ in the first place. The self consistency condition can be further simplified by noting that it should hold for all values of m and r, giving

$$\left\langle \frac{\Delta}{1 + 2\Delta\left(\widetilde{\psi}_1(\epsilon) - \widetilde{\psi}_0(\epsilon)\right)} \right\rangle = 0,$$

or

$$\int_0^\infty df \rho(f) \frac{\widetilde{\mathcal{F}}(\epsilon) - f}{1 + 2\left(\widetilde{\mathcal{F}}(\epsilon) - f\right)\left(\widetilde{\psi}_1(\epsilon) - \widetilde{\psi}_0(\epsilon)\right)} = 0. \tag{3.15}$$

Eq. (3.15) can be put [16] in a more compact form by using the fact that $\widetilde{\psi}_0(\epsilon)$ satisfies the Laplace transform of the generalized master equation, Eq. (3.10), so that

$$\epsilon\widetilde{\psi}_0(\epsilon) - 1 = \widetilde{\mathcal{F}}(\epsilon)\left(\widetilde{\psi}_1(\epsilon) + \widetilde{\psi}_{-1}(\epsilon) - 2\widetilde{\psi}_0(\epsilon)\right),$$

where we used $\psi_0(0) = 1$. This enables us to express $\widetilde{\psi}_{\pm 1}(\epsilon)$ in terms of $\widetilde{\psi}_0(\epsilon)$ and leads to

$$\int_0^\infty df \frac{\rho(f)}{f + \xi(\epsilon)} = \frac{1}{\widetilde{\mathcal{F}}(\epsilon) + \xi(\epsilon)}, \tag{3.16}$$

where

$$\xi(\epsilon) = \widetilde{\mathcal{F}}(\epsilon)\frac{\epsilon\widetilde{\psi}_0(\epsilon)}{1 - \epsilon\widetilde{\psi}_0(\epsilon)}.$$

Eq. (3.16) is a very important result [16], as it provides us with a way of calculating $\mathcal{F}(t)$ which can then be used to obtain various transport quantities, like the time dependent diffusion coefficient. In this section, we are interested in quantities that pertain to an infinite 1-D chain, for which

$$\widetilde{\psi}_0(\epsilon) = 1 \left/ \sqrt{\epsilon\left(\epsilon + 4\widetilde{\mathcal{F}}(\epsilon)\right)} \right. ,$$

and

$$\xi(\epsilon) = \frac{\epsilon}{4}\left(1 + \sqrt{1 + 4\widetilde{\mathcal{F}}(\epsilon)/\epsilon}\right).$$

In the subsequent sections, we explore the time dependence of $\mathcal{F}(t)$ by solving Eq. (3.16) for all ϵ and taking its inverse Laplace transform. In many situations, carrying out this procedure is possible only numerically because either doing the integral is cumbersome, or the equation for $\widetilde{\mathcal{F}}(\epsilon)$ is transcendental. However, it is very easy to get information about the $\epsilon \to 0$ limit. In this limit, $\epsilon \widetilde{\psi}_0(\epsilon)$ vanishes and therefore, ξ becomes zero, giving

$$\int_0^\infty df \frac{\rho(f)}{f} = \frac{1}{\widetilde{\mathcal{F}}(0)}, \qquad (3.17)$$

or $\widetilde{\mathcal{F}}(0) = \langle 1/f \rangle^{-1}$. Note that $\widetilde{\mathcal{F}}(0)$ is equal to the asymptotic diffusion coefficient as it is the integral of the memory function from 0 to ∞. This well known result is actually an exact solution in 1-D and was derived in several different ways [68, 94].

In the next section, we will see what we can infer about $\mathcal{F}(t)$ with the knowledge we already have, before considering specific distributions $\rho(f)$ and calculating the corresponding memories.

3.4   Time dependence of the memory

The solutions of the effective medium equation (3.10) need to be consistent with those of the Master equation (3.2) that are averaged over different realizations of the disorder. They should give the same results for the derivatives of $P_m(t)$ in the limit $t \to 0$ as argued in ref. [16]. That is to say

$$\left\langle \frac{d^n P_m^{\mathrm{M}}(t)}{dt^n} \bigg|_{t \to 0} \right\rangle = \frac{d^n P_m^{\mathrm{EMT}}(t)}{dt^n} \bigg|_{t \to 0},$$

where $P_m^{\mathrm{M}}(t)$ and $P_m^{\mathrm{EMT}}(t)$ obey the master equation (3.2) and the effective medium equation (3.10) respectively. Without loss of generality, we can take the initial position of the random walker to be zero, i.e. $P_m(0) = \delta_{m,0}$. As shown in ref. [16], with this choice we

have

$$\left\langle \left.\frac{dP_m^M(t)}{dt}\right|_{t\to 0}\right\rangle = -\langle F_m + F_{m+1}\rangle = -2\langle f\rangle \tag{3.18}$$

$$\left.\frac{dP_m^{EMT}(t)}{dt}\right|_{t\to 0} = \int_{0-}^{0+} ds \mathcal{F}(t-s)[P_{m+1}(s) + P_{m-1}(s) - 2P_m(s)]. \tag{3.19}$$

We immediately observe that the right hand side of Eq. (3.19) can be finite only if $\mathcal{F}(t)$ contains a δ-function centered at $t = 0$. Therefore, we must have

$$\mathcal{F}(t) = \alpha\delta(t) + \beta(t),$$

where α is a constant and $\beta(t)$ is a function of time. Using Eqs. (3.18, 3.19) and $\widetilde{\mathcal{F}}(0) = \int_0^\infty ds \mathcal{F}(s) = \langle 1/f\rangle^{-1}$ we conclude that [16]

$$\mathcal{F}(t) = \langle f\rangle\delta(t) - Q(t),$$

$$\int_0^\infty ds Q(s) = \langle f\rangle - 1/\langle 1/f\rangle.$$

Note that $\langle f\rangle - 1/\langle 1/f\rangle$ is always greater than or equal to zero as

$$\langle f\rangle - 1/\langle 1/f\rangle = \frac{\langle f\rangle\langle f^{-1}\rangle - 1}{\langle 1/f\rangle},$$

and

$$\langle f\rangle\langle f^{-1}\rangle \geq \langle ff^{-1}\rangle = 1,$$

where the last the relation is a form of the Cauchy-Schwarz inequality, $\|a\|\,\|b\| \geq \|ab\|$. Proceeding in the same manner, and equating the second derivatives give

$$\left\langle \left.\frac{dP_m^M(t)}{dt}\right|_{t\to 0}\right\rangle = 4\langle f^2\rangle + 2\langle f\rangle^2 \tag{3.20}$$

$$\left.\frac{dP_m^{EMT}(t)}{dt}\right|_{t\to 0} = 6\langle f\rangle^2 + 2Q(0), \tag{3.21}$$

which yields

$$Q(0) = 2\left(\langle f^2\rangle - \langle f\rangle^2\right).$$

Therefore, one can keep calculating the higher order derivatives of $Q(t)$ at $t = 0$ and approximate it by a Taylor series. A simple approximation to $\mathcal{F}(t)$ can be made by substituting an exponential function for $Q(t)$ with appropriate parameters [16]

$$\mathcal{F}_{apx}(t) = \langle f \rangle \delta(t) - 2\left(\langle f^2 \rangle - \langle f \rangle^2\right) e^{-t\left(2(\langle f^2 \rangle - \langle f \rangle^2)\right)/(\langle f \rangle - \langle 1/f \rangle^{-1})}, \tag{3.22}$$

which satisfies $\int_0^\infty ds \mathcal{F}(s) = \langle 1/f \rangle^{-1}$. We will compare $\mathcal{F}_{apx}(t)$ with its numerically found counterpart in the following sections.

3.5   Calculating the memory functions for specific $\rho(f)$'s

We consider three different types of transfer rate distributions $\rho(f)$ characterizing the disorder. A summary of the quantities related to each distribution that we will use in the calculations later in this section is given in Table 3.1. The first one is a sum of δ-functions

$$\rho(f) = \sum_{i=1}^{M} \alpha_i \delta(f - f_i),$$

for which the transition rates take one of M values f_i each with a weight α_i, with $\sum_{i=1}^{M} \alpha_i = 1$. For convenience, we will consider the case $M = 2$, so that

$$\rho(f) = \alpha \delta(f - f_1) + (1 - \alpha)\delta(f - f_2). \tag{3.23}$$

The distribution $\rho(f)$ for this case is shown as the two arrows in Fig. 3.1 and will be referred to as the "double-delta" distribution from now on.

The second form of $\rho(f)$ we consider is the gamma distribution given by

$$\rho(f) = \frac{\gamma^{n+1}}{\Gamma(n+1)} f^n e^{-\gamma f}. \tag{3.24}$$

A plot of $\rho(f)$ is shown for the parameter values $n = 1$ and $\gamma = 4$ in Fig. 3.1.

The last particular case we consider is the triangular distribution given by

$$\rho(f) = \begin{cases} (f - f_0 + f_b)/f_b^2 & f_0 - f_b \leq f \leq f_0, \\ (-f + f_0 + f_b)/f_b^2 & f_0 \leq f \leq f_0 + f_b, \\ 0 & \text{elsewhere.} \end{cases} \tag{3.25}$$

In this case, f can only take values between $f_0 - f_b$ and $f_0 + f_b$. As for the parameter values: f_b is half the length of the base of the triangle and f_0 is the value of the abscissa at which the distribution peaks, which also is equal to its mean value. The distribution is shown in Fig. 3.1 for $f_0 = 0.3$ and $f_b = 0.2$.

	double-delta	Gamma	Triangular
$\langle f \rangle$	$\alpha f_1 + (1 - \alpha)f_2$	$n + 1/\gamma$	f_0
$\langle f^2 \rangle$	$\alpha f_1^2 + (1 - \alpha)f_2^2$	$(n + 1)(n + 2)\big/\gamma^2$	$f_0^2 + f_b^2/6$
$\langle 1/f \rangle^{-1}$	$\frac{f_1 f_2}{\alpha f_2 + (1-\alpha)f_1}$	n/γ	$f_b \ln^{-1}\left(\left(1 + \frac{2f_b}{f_0 - f_b}\right)\left(1 - \frac{f_b^2}{f_0^2}\right)^{f_0/f_b}\right)$

Table 3.1: Summary of the distribution properties that are used in the calculations.
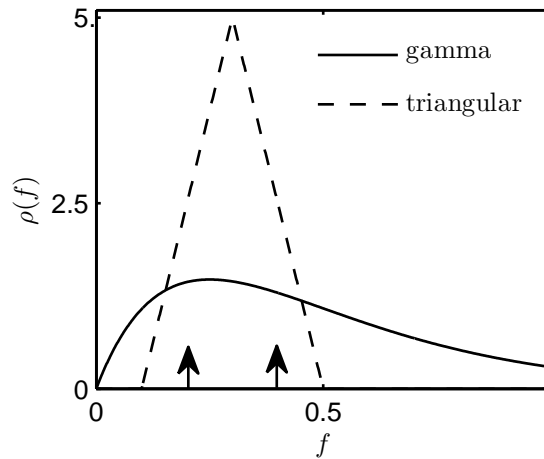
Figure 3.1: Illustration of the three different probability distributions $\rho(f)$ mentioned in the text. The two arrows show the values of f for which the double-delta distribution peaks.

3.6 Comparison of the effective medium theory and numerical solutions

After obtaining the memory function $\mathcal{F}(t)$ we can calculate various observables that can be used to compare the predictions of the effective medium theory (EMT) and numerical results. In order do so, we need to solve Eq. (3.16) for $\widetilde{\mathcal{F}}(\epsilon)$ given a particular distribution $\rho(f)$. A couple of observables that can directly be calculated from the memory function are the mean square displacement, denoted by $\text{MSD}(t)$, and the time dependent diffusion coefficient $D(t)$. In discrete space they are defined as

$$\text{MSD}(t) = \langle (ma)^2 \rangle = \sum_m (ma)^2 P_m(t),$$

$$D(t) = \frac{a^2}{2} \frac{d}{dt} \text{MSD}(t),$$

where a is the distance between two lattice sites. The way these quantities are related to $\mathcal{F}(t)$ can be found by summing Eq. (3.10) over m and solving for the $\text{MSD}(t)$. This yields,

$$\text{MSD}(t) = 2a^2 \int_0^t ds \int_0^s \mathcal{F}(u)du, \tag{3.26}$$

$$D(t) = a^2 \int_0^t \mathcal{F}(s)ds. \tag{3.27}$$

Note that $lim_{t\to\infty} D(t) = \widetilde{\mathcal{F}}(0)$. In this chapter, we will be using the dimensionless forms of $\text{MSD}(t)$ and $D(t)$. In order to simplify the notation, we are going to drop the factors of a, i.e. $a = 0$ throughout this chapter.

In the rest of this section, first we will be interested in comparing the predictions of EMT with numerical solutions for different types of disorder characterized by the three $\rho(f)$'s mentioned above. In doing this, we consider initial conditions that are of different nature which give rise to disparate ensemble averaging schemes. Next, we will explore how good the exponential approximation to the memory, given by Eq. (3.22), is and when the EMT does poorly. Finally we will compare the self propagators predicted by the EMT

to those that are calculated exactly for a specific realization of the random chain. This last task is important as it provides us with another way of testing the EMT and as the self propagators are used in calculating many observables in the system.

In order to obtain the time dependent diffusion coefficient predicted by the EMT, we need to solve Eq. (3.16) for $\widetilde{\mathcal{F}}(\epsilon)$, calculate its inverse Laplace transform and substitute the result in Eq. (3.27)[1]. To test the validity of the EMT predictions, we calculate $D(t)/D(0)$ numerically by solving the Master equation (3.2).

In order to solve the Master equation numerically, we take advantage of the fact that the matrix A in Eq. (3.6) is real and symmetric, and therefore, is diagonalizable and has real eigenvalues. Let $|\phi_\lambda\rangle$ be the eigenvector of A corresponding to the eigenvalue λ, then

$$A |\phi_\lambda\rangle = \lambda |\phi_\lambda\rangle,$$

and $|\phi_\lambda\rangle$'s are normalized such that

$$\langle \phi_\lambda | \phi_{\lambda'} \rangle = \delta_{\lambda,\lambda'}.$$

Therefore, the solution of Eq. (3.6) can be written as

$$|P(t)\rangle = \sum_\lambda e^{-\lambda t} |\phi_\lambda\rangle \langle \phi_\lambda | P(0)\rangle,$$

where we used

$$A = \sum_\lambda \lambda |\phi_\lambda\rangle \langle \phi_\lambda|,$$

$$e^{-At} = \sum_\lambda e^{-\lambda t} |\phi_\lambda\rangle \langle \phi_\lambda|.$$

Of course, this is not the only way of numerically solving Eq. (3.6), but it turns out that this method is very fast as long as the system consists of just a few thousand lattice sites or less.

---

[1]At this point, it is useful to note that dividing the Laplace transform of a function by ϵ corresponds to integrating that function from 0 to t in time.

As the EMT is concerned with ensemble averaged quantities, we need to make sure that an ensemble averaging scheme is built into the numerical solution obtained from the Master equation. In this respect, we will consider two kinds of initial conditions that are used to solve the master equation numerically. The first one will be referred to as the "localized" initial condition and it simply means that the random walker initially occupies one of the sites, for instance the 0th site. In order to calculate $D(t)/D(0)$ from the master equation, we will numerically solve it for many different realizations of the disorder and ensemble average the results. Therefore, the ensemble averaging involved in this procedure makes sure that the quantity we are calculating pertains to the effective medium chain so that it can be compared with the predictions of the EMT. The second type of initial condition we will take up is one that is extended in space, as is given by

$$P_m(0) = \frac{1}{2\mu + 1} \sum_{r=-\mu}^{\mu} \delta_{m,r}.$$

By solving the Master equation with an initial condition of this kind, we eliminate the need for ensemble averaging over different realizations of the chain because of the following reason: as the probability of occupation of the random walker is dispersed over many different sites right from the beginning, the random walker already samples a wide portion of the random chain even at small times, which is equivalent to doing an average over different realizations of the chain. The main point in using spatially extended initial conditions is that in a physical system, we are generally interested in one particular realization of the disordered structure under consideration. Therefore, ensemble averaging over many configurations may not be possible or meaningful. However, one can experimentally arrange situations in which the initial condition is spread out, which leads to the ensemble averaging in the way we described above, so that the predictions of the EMT can still be meaningful.

Let us begin with the consideration of localized initial conditions. Substituting the double-delta distribution given by Eq. (3.23) in Eq. (3.16) and doing the integral, we get

a cubic equation for the Laplace transform of the memory

$$\widetilde{\mathcal{F}}^3 - 2\widetilde{\mathcal{F}}^2 \left(2\eta^2/\epsilon + f_1 + f_2\right) + \widetilde{\mathcal{F}} \left(8\eta f_1 f_2/\epsilon + \left(2f_1 f_2 + (f_1 + f_2)^2 - \eta^2\right)\right)$$
$$-4f_1^2 f_2^2/\epsilon - (2f_1 f_2(f_1 + f_2) - 2\eta f_1 f_2) = 0,$$

where

$$\eta = (1 - \alpha)f_1 + \alpha f_2.$$

We use the cubic formula to solve this equation for $\widetilde{\mathcal{F}}(\epsilon)$ and then calculate $D(t)/D(0)$ from it. For the gamma and triangular distributions, the equations we get for $\widetilde{\mathcal{F}}(\epsilon)$ have to be solved numerically, as they turn out to be transcendental equations. This can done by using high precision arithmetics so that the results obtained are of practical value. In each case, after obtaining $\widetilde{\mathcal{F}}(\epsilon)$ either analytically or numerically, we divide it by ϵ and take its inverse Laplace transform numerically, which yields $D(t)$

$$\mathcal{L}^{-1}\left\{\frac{\widetilde{\mathcal{F}}(\epsilon)}{\epsilon}\right\} = \int_0^t ds \mathcal{F}(s) = D(t),$$

where $\mathcal{L}^{-1}$ denotes the inverse Laplace transformation operator and is defined as

$$\mathcal{L}^{-1}\widetilde{\mathcal{H}}(\epsilon)(t) = \frac{1}{2\pi i}\int_{\gamma - i\infty}^{\gamma + i\infty} d\epsilon e^{\epsilon t}\widetilde{\mathcal{H}}(\epsilon),$$

where γ is a positive real number larger than the real parts of all singularities of $\widetilde{\mathcal{H}}(\epsilon)$. The integral on the right hand side is referred to as the Bromwich integral. Undoubtedly the Laplace transform is a very useful tool in solving linear differential and integral equations by reducing them to algebraic equations. Unfortunately, taking the inverse Laplace transform of the solution can be a difficult task when it cannot be performed analytically. Most of the cases of interest, including ours, fall into this category because of the complications involved in doing the Bromwich integral involved in the inversion process. There are various ways of performing the inversion numerically and the nature of each problem determines which one is the most suitable. Some of the widely used methods are known

as the Fourier series [95], Talbot [96], Weeks [97], and Gaver-Stehfest [98, 99] methods. We chose to use the Gaver-Stehfest method because it only requires the evaluation of the Laplace transform at real values of ϵ, and is reliable when the inverse transform does not oscillate. We know from our numerical experiments that ensemble averaged mean square displacement, diffusion coefficient and probability distribution function are all monotonic functions of time. Below is a brief outline of the numerical method used, as explained in Abate and Whitt [100]. They start with the Bromwich integral

$$\mathcal{H}(t) = \frac{1}{2\pi i} \int_{\gamma - i\infty}^{\gamma + i\infty} d\epsilon\, e^{\epsilon t} \widetilde{\mathcal{H}}(\epsilon),$$

and make the change of variables $s = \epsilon t$, and obtain

$$\frac{1}{(2\pi i)\, t} \int_{t(\gamma - i\infty)}^{t(\gamma + i\infty)} ds\, e^s \widetilde{\mathcal{H}}(s/t). \tag{3.28}$$

The next step is approximating the exponential function by a sum of partial fractions [61]

$$e^s \approx \sum_{k=0}^{n} \frac{\omega_k}{\alpha_k - s}, \tag{3.29}$$

where ω_k and α_k are complex numbers and α_k's are distinct, so that the approximation of e^s has $n + 1$ simple poles and the approximation gets better as n increases. There are various ways in which one can choose α_k and ω_k to approximate e^s better, and basically the specific choice determines the name of the Laplace inversion method. Substituting the approximation Eq. (3.29) into Eq. (3.28) and doing the integration[2],

$$\mathcal{H}_n(t) = \frac{1}{t} \sum_{k=0}^{n} \omega_k \widetilde{\mathcal{H}}(\alpha_k/t). \tag{3.30}$$

Eq. (3.30) is an nth order approximation to the inverse Laplace transform of $\widetilde{\mathcal{H}}(\epsilon)$. It is quite a general result in this form because of the freedom in the choice of the complex numbers ω_k and α_k. In the Gaver-Stehfest method, ω_k and α_k are taken to be real numbers. Note that this means the Laplace transform will only be evaluated for real values of its

---

[2]Which is obviously $2\pi i$ times the residue at each simple pole.

argument. The specific way in which Gaver [98] used to approximate $\mathcal{H}(t)$ gives [100]

$$\mathcal{H}_g(t, M) = \frac{\ln 2}{t} \sum_{k=1}^{2M} \zeta_k \widetilde{\mathcal{H}}\left(k\frac{\ln 2}{t}\right),$$

$$\zeta_k = (-1)^{M+k} \sum_{j=\lfloor (k+1)/2 \rfloor}^{\min(k,M)} \frac{j^{M+1}}{M!}\binom{M}{j}\binom{2j}{j}\binom{j}{k-j},$$

where $\mathcal{H}_g(t, M)$ is the approximation to $\mathcal{H}(t)$ and $\lfloor x \rfloor$ is the greatest integer less than or equal to x. Observe that the magnitude of the terms in the alternating series can be very large. Therefore, one needs to do the arithmetic with quite high precision to obtain reliable results. When the function $\mathcal{H}(t)$ is bounded, it is possible to approximate the accuracy of $\mathcal{H}_n(t)$ and the number of significant digits that should be used to achieve that accuracy [101]. According to Abate and Whitt [100] the precision required to sum the series, i.e. the number of significant digits, is $2.2M$ while the precision of the resulting expression is $0.90M$. Practically speaking, if one uses double precision in the calculations, the value of M should not be larger than 7. As the probability distribution function and diffusion coefficient are both bounded functions in time, we can use these results to reliably perform the Laplace inversion numerically.

Following the steps that we described above, we calculate $D(t)/D(0)$ both numerically and by the EMT for the double-delta, gamma, and triangular distributions. Numerical results are carried out by calculating $D(t)$ for over 20000 different realizations of the random chain with localized initial conditions and averaging over all of them. Results are displayed in Fig. 3.2. There is excellent agreement between numerical results and the predictions of EMT for all times. Therefore, it looks like EMT can be used to make accurate predictions of time dependent transport quantities such as the diffusion coefficient.

It is natural to expect that for some parameter values, the effective medium approximation would break down. We will explore this shortly. Before that, let us consider the situation in which we employ spatially extended initial conditions and do not average over different realizations of the chain. Suppose that we use an initial condition of following
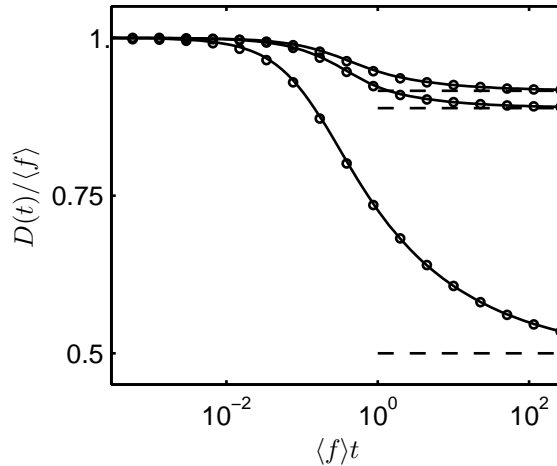
Figure 3.2: Normalized time-dependent diffusion coefficient as a function of dimensionless time $\tau = \langle f \rangle t$, for different types of disorder. From top to bottom, solid lines correspond to EMT predictions and open circles represent the numerical solutions for $\rho(f)$ being a double-delta distribution with $f_1/f_2 = 0.5$ and $\alpha = 0.5$, a triangular distribution with $f_0 = 0.3$, $f_b = 0.2$, and a gamma distribution with $n = 1$. The agreement is remarkable in all of the cases for all times. The numerical solution is found by using a localized initial condition and averaging over 20000 calculations of $D(t)/D(0)$ each involving a different realization of the disorder. Dashed lines on the right show the asymptotic values of the diffusion coefficient predicted by the EMT, which is equal to $\widetilde{\mathcal{F}}(0)$.

form

$$P_m(0) = \frac{1}{2\mu + 1} \sum_{r=-\mu}^{\mu} \delta_{m,r}. \tag{3.31}$$

With these initial conditions, we expect that the numerical solution of the Master equation for a particular realization of the disorder agrees with the EMT predictions. The non-zero width of the initial condition should play the role of ensemble averaging over different realizations of the chain, as discussed earlier. In order to test this idea, we generate a disordered chain whose transfer rates are drawn from the double-delta distribution. Always using the same chain, we calculate $D(t)/D(0)$ by varying the width of the initial condition, which is $2\mu + 1$ as seen from Eq. (3.31). Then we calculate the integrated relative difference, E_R, between the EMT predictions for $D(t)/D(0)$ and numerical solutions with

different initial condition widths. This quantity is defined by

$$E_R = \int_{-\infty}^{\infty} \frac{D^{EMT}(s) - D^{EX}(s)}{D^{EX}(s)} ds \tag{3.32}$$

where $s = \ln(\langle f \rangle t)$, and $D^{EMT}(t)$ and $D^{EX}(t)$ are the EMT prediction and exact numerical value of the diffusion coefficient. As Fig. 3.3 shows, numerical results agree with EMT as the width of the initial condition increases. The main figure shows that E_R drops quickly with the initial condition width and the inset shows $D(t)/D(0)$ for two specific initial conditions with $\mu = 5$ and $\mu = 50$. These plots in the inset demonstrate that the results obtained for the narrower initial condition (crosses) differs substantially from the EMT predictions whereas those for the broader initial condition (open circles) agree well with it.
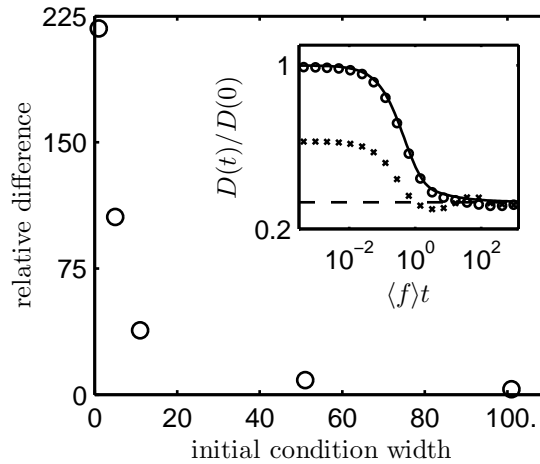
Figure 3.3: The main figure shows the behavior of E_R as given by Eq. (3.32) which is the relative difference between EMT predictions and numerical results for spatially extended initial conditions calculated for a particular realization of the disordered chain. It clearly shows that E_R monotonically decreases with increasing initial condition width. The inset shows the time evolution of $D(t)/D(0)$ for a couple of initial conditions, one of which is narrower (crosses, $\mu = 5$) and the other being broader (open circles, $\mu = 50$), along with the EMT prediction. The results that correspond to the broader initial condition agree surprisingly well with the EMT prediction for all times.

Next, we will explore how the exponential approximation to the memory, Eq. (3.22)

compares with the exactly calculated memory functions and when the effective medium approximation breaks down. In order to address the first of these issues we need to find an alternative way of calculating the memory without using Eq. (3.16). Our aim is to calculate the matrix elements $\mathcal{W}_{mn}(t)$ in

$$\frac{dP}{dt} + \int_0^t ds \mathcal{W}(t-s)P(s) = 0,$$

where $\mathcal{W}_{mn}(t) = -\mathcal{F}_{mn}(t)$, $\mathcal{W}_{mm}(t) = \sum_n \mathcal{F}_{nm}(t)$ and $\mathcal{F}_{mn}(t)$'s are the memory functions we are looking for. The solution of this equation in the Laplace domain can be expressed as

$$\widetilde{P}(\epsilon) = \left(\epsilon + \widetilde{\mathcal{W}}(\epsilon)\right)^{-1} P(0), \tag{3.33}$$

where $\left(\epsilon + \widetilde{\mathcal{W}}(\epsilon)\right)^{-1}$ is a translationaly invariant matrix. Meanwhile the master equation that describes the evolution of probabilities in a disordered chain is

$$\frac{dP}{dt} + AP = 0,$$

where $A_{mn} = -F_{mn}$ and $A_{mm} = \sum_m F_{nm}$ and $F_{mn} = F_{|m-n|}$'s are independently distributed random variables. Its formal solution in the Laplace domain is

$$\widetilde{P}(\epsilon) = (\epsilon + A)^{-1} P(0).$$

If we average both sides of this equation over each possible realization of the disordered chain, we get

$$\widetilde{P}(\epsilon) = \langle(\epsilon + A)^{-1}\rangle P(0). \tag{3.34}$$

Note that $\langle(\epsilon + A)^{-1}\rangle$ should be a translationaly invariant matrix because ensemble averaging wipes out all inhomogeneities originally present in A. Note that Eqs. (3.33) and (3.34) should be equivalent as we are arguing that the effective medium equation (3.33) describes the evolution of probabilities in the ensemble averaged chain. Therefore

$$\langle(\epsilon + A)^{-1}\rangle = \left(\epsilon + \widetilde{\mathcal{W}}(\epsilon)\right)^{-1},$$

$$\widetilde{\mathcal{W}}(\epsilon) = \epsilon - \langle(\epsilon + A)^{-1}\rangle^{-1},$$

$$\widetilde{\mathcal{F}}_{mn}(\epsilon) = \left[\langle(\epsilon + A)^{-1}\rangle^{-1} - \epsilon\right]_{mn}. \tag{3.35}$$

Therefore, what we need to do to get the memory functions $\mathcal{F}_{mn}(t)$ is to perform the average in Eq. (3.35) for a large number (ideally infinite) of different realizations of the matrix A, and then doing an inverse Laplace transformation. In Fig. 3.4, we display both the exponential approximation given by Eq. (3.22) and the exact memory obtained from Eq. (3.35) when $\rho(f)$ is a double-delta distribution. The agreement between them is very good, but in some cases exponential approximation may lead to erroneous results because of its simple nature, as we will see shortly. We will also make use of Eq. (3.35) later to calculate memory functions while investigating non-nearest neighbor memories and effects of finite system size.
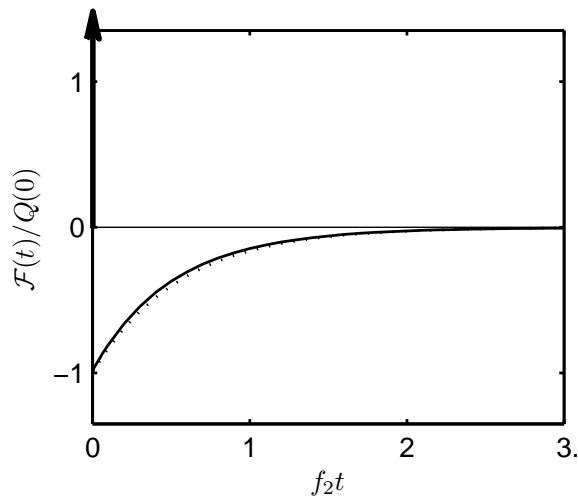
Figure 3.4: Exponential approximation to the memory function calculated by Eq. (3.22) (dotted line) and its exact counterpart given by Eq. (3.35) (solid line), as a function of dimensionless time $f_2 t$. The agreement is good considering the simple nature of the approximation. $\rho(f)$ which characterizes the disorder in this case is a double-delta distribution with $\alpha = 0.1$, and $f_1/f_2 = 10$.

The results we displayed so far show that the agreement between EMT and numerical calculations is remarkably good. However some discrepancy should be expected at least for certain values of the parameters. We find that the difference between $D(t)/D(0)$ found numerically and predicted by the EMT, which from now on will simply be referred to as

difference, increases with the fraction of links that have very low transfer rates. In order to study this effect quantitatively, we take $\rho(f)$ to be a double-delta distribution with $\alpha = 0.5$, so that it is equally likely to find either of the rates f_1 and f_2. We choose this value of α on purpose as it makes the configuration maximally disordered, and we are interested in the cases for which the effective medium approximation may break down. In Fig. 3.5, we show the comparison between EMT and numerical results for decreasing values of f_1 so that from top to bottom the ratio f_1/f_2 takes the values 0.5, 0.1, 0.01. Note that the EMT predictions deviate from the numerical findings more and more as one of the rates gets closer and closer to zero. Therefore, if one of the rates is equal to zero, the difference should be maximal. The main graph in Fig 3.6 shows the mean square displacement as a function of dimensionless time $\langle f \rangle t$ when one of the rates is equal to zero with concentration $\alpha = 0.01$ and 0.1, again for a double-delta distribution. There are two reasons why we chose the mean square displacement as the observable instead of the diffusion coefficient. First of all, when the EMT predictions deviate more from the numerical findings, the magnitude of deviation is larger for the mean square displacement than what it is for the diffusion coefficient, as the latter is the integral of the former. Secondly, we can exactly calculate the saturation value of the mean square displacement when one of the rates is zero. Therefore, we can easily compare the exact saturation value of the mean square displacement with the EMT predictions and the one obtained from the exponential approximation to the EMT memory to further test its applicability. As explained in ref. [16], in order to obtain the saturation value of the mean square displacement in the exponential approximation, we substitute Eq. (3.22) in Eq. (3.26) to get

$$\langle m^2 \rangle = \frac{2}{\langle 1/f \rangle}t + \frac{\left(\langle f \rangle - \langle 1/f \rangle^{-1}\right)^2}{\langle f^2 \rangle - \langle f \rangle^2}\left(1 - e^{-t/\tau}\right),$$

$$\tau = \frac{\langle f \rangle - (\langle 1/f \rangle)^{-1}}{2(\langle f^2 \rangle - \langle f \rangle^2)},$$

whose long time limit gives the saturation value is

$$\lim_{t \to \infty}\langle m^2 \rangle = \frac{\langle f \rangle^2}{\langle f^2 \rangle - \langle f \rangle^2},$$

where we used the fact that $\langle 1/f \rangle^{-1}$ vanishes when one of the rates is zero. It is clearly seen in the main graph in Fig. 3.6 that the saturation value predicted by the EMT is different from what is found numerically. The inset shows the mean square displacement as a function of time for $\alpha = 0.1$ case but on semilogarithmic axes, so that the deviation is clearly visible. Dotted and solid vertical lines correspond to the prediction of the exponential approximation to the EMT and the exactly calculated saturation value[3], whereas the solid curve is the EMT prediction. Apparently EMT predictions are not reliable when the chain has broken bonds. Not surprisingly, the exponential approximation is not accurate either, as it is an approximation on the EMT.
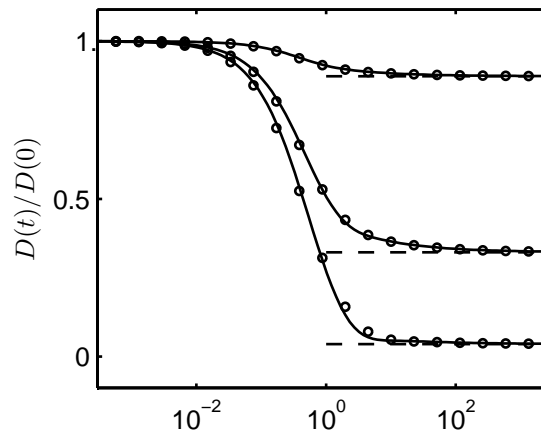
Figure 3.5: Normalized diffusion coefficient is plotted as a function of the dimensionless time $\tau = \langle f \rangle t$ for the double-delta distribution. Solid lines correspond to EMT predictions and open circles correspond to numerical results. From top to bottom, the ratio f_1/f_2 is equal to 0.5, 0.1, and 0.01 with $\alpha = 0.5$ being equal for all of them. Note that the agreement between EMT and numerical results gets slightly worse as the rates become more and more disparate (when one of the rates gets closer and closer to zero).

As we mentioned in the introduction of this section, there is one more quantity that we are interested in calculating: the self propagators. We would like to see how well EMT predicts the self propagators for the disordered chain as they are involved in the calculation of many observables relevant to a system. We start with a particular realization

---

[3]This is equivalent to calculating the average size of connected clusters of links.
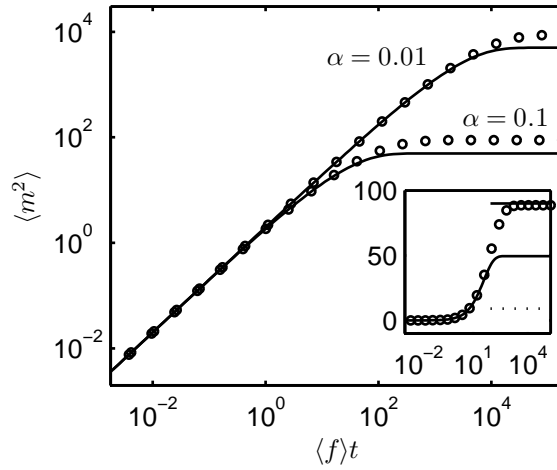
Figure 3.6: Mean square displacement as a function of dimensionless time, for a double-delta distribution with $f_1 = 0$, $f_2 = 0.2$ and two different values of α. Again, solid lines and open circles correspond to EMT predictions and numerical results, respectively. Apparently, the saturation value of the mean square displacement predicted by the EMT is different from the numerical results. To emphasize the deviation between them, in the inset we plot the $\alpha = 0.1$ by itself on semilogarithmic axes. In addition, the solid horizontal line correspond to the exact value of the long time limit of the mean square displacement (saturation value) while the dotted horizontal line shows the value of its counterpart obtained by using the exponential approximation to the EMT memory Eq. (3.22).

of the disordered chain and calculate self propagators at the $2\mu + 1$ sites around the zeroth site. Then we average over them to get the quantity

$$\Psi_\mu = \frac{1}{2\mu + 1} \sum_{\ell=-\mu}^{\mu} \psi_{\ell,\ell}.$$

As we average over more and more self propagators at different sites, we would expect Ψ_μ to approach the self propagator that the EMT predicts for the effective medium chain. That is to say,

$$\Psi_\infty = \lim_{\mu \to \infty} \frac{1}{2\mu + 1} \sum_{\ell=-\mu}^{\mu} \psi_{\ell,\ell}, \tag{3.36}$$

Should be approximated well by the effective medium self propagator. In Fig. 3.7, averaged self propagators calculated numerically for a particular realization of the disordered

chain is shown for $\mu = 3\,, 9\,, 15\,, 25$ and 401 for a chain with 801 sites. The comparison between numerically found self propagator, for $\mu = 401$, and the one predicted by the EMT is shown in Fig. 3.8 by open circles and the solid line respectively. Good agreement between them confirms the hypothesis that the self propagator given by Eq. (3.36) is approximated well by the EMT. EMT provides us with the effective transfer rate $F_{\text{eff}} = \widetilde{\mathcal{F}}(0)$ for the disordered chain[4]. This means, for long times, we can replace the disordered chain by one which has uniform transfer rates F_{eff}. Then it is natural to ask what the difference is between the time evolution in a chain that has uniform transfer rates F_{eff}, or equivalently uniform Markoffian memory $F_{\text{eff}}\delta(t)$, and in the effective medium chain with non-Markoffian memory $\mathcal{F}(t)$. The dashed line in Fig. 3.8 represents the self-propagator for a chain which has uniform transfer rates F_{eff}. Therefore, the difference between the time evolution shown by the dashed and solid lines are due to memory effects, which are significant at intermediate times.

3.7   Significance of higher order memory functions

We have implicitly assumed that long range memory functions in the effective medium equation (3.10) can be neglected and expressed all of our results in terms of the nearest neighbor memory function $\mathcal{F}_1(t)$ (without using the subscript 1). In this section we would like to verify the validity of this assumption by calculating higher order memory functions $\mathcal{F}_2(t)$, $\mathcal{F}_3(t)$, ... that connect sites that are farther apart. We consider a chain of 100 sites with disordered links whose transfer rates are characterized by a double-delta distribution with $\alpha = 0.5$ and $f_1/f_2 = 0.1$. By using Eq. (3.35), we numerically calculate the memory functions $\mathcal{F}_n$ for $n = 1, 2, 3,$ and 4 and display the results in Fig. 3.9. Fig. 3.9(a) shows the comparison between EMT nearest neighbor memory (open circles), and its numerically calculated counterpart. We note the excellent agreement between the two, which gets even

---

[4]F_{eff} is equivalent to the diffusion coefficient divided by a^2 but the value of a is irrelevant in our calculations so we may as well take it to be 1.
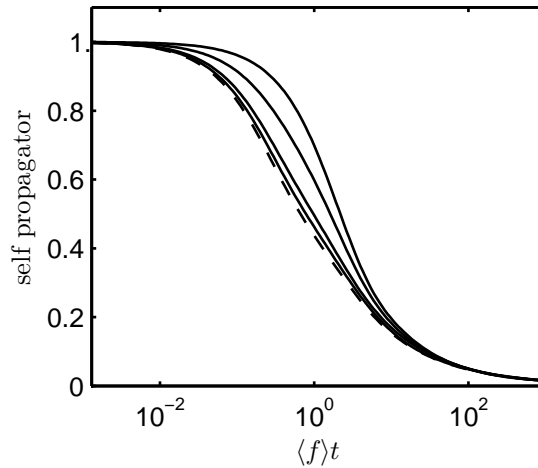
Figure 3.7: Average self propagators for a particular realization of the chain as a function of dimensionless time. Disorder is characterized by a double-delta distribution with $f_1/f_2 = 0.1$ and $\alpha = 0.5$. A total of 401 self propagators at the 200 sites to the left and right of the 0th site are calculated numerically. The dashed line shows the average of all of the 401 self propagators whereas the solid lines correspond to averaging over 3, 9, 15 and 25 (from top to bottom) of the self propagators around the origin.

better as the size of the ring increases. The first few higher order memory functions are shown in Fig. 3.9(b), that are calculated numerically. As the scale of y-axis indicates, the amplitude of higher order memories are negligible compared to $\widetilde{\mathcal{F}}_1(\epsilon)$, especially for $\epsilon \gg 1$ and $\epsilon \ll 1$. Therefore, it is reasonable to discard higher order memory functions and calculate the observables using the nearest neighbor memory function $\widetilde{\mathcal{F}}_1(\epsilon)$.

3.8 Effects of finite system size

As we have seen previously, EMT correctly predicts the long time diffusion coefficient for a disordered infinite 1-D chain, which is given by $\widetilde{\mathcal{F}}(0)$. In this section we describe the results of applying the EMT to a system of finite size, as reported in ref. [16]. We consider a ring of N sites with periodic boundary conditions and for simplicity, we choose the transfer rates from a double-delta distribution with $\alpha = 0.5$. Laplace transform of the
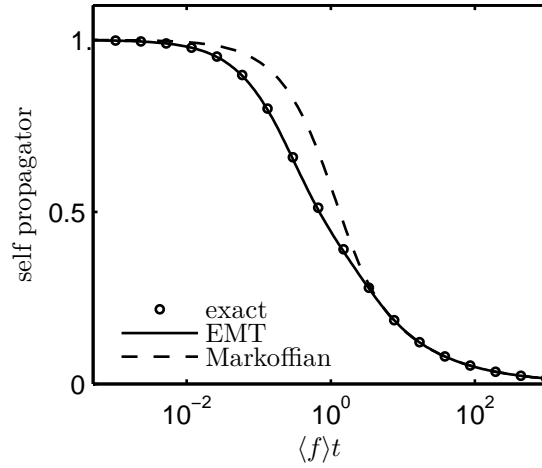
Figure 3.8: Self propagators as a function of dimensionless time for various cases. Open circles represent numerically found average of the 401 self propagators mentioned in the caption of Fig. 3.7. Solid line corresponds to the EMT prediction. The dashed line shows the behavior of the self propagator for a chain has transfer rates F_{eff} throughout. It is included to emphasize the effects of having a non-δ memory.

self propagator for a finite ring of N sites is given by

$$
\widetilde{\psi}_0(\epsilon) = \frac{1}{N} \sum_k \frac{1}{\epsilon + 2\mathcal{F}(\epsilon)(1 - \cos k)}. \tag{3.37}
$$

In order to find the effective transfer rate $F_{\text{eff}} = \widetilde{\mathcal{F}}(0)$, we need to solve Eq. (3.16) with ξ calculated with the propagator given by Eq. (3.37). Note that $\lim_{\epsilon \to 0} \epsilon\widetilde{\psi}_0(\epsilon)$ that appears in ξ is the asymptotic value of $\psi_0(t)$, the probability of finding the random walker at the 0th site at long times, which is simply equal to $1/N$. Therefore, Eq. (3.16) becomes

$$
\frac{1}{F_{eff}} = \frac{N}{N-1} \int_0^\infty df \frac{\rho(f)}{f + F_{\text{eff}}(\frac{1}{N-1})}.
$$

After evaluating the integral with $\rho(f) = \alpha\delta(f - f_1) + (1-\alpha)\delta(f - f_2)$, we obtain an equation for the effective transfer rate

$$
F_{\text{eff}} = \frac{N-1}{N} \left[\frac{\alpha}{f_1 + \frac{F_{\text{eff}}}{N-1}} + \frac{1-\alpha}{f_2 + \frac{F_{\text{eff}}}{N-1}} \right]^{-1},
$$
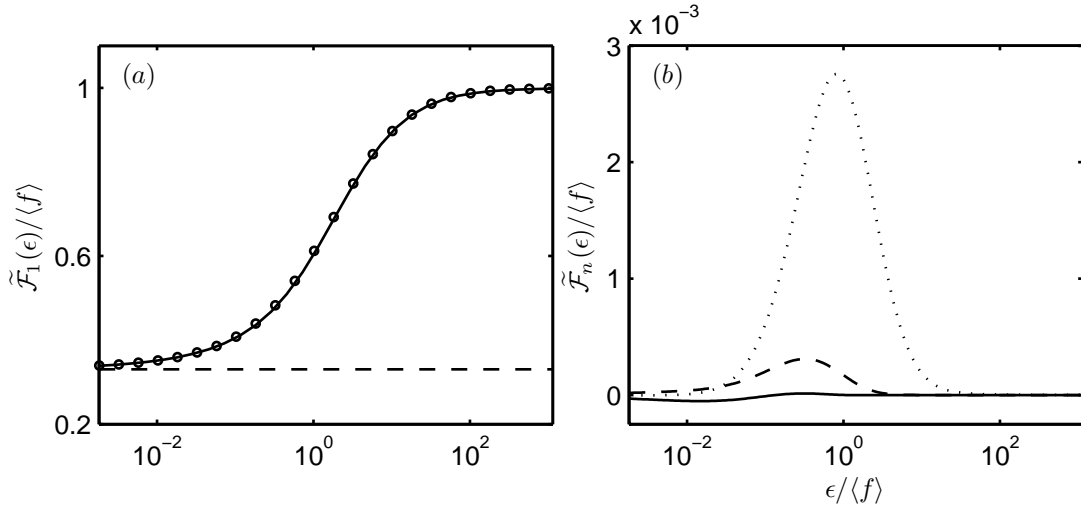
Figure 3.9: In (a) the nearest neighbor memory function obtained from EMT (open circles), and numerically by using Eq. (3.35) (solid line) is shown. Numerical results are obtained by considering a chain of 100 sites and double-delta distribution with $\alpha = 0.5$, and $f_1/f_2 = 0.1$ for the disorder in transfer rates. In (b), higher order memory functions $\widetilde{\mathcal{F}}_2(\epsilon)$, $\widetilde{\mathcal{F}}_3(\epsilon)$, and $\widetilde{\mathcal{F}}_4(\epsilon)$ for the same chain and disorder type are shown. Note that the amplitude of higher order memory functions are negligible compared to that of the nearest neighbor memory $\widetilde{\mathcal{F}}_1(\epsilon)$.

whose solutions are given by

$$F_{\text{eff}} = \frac{j \pm \sqrt{j^2 + 4(N-1)f_1 f_2}}{2}, \tag{3.38}$$

where $j = f_1(1 - N + N\alpha) + f_2(1 - N\alpha)$. When both of f_1 and f_2 are nonzero, one of the roots of Eq. (3.38) is always negative, therefore we need to discard it and use the positive root only. On the other hand if one of the rates is zero, say $f_1 = 0$, then one root is always zero and the other changes sign when the concentration of broken bonds reach $\alpha = 1/N$. A plot of F_{eff} as a function of α is shown in Fig. 3.10. It is interesting to note that this plot looks like the diagram of a transcritical bifurcation [102] in which the two solutions of Eq. (3.38) exchange stability at $\alpha = 1/N$. As N tends to infinity, F_{eff} can only be zero. Therefore, for an infinite chain, if the probability of having a broken bond is greater than zero, F_{eff} vanishes.
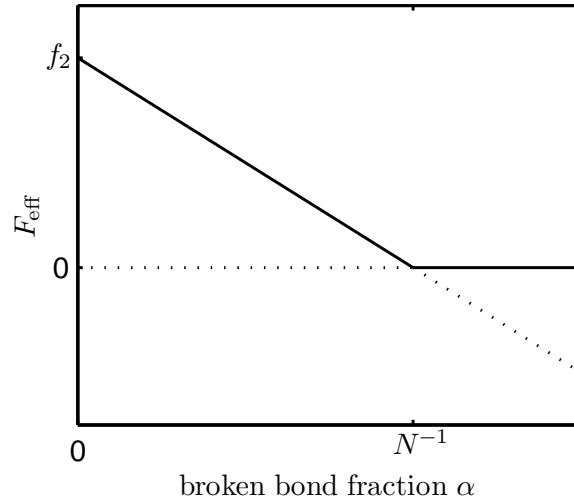
Figure 3.10: Bifurcation of the effective long time transfer rate for a double-delta distribution in a finite system of N sites. Plotted is F_{eff} as a function of the concentration of broken bonds (i.e., bonds with the rate $f_1 = 0$), the rate associated with the remaining fraction $1 - \alpha$ of unbroken bonds being equal to f_2. A transcritical bifurcation occurs when α equals $1/N$. For concentrations higher than this value, the effective rate vanishes but changes linearly with the concentration for lower α. Solid (dotted) lines denote the stable (unstable) solution.

Lastly, we would like to compare the $\epsilon \to 0$ limit of memory functions calculated exactly and by the EMT for finite rings. For finite rings we can use Eq. (3.35) to calculate the nearest neighbor memory function $\widetilde{\mathcal{F}}_1(\epsilon)$ exactly, as the number of all possible realizations of the disorder in finite. The $\epsilon \to 0$ limit of $\widetilde{\mathcal{F}}_1(\epsilon)$ calculated in this manner for rings of size $N = 2, 3, 4,$ and 5 are given below,

$$\widetilde{\mathcal{F}}_1^{\text{ex}}(0)$$

$$= \begin{cases} 2f_2 \dfrac{r}{r+1} & \text{N=2,} \\[2mm] 8f_2 \dfrac{r(r+2)(2r+1)}{(5r+1)(r+5)(r+1)} & \text{N=3,} \\[2mm] 16f_2 \dfrac{r(1+3r)(3+r)(r+1)}{124r(1+r^2)+230r^2+17(1+r^4)} & \text{N=4,} \\[2mm] 16f_2 \dfrac{r(3+2r)(2+3r)(1+4r)(4+r)}{(7+3r)(3+7r)(r+1)(7+36r+7r^2)} & \text{N=5,} \end{cases} \tag{3.39}$$

where the superscript ex emphasizes that these are exact values, and r is the ratio f_1/f_2. We

calculate the relative difference between $\widetilde{\mathcal{F}}_1^{\text{ex}}(0)$ and the $\epsilon \rightarrow 0$ limit of the EMT nearest neighbor memory, F_{eff}, given by Eq. (3.38) as follows

$$\frac{1}{f_2} \left[\frac{F_{\text{eff}} - \widetilde{\mathcal{F}}_1^{\text{ex}}(0)}{\widetilde{\mathcal{F}}_1^{\text{ex}}(0)} \right],$$

and plot it in Fig. 3.11 for $N = 3, 4, 5$. Relative difference decreases with increasing system size or when the ratio f_1/f_2 gets closer to 1. EMT predicts the correct value for $f_1/f_2 = 1$ as expected.
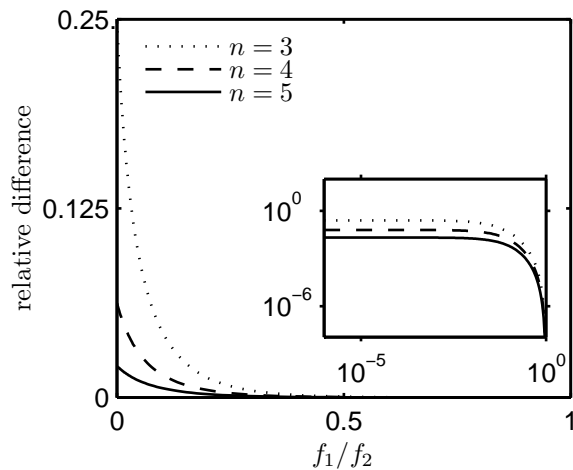
Figure 3.11: Relative difference between the nearest neighbor effective rates calculated from the EMT and an exact numerical procedure as given by Eqs. (3.38) and (3.39), respectively as a function of f_1/f_2. The disorder is characterized by a double-delta distribution with $\alpha = 0.5$.

3.9 Effects of correlations

In this section we go beyond the results obtained by Kenkre, Kalay and Parris [16], and report new results not published elsewhere.

Suppose that we generate random chains with bonds whose transfer rates are drawn from a distribution $\rho(F_1, F_2, ...F_N)$, which is simply the probability that the bond between

sites 1 and 2 has transfer rate F_1 and the one between sites 2 and 3 has F_2 and so on. We will focus our interest on infinite chains so, $N \to \infty$. If we perform an ensemble average over all random chains generated in this fashion, the result will be translationally invariant and we can describe the system by using the effective medium equation (3.10) as we discussed earlier. Let $\widetilde{\mathcal{F}}(\epsilon)$ be the Laplace transform of the EMT memory for this chain. Consider replacing two of the bonds, say the one between sites q and $q + 1$, and r and $r + 1$ with bonds that have transfer rates f_q and f_r instead of the memory $\widetilde{\mathcal{F}}(\epsilon)$. Then the generalized master equation

$$\frac{dP_m}{dt} = \int_0^t ds \mathcal{F}(t - s)(P_{m+1} + P_{m-1} - 2P_m) + \Delta_m \tag{3.40}$$

where

$$\Delta_m = \sum_{i=q,r} \left[\int_0^t ds \mathcal{F}(t - s)(P_{i+1} - P_i) - f_i(P_{i+1} - P_i) \right] (\delta_{m,i+1} - \delta_{m,i}). \tag{3.41}$$

describes non-Markoffian transport in a 1-D chain that is translationally invariant except for two links between the sites q and $q + 1$ and r and $r + 1$. The Laplace transform of the solution of Eq. (3.40) can be written as

$$\widetilde{P}_m = \sum_n P_n(0)\widetilde{\psi}_{m-n} + \sum_n \widetilde{\Delta}_n\widetilde{\psi}_{m-n}, \tag{3.42}$$

where $\widetilde{\psi}_l$ is the propagator for the infinite translationally invariant chain in the Laplace domain, given by

$$\widetilde{\psi}_l = \frac{1}{\sqrt{\epsilon\left(\epsilon + 4\widetilde{\mathcal{F}}\right)}} \left[\frac{\epsilon + 2\widetilde{\mathcal{F}} - \sqrt{\epsilon\left(\epsilon + 4\widetilde{\mathcal{F}}\right)}}{2\widetilde{\mathcal{F}}} \right]^{|l|} \tag{3.43}$$

After doing some algebra, the solution of Eq. (3.40) can be written as

$$\widetilde{P}_m = \widetilde{\eta}_m + \Omega_m, \tag{3.44}$$

where $\widetilde{\eta}_m = \sum_n P_n \widetilde{\psi}_{m-n}$, and Ω_m is

$$
\begin{aligned}
\Omega_m = & \left[F^q \left(\widetilde{\psi}_{m-q-1} - \widetilde{\psi}_{m-q} \right) \right] \left[F^r \widetilde{\phi}_{q-r} \eta^r + \left(1 - 2F^r \left(\widetilde{\psi}_0 - \widetilde{\psi}_1 \right) \right) \widetilde{\eta}^q \right] \\
& + F^r \left(\widetilde{\psi}_{m-r-1} - \widetilde{\psi}_{m-r} \right) \left[F^q \widetilde{\phi}_{q-r} \eta^q + \left(1 - 2F^q \left(\widetilde{\psi}_0 - \widetilde{\psi}_1 \right) \right) \widetilde{\eta}^r \right] \\
& \times \left[\left(1 - 2F^q \left(\widetilde{\psi}_0 - \widetilde{\psi}_1 \right) \right) \left(1 - 2F^r \left(\widetilde{\psi}_0 - \widetilde{\psi}_1 \right) \right) - F^r F^q \widetilde{\phi}_{q-r}^2 \right]^{-1},
\end{aligned} \tag{3.45}
$$

with $F^i = \widetilde{\mathcal{F}} - f_i$, $\widetilde{\phi}_i = 2\widetilde{\psi}_i - \widetilde{\psi}_{i+1} - \widetilde{\psi}_{i-1}$ and $\widetilde{\eta}^i = \widetilde{\eta}_{i+1} - \widetilde{\eta}_i$.

Our aim is to average over f_q and f_r in a proper way that depends on the correlations between them to restore the translational invariance and obtain a self-consistency equation analogous to Eq. (3.14) which was obtained for the case in which disorder is uncorrelated.

To do this, we focus on a chain in which transfer rates can take only two values, like in the double-delta distribution. In this picture, the transfer rates of bonds between different sites, say f_q and f_r, are correlated random variables that take on one of the two values f_1 or f_2. Correlation between the values of f_q and f_r arise according to the nature of interactions between the two. We consider a situation in which neighboring bonds with transfer rate f_2 interact with energy $-\Delta$ so that they attract or repel each other when $\Delta > 0$ and $\Delta < 0$ respectively. This system can be thought as a 1-D Ising model in which the mth spin is analogous to the mth link in the chain, so that $\sigma_m = 1$ and $\sigma_m = -1$ correspond to transfer rates f_1 and f_2 respectively. As two point correlation functions in the 1-D Ising model is analytically calculable, we find the joint probability distribution, $P(f_q, f_r)$, that the bond between sites q and $q + 1$ has transfer rate f_q and the bond between sites r and $r + 1$ has transfer rate f_r to be

$$
\left\langle \left(\frac{1 - \sigma_q}{2} \right) \left(\frac{1 - \sigma_r}{2} \right) \right\rangle = P(f_1^q, f_1^r) = \alpha^2 + \alpha \left(1 - \alpha \right) x^{|q-r|}, \tag{3.46}
$$

$$
\left\langle \left(\frac{1 - \sigma_q}{2} \right) \left(\frac{1 + \sigma_r}{2} \right) \right\rangle = P(f_1^q, f_2^r) = P(f_2^q, f_1^r) = \alpha \left(1 - \alpha \right) \left(1 - x^{|q-r|} \right), \tag{3.47}
$$

$$
\left\langle \left(\frac{1 + \sigma_q}{2} \right) \left(\frac{1 + \sigma_r}{2} \right) \right\rangle = P(f_2^q, f_2^r) = \left(1 - \alpha \right)^2 + \alpha \left(1 - \alpha \right) x^{|q-r|}, \tag{3.48}
$$

where

$$x = \frac{\sqrt{1 - 4\alpha(1 - \alpha)\left(1 - e^{\beta\Delta}\right)} - 1}{\sqrt{1 - 4\alpha(1 - \alpha)\left(1 - e^{\beta\Delta}\right)} + 1},$$

α is the fraction of bonds that have transfer rate f_1, which is equivalent to the probability of finding a bond with transfer rate f_1, and $\beta = 1/k_B T$. Note that α is a quantity proportional to the external field in the analogous Ising model picture.

Now we are in a position to suggest the proper averaging scheme we mentioned earlier which restores translational invariance. Remember that the Laplace transform of the probability of finding the random walker at site m, is given by

$$\widetilde{P}_m = \widetilde{\eta}_m + \Omega_m. \tag{3.49}$$

Ensemble averaging over all different realizations of the chain, we get

$$\left\langle \widetilde{P}_m \right\rangle_{ens} = \widetilde{\eta}_m + \langle \Omega_m \rangle_{ens}. \tag{3.50}$$

As the ensemble averaging makes the system translationally invariant, $\langle \Omega_m \rangle_{ens}$ must vanish so that the $\left\langle \widetilde{P}_m \right\rangle_{ens}$'s are identically equal to $\widetilde{\eta}_m$'s which are the solutions in the absence of the defective bonds. For the type of bond-bond interactions considered here, the two point correlation functions are known. Using this knowledge, we propose that the ensemble averaging $\langle \cdot \rangle_{ens}$ is explicitly given as

$$\langle \cdot \rangle_{ens} = \sum_{\substack{q=0 \\ r=0}}^{N} \sum_{f_q, f_r = f_1, f_2} P(f_q, f_r) [\cdot]. \tag{3.51}$$

The summations in Eq. (3.51) makes sure that correlations between the pairs f_q and f_r are going to be washed out, by averaging over all possible configurations, i.e. all possible (f_q, f_r) pairs for all q and r, according to the joint probability distribution $P(f_q, f_r)$.

Therefore, we have

$$\langle \Omega_m \rangle_{ens} = \sum_{\substack{q=0 \\ r=0}}^{N} \sum_{f_q, f_r = f_1, f_2} P(f_q, f_r) \Omega_m = 0, \tag{3.52}$$

for all m. The expressions simplify greatly in the limit $\epsilon \to 0$. In this limit we have

$$\lim_{\epsilon \to 0} \left(\widetilde{\psi}_{m-q-1} - \widetilde{\psi}_{m-q} \right) = \lim_{\epsilon \to 0} \left(\widetilde{\psi}_{m-r-1} - \widetilde{\psi}_{m-r} \right) = \lim_{\epsilon \to 0} \left(\widetilde{\psi}_0 - \widetilde{\psi}_1 \right), \tag{3.53}$$

$$\lim_{\epsilon \to 0} \widetilde{\eta}^q = \lim_{\epsilon \to 0} \widetilde{\eta}^r = -\frac{1}{\widetilde{\mathcal{F}}(0)} \sum_n P_n(0), \tag{3.54}$$

$$\lim_{\epsilon \to 0} \widetilde{\phi}_k = 0 \quad \text{for } k > 0. \tag{3.55}$$

Therefore, in the limit $\epsilon \to 0$ Eq. (3.52) becomes

$$\sum_{f_q, f_r = f_1, f_2} \sum_{\substack{q=0 \\ r=0}}^{N} P(f_q, f_r) \left[\frac{\widetilde{\mathcal{F}}(0) - f_q}{f_q} + \frac{\widetilde{\mathcal{F}}(0) - f_r}{f_r} \right] = 0,$$

which is also equal to

$$\sum_{q=0}^{N} \sum_{f_q = f_1, f_2} P(f_q) \left[\frac{\widetilde{\mathcal{F}}(0) - f_q}{f_q} \right] + \sum_{r=0}^{N} \sum_{f_r = f_1, f_2} P(f_r) \left[\frac{\widetilde{\mathcal{F}}(0) - f_r}{f_r} \right] = 0, \tag{3.56}$$

where

$$P(f_r) = \sum_{q=0}^{N} \sum_{f_q = f_1, f_2} P(f_q, f_r),$$

$$P(f_q) = \sum_{r=0}^{N} \sum_{f_r = f_1, f_2} P(f_q, f_r),$$

are the marginal probability distributions. Note that

$$P(f_1) = \alpha,$$

$$P(f_2) = 1 - \alpha,$$

for the marginal probability distributions, regardless of the values of q and r. Therefore, Eq. (3.56) is equivalent to Eq. (3.17) which we obtained for uncorrelated disorder. Therefore, this indicates that at long times, diffusion coefficient does not depend on the type of correlations. In order to test the validity of this, we generate disordered lattices by simulating the 1-D Ising model with external magnetic field. This way we guarantee that correlations between links with different transfer rates are such that Eqs. (3.46-3.48) are

α	$J = -1$		$J = 1$	
0.75	$B = 2.1$	$\beta = 1.46$	$B = 0.02$	$\beta = 1.48$
0.5	$B = 0$	$\beta = 1.00$	$B = 0$	$\beta = 1.00$
0.25	$B = -2.1$	$\beta = 1.46$	$B = -0.02$	$\beta = 1.48$

Table 3.2: Parameters used in the generation of chains with correlated disorder. Similar links repel or attract each other for $J = -1$ and $J = 1$, respectively.

satisfied. In order to simulate the Ising model, we start with a chain in which the ratio of the number of links with transfer rate f_1 to those with f_2 is approximately $\alpha/(1 - \alpha)$ and use the Metropolis algorithm to minimize the energy of the total system, which is given by

$$E = -J \sum_{i,j}' \sigma_i \sigma_j - B \sum_i \sigma_i,$$

where the primed sum is over nearest neighbors only and $\sigma_i = 1$ and $\sigma_i = -1$ represent the two possible values of the transfer rate of the ith link, which are f_1 and f_2, respectively. At each step of the simulation, we calculate what would the change in the energy of the system be if we change the transfer rate of a randomly chosen link from f_1 to f_2 or from f_2 to f_1 depending on its value just before that step of the simulation. If the change lowers the energy of the system, we modify the transfer rate of the chosen link. However if the change increases the energy of the system, then we accept it with probability $e^{-\Delta E \beta}$. This helps avoid the system from getting stuck in a local minimum in the energy landscape. Following this procedure, we generate random chains in which similar links either repel or attract each other. When the interaction between similar links is repulsive ($J < 0$) the chain ends up having a grained structure and when it is attractive ($J > 0$), clusters of links that have the same transfer rate form. An illustration of various random chains generated in this way are displayed in Fig. (3.12). Typical parameter values used in different cases are given in the Table 3.2.

In Fig. 3.13, we plot $D(t)$ as a function of dimensionless time for random chains with different correlation types. From top to bottom each set of 3 curves correspond to
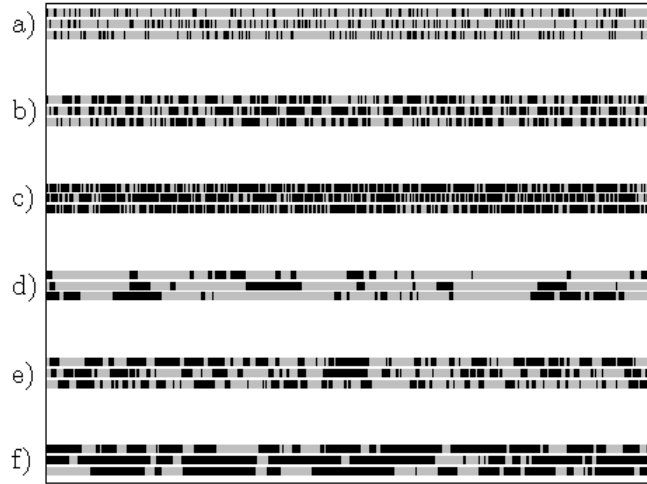
Figure 3.12: Illustration of various realizations of the random chain with repulsive and attractive link interactions. Black and gray indicate bonds with different transfer rates. The cases a,b, and c correspond to repulsive link interactions ($J < 0$) for various concentrations of different types of links. For each case, three different realizations of the chain are displayed. The cases d, e and f display the same information for when the interaction is attractive ($J > 0$).

a different value of α, the concentration of f_1. In each set, data represented by the thick solid line, dashed line and thin solid line correspond to attractive, neutral, and repulsive link-link interactions. Although the behavior of $D(t)$ for different correlation types is quite different for intermediate times, its asymptotic value seems to depend only on α. This outcome supports the statement we made earlier about the asymptotic value of $D(t)$ being independent from the correlations in the disorder (see Eq. (3.56)).

Another result we would like to mention in passing is about the asymptotic value of $d\langle m \rangle / dt$ for different correlation types, within the presence of an external field that introduces a bias in transfer rates. $d\langle m \rangle / dt$ is proportional to the mobility of particles which is a common and important transport property in many systems. Previously, it was found that [103] for particles that move under the influence of an external field in a random po-
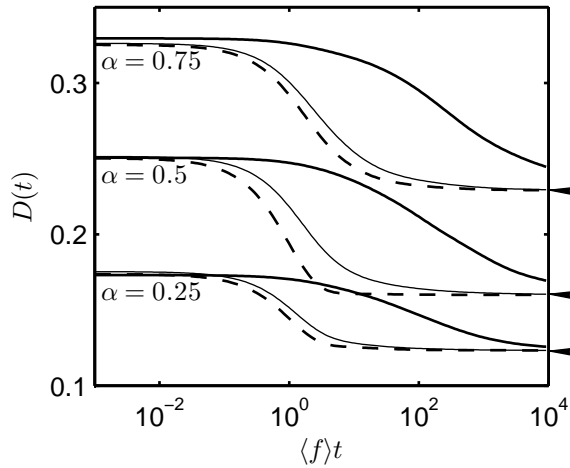
Figure 3.13: Diffusion coefficient as a function of dimensionless time for various different correlation types. Disorder is characterized by a double-delta distribution with $f_1 = 0.4$, $f_2 = 0.1$ and α, the concentration of f_1, takes the values 0.75, 0.5 and 0.25 from top to bottom. Thick solid lines and dashed lines correspond to attractive and repulsive link interactions, respectively, whereas the thin solid line shows the behavior of $D(t)$ when the interactions are neural (uncorrelated disorder). The arrowheads on the right represent the asymptotic value of $D(t)$ obtained from the EMT. It is seen that $D(t)$ is not modified by the different correlation types we consider here.

tential, mobility depends on the spatial correlations present in the random potential. We numerically calculate $d\langle m \rangle/dt$ for different types of correlations when the transfer rates are uniformly biased to the right by an amount Δf. Fig. 3.14 shows the results for a couple of different values of the bias Δf. Interestingly, asymptotic value of the mobility does not depend on the correlation type in our system.

3.10 Concluding remarks

Our objective in this chapter is to explore the properties of random walk in disordered lattices in 1-D, by using the effective medium theory. In the past, the effective medium theory was used to calculate the properties of many disordered systems including transport in disordered lattices, but most of these treatments were restricted to calculating steady
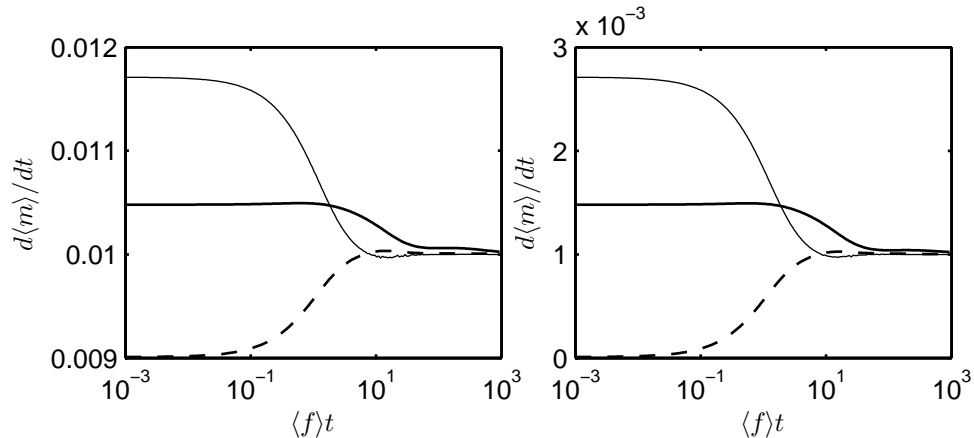
Figure 3.14: Ensemble averaged velocity as a function of dimensionless time for different values of the bias Δf. Disordered transfer rates are sampled from a double-delta distribution with $f_1 = 0.4$, $f_2 = 0.1$ and $\alpha = 0.25$. The dashed, the thick and the thin solid lines correspond to repulsive, attractive and neutral link interactions. The value of the bias is $\Delta = 0.01$, and $\Delta = 0.001$ for the plot on the left and the right, respectively. For larger values of the bias, we observe similar behavior. Here we display results for small values of Δf in order to make sure that the mobility does not saturate (see ref. [103], Fig. 2).

state values of the quantities of interest (see references in the introduction for some exceptions). Here, we show how one can obtain a prescription that can be used to calculate time-dependent quantities that pertain to random walk in a disordered lattice, and obtain expressions for the time-dependent diffusion coefficient and mean square displacement in 1-D. We consider a 1-D chain of sites with nearest neighbor interactions and disordered transfer rates, and show how to convert the disorder in space into nonlocal evolution in time. In other words, we show that it is appropriate to replace the Master equation (3.1) by the generalized master equation (3.3) which has the memory $\mathcal{F}(t)$. The prescription of obtaining $\mathcal{F}(t)$ given the characteristic properties of the disorder is contained in Eq. (3.16), as given in ref. [16]. One of our most important results is that in most of the cases, this replacement is meaningful not just for asymptotic times, but for all times, provided that we are interested in quantities that are ensemble averaged over the different realizations of the disorder. Figs. 3.2 and 3.3 show the comparison between simulations and theoretical findings concerning the diffusion coefficient for all times, and for different initial conditions.

We also show the cases in which the effective medium theory makes poor predictions in Figs. 3.5 and 3.6, which corresponds to the cases in which the transfer rates of some of the links in the chain vanish.

In this chapter, we also present a few other interesting findings that have not been previously explored in detail. These are the appearance of long range memories and the effects of finite system size as discussed in ref. [16], and the effects of correlated disorder.

The disordered system we consider is a chain of sites that are connected with disordered transfer rates and the random walker is allowed to hop back and forth between nearest neighbor sites only. An immediate question that arises is: how long will the range of the memory functions be, in the generalized master equation (3.3) ? By calculating memory functions that connect sites that are not necessarily nearest neighbors, we find that even though the original system only has nearest neighbor interactions, longer range memory functions naturally develop in the effective medium description. In Fig. 3.9 we display results corresponding to memory functions with longer range (or of higher order). However, it should be noted that the amplitude of the longer range memory functions are much smaller than the nearest neighbor memory function so that in most of the cases they can be neglected.

For the most part, we are interested in infinite chains, but we also include results about the effects of finite system size in our study. When the system size gets smaller and smaller, the predictions of the effective theory made by using the nearest neighbor memory function deviate more and more from the numerically found results as shown in Fig. 3.11. One of the reasons for this growing deviation is the increasing importance of long range memory functions in small systems. Another interesting behavior that is observed in systems of finite size is the vanishing of the effective transfer rate at a nonzero concentration of broken links. In an infinite chain, if the probability of finding a link with zero transfer rate, a broken link, is nonzero, then the effective transfer rate will vanish. However, for finite systems, our findings [16] indicate that the effective transfer rate can be nonzero even for

a nonzero concentration of broken links, as shown in Fig. 3.10.

Lastly, we present some findings on random walks in a 1-D chain with correlated disorder in Sec. 3.9. Our results indicate that, interestingly, at asymptotic times, the diffusion coefficient does not depend on whether the random variables that characterize the transfer rates of the links are correlated or not. However, for intermediate times, we see a consistent difference in the diffusion coefficient when the characteristics of the joint probability of the distribution of transfer rates change.

Chapter 4

An analysis of transient dynamics and pattern formation in some reaction-diffusion systems

4.1   Introduction

Reaction-diffusion systems have been used to model a large number of phenomena, mainly in physics, chemistry and biology. Many chemical reactions occur in a medium in which reactants diffuse and encounter each other which results in a set of products. The concentration of chemical species in such chemical reactions can naturally be described with the following set of partial differential differential equations

$$\frac{\partial u_i}{\partial t} = D_i \nabla^2 u_i + f_i(u_1, u_2, ..., u_N), \tag{4.1}$$

where ∇ is the Laplacian operator in the space that the system occupies, D_i is the diffusion coefficient of the ith species, and f_i is a, usually nonlinear, function of u_i's that describes how species react with each other. A well known class of chemical reactions that have been

modeled in this way is the Belusov-Zhabotinskii reaction [20, 21]. The time evolution of the concentrations u_i in these type of systems turns out to be very rich, and can involve periodic oscillations or may display chaotic behavior [104, 105].

One of the first problems that was studied using reaction-diffusion equation is about population genetics. In his seminal paper published in 1937 [17], Fisher employed an equation of the following form to describe the spread of advantageous genes in a population

$$\frac{\partial u}{\partial t} = D\frac{\partial^2 u}{\partial x^2} + au(1 - u), \tag{4.2}$$

where D is a diffusion constant and a is a characteristic rate. This equation was also used by Kolmogorov, Petrovskii and Piskunov [18] around the same time, and now it is referred to as the Fisher-Kolmogorov-Petrovskii-Piskunov(FKPP) equation. For more examples on the use of reaction-diffusion equations in population dynamics and ecology, see e.g. refs. [106, 107]. Recent work on those equations particularly directed at animal movement in the theory of the spread of epidemics such as in the Hantavirus, is due to Kenkre and collaborators [108, 109, 110, 111, 112, 113].

Another interesting aspect of the reaction-diffusion systems is that they can produce patterns. In many biological systems, patterns arise in a homogeneous distribution of matter, for instance during the process of morphogenesis [106]. Therefore, many problems in developmental biology include reaction-diffusion systems, and can be quantitatively modeled by using systems of equation such as Eq. (4.1). Patterns can also arise in reaction-diffusion systems as a result of spatially nonlocal interactions [114, 22, 115].

Some other examples of studies that involve reaction-diffusion systems are: flame propagation [116, 117], propagation of pulses in nerves [118, 119], aggregation [120], and deposition [121]. In addition to these, there are many studies whose goals are to generalize the reaction-diffusion systems so that they display richer phenomena. A couple of studies in this direction include allowing for convective transport [122, 123], and non-diffusive

transport [124, 125] in the system.

This chapter is divided into two parts and the first part is about investigating the time evolution of an initial condition in three reaction-diffusion systems that give rise to front propagation. The traveling front speeds and shapes can be analytically calculated in the cases that we consider, providing us with more motivation for choosing them. A great deal of the results presented in this section are published in the article of Giuggioli, Kalay, and Kenkre [126] in which the author of this thesis took part. The second part is about pattern formation in a reaction-diffusion system with spatially non-local interactions. In this part, we first summarize some results that are already known in the literature for the FKPP equation and then present new results on the generalization of the problem.

This chapter is organized in the following way. The first part on understanding the transient behavior in some reaction systems and spans the sections 4.2 through 4.5. The second part begins in Sec. 4.6 and is concerned with pattern formation in reaction-diffusion systems with nonlocal interaction terms. In Sec. 4.3, we present the nonlinear reaction terms associated with the reaction-diffusion systems we are interested in, give the corresponding traveling front solutions that are obtained analytically, and for a particular case, show how to solve a reaction-diffusion equation for traveling fronts, for illustrative purposes. In Sec. 4.4 the method we use to study the transient behavior is explained in detail and the results of our analysis are given. The next section, Sec. 4.5 is concerned with the linear stability analysis of the traveling fronts we consider and is included for the completeness of our analysis. Sec. 4.6 marks the beginning of the second part of this chapter, and is about a different sub-topic, viz., pattern formation in a reaction-diffusion system. In this section, we first examine the formation of patterns in FKPP equation with a spatially nonlocal interaction term and then present a generalization of it by allowing for anomalous diffusion. In Sec. 4.7, we present the method used in the numerical solution of the reaction-diffusion equation involved and present our results. This chapter ends with Sec. 4.8 and is reserved for concluding remarks.

4.2 A brief introduction to traveling fronts

As the examples we gave in the introduction show, reaction-diffusion systems can display a wide range of features. In this section we will only be interested in a particular feature of the reaction-diffusion (R-D) systems, which is giving rise to traveling fronts. A traveling front is a particular kind of wave that propagates along the medium while preserving its shape. Front propagation in many R-D systems has been extensively studied and a vast amount of results have been collected [127, 128, 129]. A couple of problems that attracted a substantial amount of attention in this field include: finding the relation between initial conditions and the final front speed and shape [130, 131], and investigating the relaxation behavior in the system while the front speed approaches its asymptotic value [127, 128, 129].
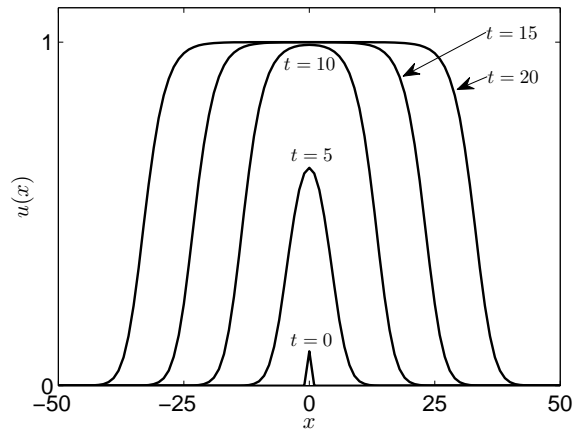
Figure 4.1: Time evolution in the FKPP equation, given in Eq. (4.2) with $D = 1$. The initial condition is $u(x, 0) = 0.1$ for $x = 0$ and 0 elsewhere.

In Fig. 4.1, we show the time evolution of an initial condition in the 1-D FKPP equation, given in Eq. (4.2). Initially $u(x) = 0.1$ for $x = 0$ and 0 otherwise. After a transient period, the solution of the FKPP equation takes the form of a traveling front. For the FKPP equation initial conditions that have compact support always lead to the formation of a traveling front that moves with the speed $v = 2\sqrt{D}$ [129]. The relation between

the initial conditions and the speed of the traveling front it evolves into has been studied extensively and some references on this subject will be given below.

In this chapter we restrict our attention to R-D systems in 1-D, which are described by

$$\frac{\partial u}{\partial t} = D\frac{\partial^2 u}{\partial x^2} + af(u),$$
(4.3)

where $u = u(x, t)$ is the density of the entity under consideration, D is the diffusion constant, a a growth rate and $f(u)$ the nonlinearity. The nonlinearities that we are interested vanish at $u = 0$ and $u = 1$, such that $u = 0$ and $u = 1$ are steady states.
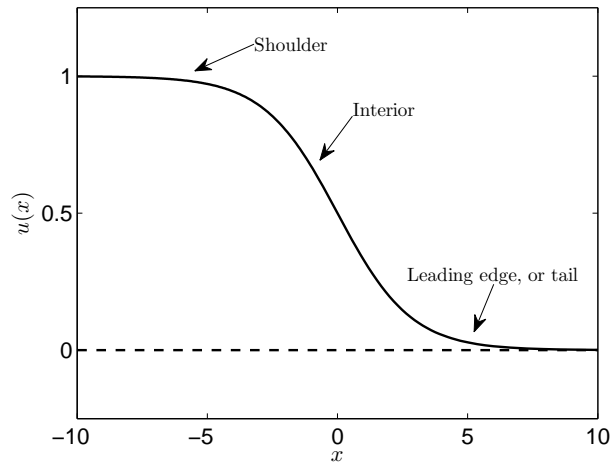
Figure 4.2: Schematic illustration of a traveling front. Here we label the regions of the front to which we will refer frequently in the text.

The characteristics and propagation mechanism of the front depends on the stability properties of the states that it connects. The traveling front connects states that are the fixed points of the R-D equation, i.e. the values of u for which $\partial u/\partial t = 0$. If the nonlinearity satisfies the following conditions

$$f'(0) > 0,$$
(4.4)

$$f'(u) < f'(0)$$
(4.5)

for $0 < u \leq 1$, then the characteristics of the traveling front are dominantly determined by its leading edge [132, 127], where $u \approx 0$. See Fig. 4.2 for the terminology used in describing different parts of a traveling front. Fronts of this type are commonly called pulled fronts as the leading edge determines the essential dynamics, and thus pulls the rest of the front [127, 133, 129]. In this case, it is possible to calculate the speed of the front by considering the R-D equation obtained by linearizing $f(u)$ around $u = 0$. The FKPP equation is one of the equations that give rise to pulled fronts. In this regime, the speed of the front relaxes to its asymptotic value algebraically [128, 129]. It turns out that for pulled fronts, the speed of the front can assume many values that are greater than a minimum speed v_{min}. The problem of which speed is selected was analyzed by using the linear marginal stability condition (see Van Saarloos [127] and references therein for details).

When the nonlinearity does not satisfy the conditions given by Eqs. (4.4) and (4.5) such that $f'(u)$ is not equal to its maximum value at $u = 0$, linearizing $f(u)$ around u does not give correct results for the speed of the front. In this case the dynamics of front propagation is predominantly determined by the interior of the front [128, 133, 129], where $f'(u)$ attains its maximum value. These types of fronts are called pushed fronts [134], as the interior of the front drives it. The speed of the traveling fronts of this kind converges to its asymptotic value exponentially [128]. The problem of speed selection for this regime was analyzed by employing the nonlinear marginal stability condition [128].

The nonlinearities we will consider in this chapter all satisfy $f'(0) = 0$ and attain a nonzero maximum value for $u > 0$. Therefore, the R-D systems we will be interested in give rise to pushed fronts. As mentioned in ref. [126], nonlinearities of this form have been used to study flame propagation [116, 117], certain autocatalytic chemical reactions [135] and calcium deposition in bone formation [21]. In flame propagation, the traveling front may represent the temperature profile [116] as well as the concentration of the reacting species [117], in chemical reactions, the order of the autocatalysis [135], and in calcium

deposition, the crystalline clusters that grow over the bulk of the bone proportionally to the square of its mass [136]. In population dynamics, diffusion-reaction systems with this type of nonlinearity can be used to model populations that display the weak Allee effect [137, 138]. If the growth rate of a population becomes negative for very low population densities, the system is said to display a strong Allee effect. If the growth rate is vanishingly small but positive for low population densities, the term "weak Allee effect" is used to describe the situation. The nonlinearities we consider have the properties $f(0) = 0$ and $f'(0) = 0$. Therefore, they can be employed to study populations that exhibit the weak Allee effect.

It is only in very rare instances that it is possible to obtain the analytic solution of a diffusion-reaction equation with a nonlinear term, as a function of time. Therefore, it is a difficult task to predict how an initial condition is going to evolve in these systems. Our aim is to contribute to the understanding of this problem by focusing on a particular aspect of it. In our study, we consider three R-D equations that can be solved exactly for the traveling front. If we use the traveling front solution as the initial condition in these equations, we know that it will not change in time. Instead, we slightly modify the traveling front solution in a few different ways, use it as the initial condition and observe a quantity that measures the difference between the evolving solution and the eventual traveling front solution. We describe this procedure in detail in Sec. 4.4 where we also give a quantitative as well as a qualitative interpretation of the results.

4.3   The reaction terms and corresponding traveling wave solutions

We will consider three different nonlinear terms $f(u)$ such that $f'(0) = 0$, and the corresponding traveling wave solutions. Among these, two of them behave like a quadratic for

$u \approx 0$, whereas the third behaves like a cubic. For demonstrative purposes, we will show the details of obtaining the traveling wave speed and shape for the Zel'dovich - Frank-Kamenetskii (ZF) equation [139]. Then the explicit forms of these nonlinearities along with the traveling wave solutions they lead to will be presented. In Sec. 4.5 of this chapter, the stability of these traveling fronts will be discussed.

4.3.1 Solution of the ZF equation in a moving frame

The ZF equation is given by [139]

$$\frac{\partial u}{\partial t} = \frac{\partial^2 u}{\partial x^2} - \gamma(1 - u)(\mu - u)u, \tag{4.6}$$

where t and x are appropriately redefined to eliminate the diffusion coefficient D. Fig. 4.3 shows a plot of the nonlinear term of this equation with a particular choice of parameters γ and μ. Later on, we will focus on a particular form of this nonlinearity with $\gamma = 1$ and $\mu = 0$. We are interested in solving Eq. (4.6) for traveling fronts. Solutions of this type
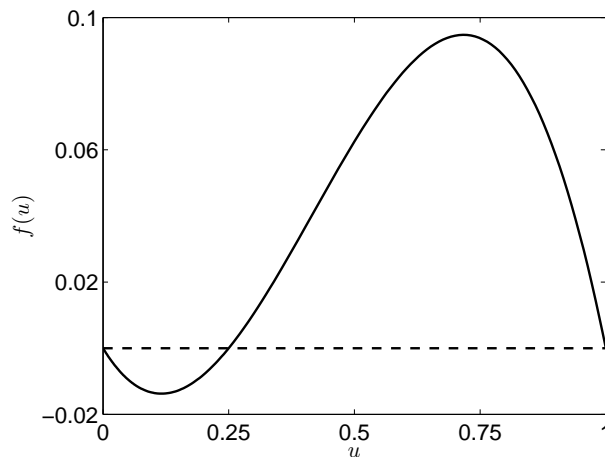
Figure 4.3: The nonlinear reaction term of Eq. (4.6) as a function of u for $\gamma = 1$ and $\mu = 0.25$.

have a fixed shape and move with constant speed. Therefore, if we switch to a reference

frame that moves with the speed of the traveling front, we should see a profile that does not change in time. To do this, we follow the standard procedures (see for instance refs. [129, 106]), and define a new variable $z = x - vt$ where v is the speed of the traveling front. As a result of this change of variables, the differentials transform in the following way

$$\frac{\partial}{\partial t} = \frac{\partial z}{\partial t}\frac{\partial}{\partial z} = -v\frac{\partial}{\partial z},$$
$$\frac{\partial}{\partial x} = \frac{\partial z}{\partial x}\frac{\partial}{\partial z} = \frac{\partial}{\partial z},$$

so that Eq. (4.6) can be rewritten as

$$\frac{d^2\tilde{u}}{dz^2} + v\frac{d\tilde{u}}{dz} - \gamma(1 - \tilde{u})(\mu - \tilde{u})\tilde{u} = 0 \tag{4.7}$$

where $\tilde{u} = \tilde{u}(z)$. For convenience we are going to drop the tildes on u from now on and u will be taken as a function of z only, unless otherwise stated. Let $J(u) = -du/dz$, then Eq. (4.7) becomes

$$\frac{dJ}{dz} + vJ + \gamma(1 - u)(\mu - u)u = 0. \tag{4.8}$$

Note that

$$\frac{dJ}{dz} = \frac{dJ}{du}\frac{du}{dz} = -J\frac{dJ}{du}.$$

Using this relation Eq. (4.8) can be expressed as

$$\frac{dJ}{du}J + vJ + \gamma(1 - u)(\mu - u)u = 0. \tag{4.9}$$

Suppose that we are interested in finding the traveling front solutions that connect the stable states $u = 0$ and $u = 1$. As a function of z, these fronts will look like the curve illustrated in Fig. 4.4, and they clearly satisfy

$$\lim_{z \to \infty} u = 0,$$

$$\lim_{z \to -\infty} = 1,$$

$$J(u) = -\frac{du}{dz}, \quad J(0) = J(1) = 0.$$
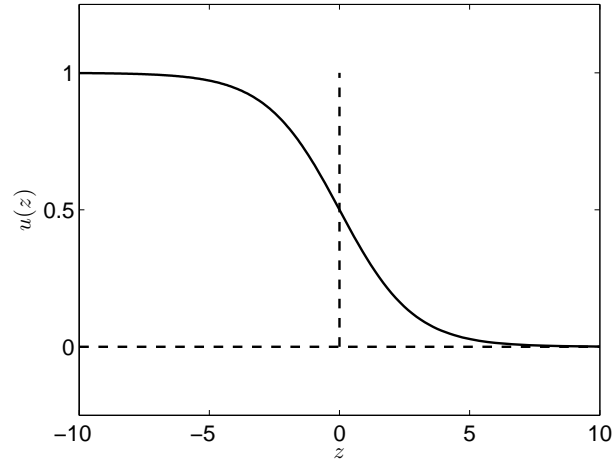
Figure 4.4: Schematic illustration of a traveling front that connects the states $u = 0$ and $u = 1$.

The properties of $J(u)$ leads one to consider the ansatz

$$J = \zeta u(1 - u),$$

where $\zeta \geq 0$ as $du/dz \leq 0$. Substituting this ansatz in Eq. (4.9), one obtains

$$u\left(2\zeta^2 - \gamma\right) + v\zeta + \mu\gamma - \zeta^2 = 0. \tag{4.10}$$

In order that Eq. (4.10) is satisfied, the coefficients of u and $u^0 = 1$ must vanish identically. Imposing this condition results in the following relations

$$\gamma = 2\zeta^2,$$

$$v = \sqrt{\frac{\gamma}{2}}(1 - 2\mu).$$

Therefore, the speed at which the front moves depends on the parameters γ and μ.

The shape of the front can be found by integrating $J(u)$

$$\int_{u(0)}^{u(z)} \frac{du}{u(1 - u)} = -\zeta \int_0^z dz.$$

In order to do the integration, we need to specify the value $u(0)$. Because we can take any point z in the moving frame as a reference point, $u(0)$ can be assigned any value in the

111

interval $(0, 1)$ without loss of generality. Choosing $u(0) = 1/2$ and evaluating the integral, one obtains the front shape

$$u(z) = \frac{1}{1 + e^{\sqrt{\frac{\gamma}{2}}z}}. \tag{4.11}$$

Note that the shape of the front does not depend on where the unstable fixed point μ is. The speed however, depends on μ and is positive for $\mu < 1/2$ and negative for $\mu > 1/2$. This is the exact and only traveling front solution of the ZF equation which connects the states $u = 0$ and $u = 1$, as it is known that [127, 128, 132] when the front connects two stable states, there can only be one solution. An intuitive way of understanding why the solution must be unique is thinking of the R-D equation as a Newton's equation of motion [127, 128, 132]. Replacing the variable z by t, which corresponds to time, in Eq. (4.7) gives

$$\frac{d^2u}{dt^2} = -v\frac{du}{dt} - \frac{dV}{du}, \tag{4.12}$$

where u is treated like the position variable of a particle moving under the influence of the potential $V(u)$ whose derivative is

$$-\frac{dV}{du} = \gamma(1 - u)(\mu - u)u, \tag{4.13}$$

and subject to a frictional force $-vdu/dt$, where the speed of the front acts like the friction coefficient. Fig. 4.5 shows $V(u)$ as a function of u. Note that $V(u)$ has a minimum at $u = \mu$. For illustrative purposes $\mu = 0.25$ in the plot. If the particle starts at $u = 0(u = 1)$, it will reach the point $u = 1(u = 0)$ if and only if the friction coefficient v has the right value. Otherwise, it will undershoot, or go over the destination point. The velocity of the traveling front, which is equal to the right value of the friction coefficient, is therefore unique. Note that this is not true for fronts connecting an unstable fixed point to a stable one, for instance in the FKPP equation.
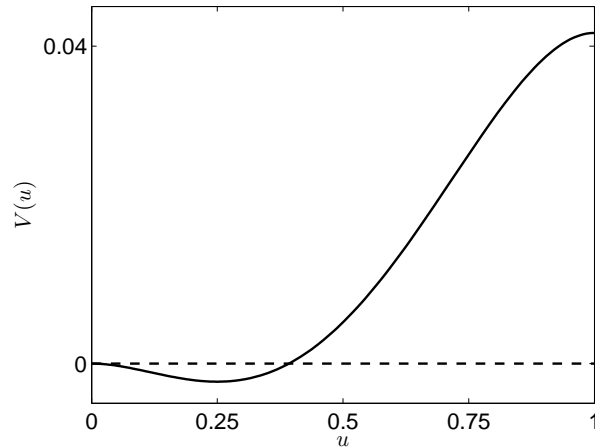
Figure 4.5: The potential $V(u)$ obtained by integrating Eq. (4.13) with respect to u. The parameter values are: $\gamma = 1$, $\mu = 0.25$

4.3.2 The three cases we consider

A particular form of the ZF nonlinearity

The nonlinear term that one obtains by setting b equal to 0 in the ZF equation [139] is

$$f(u) = u^2(1 - u). \tag{4.14}$$

In the rest of this chapter, we will refer to this function as the quadratic nonlinearity, because $f(u) \approx u^2$ for $u \approx 0$. Substituting it in Eq. (4.3) and solving the resulting equation for traveling waves, we get

$$u(z) = \frac{1}{1 + e^{z\sqrt{a/2D}}}, \tag{4.15}$$

where $c = \sqrt{Da/2}$ is the speed of the front.

A logarithmic nonlinearity

Another nonlinearity that behaves quadratically around $u = 0$ and has a shape similar to the previous one is

$$f(u) = (u + 1)\,[2 - \ln(2) + \ln(u + 1)]\ln^2(u + 1)\,[\ln(2) - \ln(u + 1)]. \qquad (4.16)$$

Although this expression looks complicated, the R-D equation it leads to can be solved analytically for traveling fronts [126]. Following the procedure we reviewed earlier, the traveling front shape and speed can be obtained as

$$u(z) = -1 + 2^{\left[1 + \frac{\ln(4/3)}{\ln(3/2)} 2^{z\sqrt{a/D}}\right]^{-1}}, \qquad (4.17)$$

$$c = \sqrt{Da}\,\ln(2). \qquad (4.18)$$

In all of the discussions that follow, we will call Eq. (4.16) the logarithmic nonlinearity.

A cubic nonlinearity

The last form of $f(u)$ that we are interested in studying differs from the others for small u, and behaves like a cubic around $u = 0$. It is expressed as

$$f(u) = \eta \sin(\pi u)\,[1 - \cos(\pi u)]. \qquad (4.19)$$

A nonlinear term of this form has been used in studying the dynamics of the angle between the electric field and the polarization in ferroelectric chiral smectic liquid crystals [140]. Note that it is periodic in u with period 2. In this study, we are interested in the cases for which $u \leq 1$. Hence, the periodicity of this nonlinear term does not cause any effects. The R-D equation that has this nonlinear term can be solved exactly for both the shape and speed of the traveling front. The results are

$$u(z) = \frac{2}{\pi}\arctan\left(e^{-z\sqrt{\eta\pi a/D}}\right), \qquad (4.20)$$

$$c = \sqrt{\eta\pi Da}. \qquad (4.21)$$

The main reason we consider the cubic nonlinearity is that while it is qualitatively very similar to the other two, it behaves quite differently for $u \approx 0$. Therefore, studying it can give us an idea about the effects of growth rate for small u on transient dynamics. Motivated by this, the parameter η, which controls the amplitude of the nonlinearity, is set equal to $\eta = 16/(81\sqrt{3})$ so that the peaks of the cubic and quadratic nonlinearities coincide.

In Fig. 4.6, each of these nonlinearities are plotted as function of u with the parameter values indicated above.
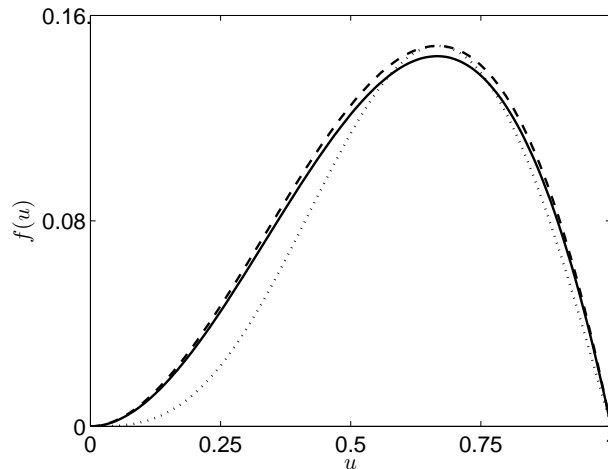
Figure 4.6: Plots of the logarithmic (solid curve), quadratic(dashed curve), and cubic(dotted curve) nonlinearities given by Eqs. (4.19), (4.14), and (4.19), respectively. For the cubic nonlinearity the value of η is chosen to be $16/(81\sqrt{3})$.

4.4 Our method of studying the transients and the results

As we stated in the introduction of this chapter, our interest lies in studying how slightly modified traveling front solutions evolve according to the R-D equations we consider, as they approach the exact front solution. This is what we mean by the transient and we do not consider the full time evolution in the system starting from an arbitrary initial condition.

In Fig. 4.2, we labeled the different parts of the front as the shoulder, the interior, and the tail. In obtaining the modified traveling fronts we would like to use as our initial condition, we modify either of these three parts of the exact traveling front solution, or a combination of them. Our analysis showed that modifying only the shoulder of the exact front does not result in very interesting behavior. Here, we will show results for three different modification types, which are

A) Changing the characteristic length $\sqrt{D/a}$ in the exact front solution, which modifies all three parts.

B) Replacing the interior of the front with a line segment, starting at $u = 0$ and ending at a point $u < 0$ where the line segment intersects the shoulder of the front.

C) Modifying both the interior and the tail of the front. In this case the interior is a function that is obtained by changing the characteristic length of the exact solution, and the tail is replaced by a line segment.

Fig. 4.7 illustrates all three types of modifications to the exact front solution.

In our analysis, for each nonlinearity we first consider an initial condition $u(x, 0)$ generated according to one of the cases A,B or C described above and numerically calculate a quantity that measures an aspect of the difference between the numerical solution and the exact traveling front. The quantity we chose is the relative excess speed defined as $(v(t) - c)/c$, where c is the speed of the exact front solution and $v(t)$ is the instantaneous speed of the evolving numerical solution given by

$$v(t) = \frac{d}{dt} \int_{-\infty}^{\infty} dx u(x, t), \tag{4.22}$$

which is the rate of change of area under the curve $u(x, t)$ and a natural definition of the speed. A similar approach is adopted in other studies also (see for instance ref. [122]). After calculating the behavior of the excess speed as a time series, we try to explain the
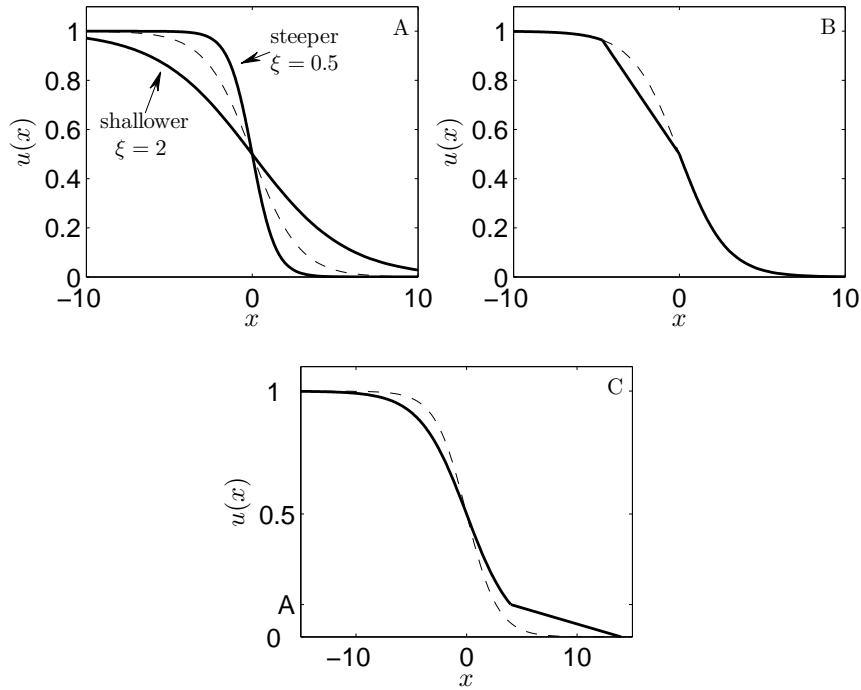
Figure 4.7: Illustration of the initial conditions employed in Secs. 4.4.1, 4.4.2, and 4.4.3. In (A), The initial condition is obtained by replacing the characteristic length $\sqrt{D/a}$ by $\sqrt{D/a}/\xi$ in the exact front solutions. For $\xi > 1$ and $\xi < 1$, the initial conditions formed are termed shallower and steeper than the exact front, respectively. In (B), the modification to the exact front consists of replacing a portion of its interior part with a line segment. The line segments begins at $u = 1/2$ and ends at a point with $u > 1/2$ where the line intersects the shoulder of the front. In (C), we modify both the interior and tail of the exact front to obtain the initial condition. The interior is made shallower than the exact front by adjusting the characteristic length as in (A), and the tail is simply replaced by a line segment starting at $u = A$ and going down to $u = 0$. We generate initial conditions of this type by modifying A while keeping the projection of the line segment on the x-axis at a constant length.

significance of its features and their dependence on the initial conditions. In the rest of this chapter, we will simply call $(v(t) - c)/c$ the excess speed.

In solving the reaction-diffusion equations numerically, we use an adaptive Adams-Bashforth-Moulton multistep integration method. The step size we used in discretizing the space variable x is 0.08 in units of $\sqrt{D/a}$, which is the characteristic length in the R-D

equations we consider. If the excess speed is is less than or equal to 10^{-8}, we argue that the numerical solution approached its asymptotic form, which is the exact traveling front solution.

In the next three subsections, we will present the time dependence of the excess speed as a function of initial condition parameters for each nonlinearity.

4.4.1 Case A

Suppose that we replace the characteristic length $\sqrt{D/a}$ in Eqs. (4.15, 4.17) and (4.20) by $\sqrt{D/a}/\xi$, where ξ is a dimensionless parameter. For $\xi > 1$, the derivative of this modified front will vary in a slower fashion compared to the case $\xi = 1$, which corresponds to the exact traveling front. In other words, this type of modified fronts are shallower than the exact front for all x. On the other hand, for $\xi < 1$ the modified front will be steeper than the exact front. Plots of modified fronts of this kind along with the exact front is given in Fig. 4.7 (A).

Considering such initial conditions and calculating the excess speed for each nonlinearity, we found that the instantaneous speed of the numerical solutions defined by Eq. (4.22) changes monotonically in time. Moreover, the relaxation to the asymptotic value of the front speed seems to be exponential in time. The inset in Fig. 4.8 shows the magnitude of the excess speed on semilogarithmic axes for different values of ξ, which indicates that at long times the excess speed decays exponentially. Therefore, one can find an exponential decay constant τ, which has the dimensions of $1/a$, for various values of ξ by appropriately performing a linear fit to the excess speed versus time plots. The main plot shows this decay constant τ as a function of the steepness of the modified front ξ. We immediately note that if the initial conditions are steeper than the exact front, $\xi < 1$, then τ does not depend on ξ and varies with the type of nonlinearity. Hence, initial conditions that are steeper than the exact front relax to the asymptotic speed in the same way. How-

ever, this is not true for $\xi > 1$. For initial conditions that are shallower than the exact front, τ depends on ξ as well as the type of nonlinearity. Similar qualitative results on the relaxation behavior have also been reported by Van Saarloos [128].
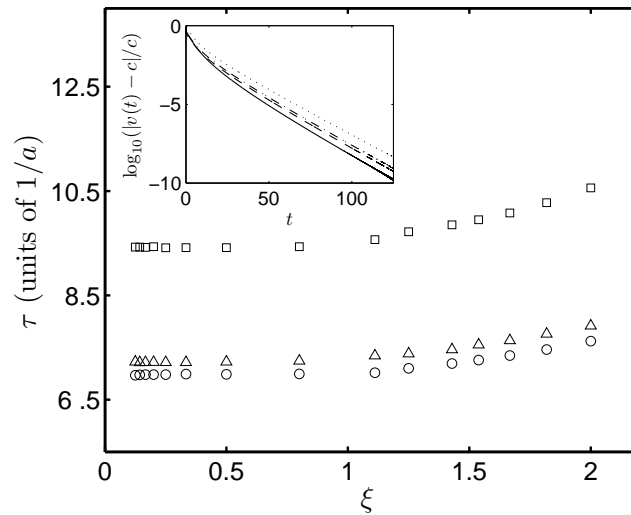
Figure 4.8: Characteristic decay time τ in units of $1/a$, plotted against the steepness of the initial condition ξ. For $\xi > 1$, the initial condition is shallower than the exact front, and for $\xi < 1$ it is steeper. The magnitude of the excess speed for various values of ξ is plotted on semilogarithmic axes in the inset. The solid, dashed, dash-dotted and dotted curves correspond to an initial condition with $\xi = 1.250, 1.429, 1.539,$ and 2, respectively.

The characteristic decay time τ is largest for the cubic nonlinearity and it is followed by the logarithmic and quadratic nonlinearities. This is not surprising as the time scales in the dynamics of the system should depend on the strength of the nonlinear term. as seen in Fig. 4.6, the quadratic nonlinearity is stronger than the logarithmic followed by the cubic for most values of u. Furthermore the cubic nonlinearity which gives rise to the largest decay times is significantly weaker than the other two around $u = 0$.

4.4.2   Case B

The transient behavior we saw in Case A was monotonic and not so interesting. Here we consider a different initial condition that gives rise to a slightly richer time evolution. Suppose that we modify the interior of the exact front solution so that part of it is replaced by a line segment. Obviously one can make a modification to the interior in many different ways, but it is convenient to consider a line segment as it is simple enough to be described by a single parameter. The initial conditions we consider in this subsection are depicted in Fig. 4.7. The modification consists of replacing the part of the interior by a line segment starting at $u = 1/2$ and ending at some value $u > 1/2$ at which the line segment and the exact front intersect. In order to characterize initial conditions of this type, we introduce the parameter α which is the ratio of the slope of the line segment to the slope of the exact front at $u = 1/2$. We are interested in assuming α values that lie in the interval $(0, 1)$ so that the initial condition we generate is shallower that the exact solution over its modified part.

In Case A, we saw that when the initial condition is shallower than the exact front for all x, the excess speed decays monotonically. In this case, the initial condition we consider is shallower than the exact front only over a finite portion of the space. At first one may expect to observe similar monotonic behavior again, but it turns out that the excess speed behaves quite differently for the interior-modified initial condition.

Fig. 4.9 shows the time evolution of the excess speed for each nonlinearity, for a particular value of α (Dependence of the features of the excess speed on α will be demonstrated in Fig. 4.10). Note that the excess speed no longer decays monotonically. A maximum in the excess speed versus time plot appears because of the following development. Instead of just reforming and approaching the exact front shape, the modified part of the front induces the lower part of the interior and the tail to become shallower than the interior and the tail of the exact front solution. Therefore, for a brief amount of time, the solu-

tion is shallower than the exact traveling front, and then it relaxes to the exact front shape which is steeper. It is well known that shallower fronts travel faster than steeper fronts [127, 128]. Therefore, it is natural to expect a maximum in the excess speed in the light of this argument.
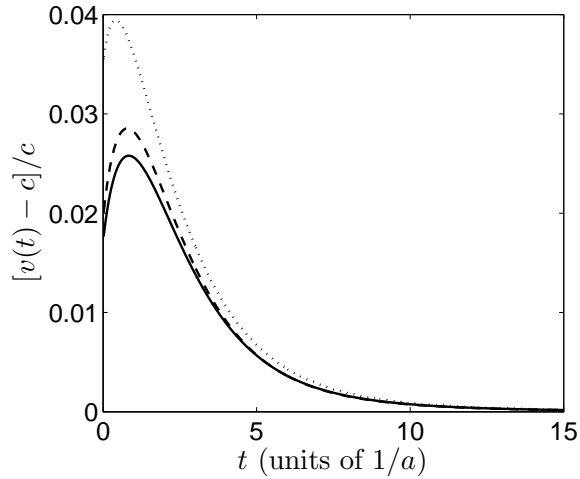
Figure 4.9: The nonmonotonic time evolution of the excess speed for interior modified initial conditions (see Fig. 4.7). The solid, dashed and dotted curves correspond to results for the logarithmic, quadratic and cubic nonlinearities, respectively.

In Fig. 4.10 we display results concerning the relation between the parameter α and the location and magnitude of the maximum. One our our findings is that for $\alpha \gtrsim 0.85$ and $\alpha \lesssim 0.5$ the maximum disappears and the time evolution becomes monotonic. The reason for this in each of these cases is different. When $\alpha \lesssim 0.5$, the initial condition is very shallow so that the diffusion is negligible compared to the effects of the nonlinearity. Therefore, the modified part of the front grows extremely rapidly and takes a steeper form while approaching the exact front shape so that its speed continuously decreases. In the opposite limit, when $\alpha \gtrsim 0.85$, the modification from the exact front shape is slight, so that it can be regarded as a small perturbation. This small perturbation monotonically decays and the excess speed does not show a maximum. For intermediate values of α, we display the results for the location and magnitude of the maximum of excess speed in Fig. 4.10.

We define T_1 to be the time it takes for the excess speed to reach a maximum, and H to be the magnitude of this maximum. The main graph and the inset in Fig. 4.10 show the behavior of T_1 and H as a function of α, respectively.
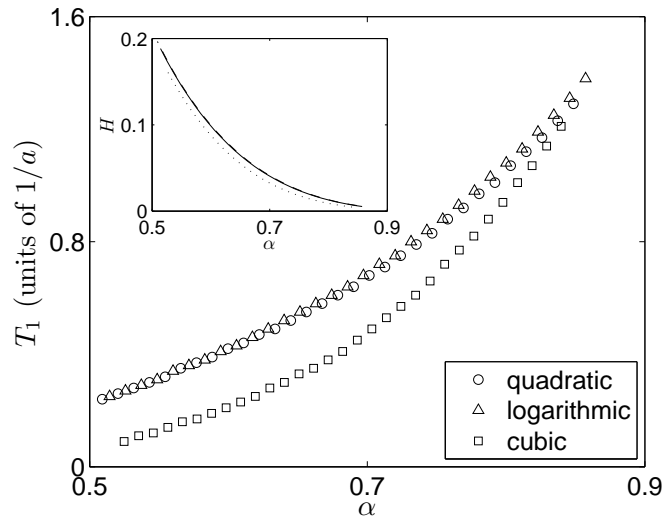
Figure 4.10: The behavior of T_1, the time it takes for the excess speed to reach a maximum, as a function of the initial condition parameter α. In the inset, we plot the magnitude of the same maximum again as a function of α. The solid, dashed and dotted curves correspond to results for the logarithmic, quadratic and cubic nonlinearities, respectively.

4.4.3   Case C

The last type of initial conditions we consider is obtained by modifying both the interior and the tail of the exact front, and gives rise to the richest transient behavior. An illustration of an initial condition of this kind is provided in Fig. 4.7 (C). The interior is modified such that it is shallower than the exact front by changing the characteristic length as described in Sec. 4.4.1. The tail is replaced by a line segment which starts at $f(u) = A$ and goes down until it reaches zero. In order to generate different initial conditions, we adjust the parameter A while keeping the projection of the line segment on the x-axis constant. A common feature of the nonlinearities we consider is that they are very weak around $u = 0$,

i.e. $f(u \approx 0) \approx 0$. If the initial condition has a substantial part which is nonzero for small values of u, we may expect the dynamics to be very slow around that region. Therefore, some parts of the front will change rapidly and some will not, and this may give rise to rich transient behavior.

In Fig. 4.11 we show the qualitative behavior of the excess speed as a function of time for the logarithmic nonlinearity given by Eq. (4.16). The results for other nonlinearities are essentially very similar and not shown in this figure. Note that now there is a minimum in addition to a maximum in the excess speed versus time plot. To make things easier, we include the plots of the numerical solution and the exact front solution at three points in time, whose significance we are set to understand.

The excess speed decreases as the interior part of the front, which evolves faster than the tail, becomes less and less steep and approaches the exact front shape as shown in the center inset in Fig. 4.11. After the minimum is reached, the part of the front where the interior and the tail meet starts to grow as the top left inset of Fig. 4.11 shows. This growth induces the whole front to become shallower than the exact front and keeps going until the maximum point is reached. At the maximum point, the whole profile is shallower than the exact front as shown in the top right inset of Fig. 4.11. The time evolution after this point is monotonic and is almost identical to what we had in Case A above.

The main graph in Fig. 4.12 shows the excess speed as a function of time for the logarithmic nonlinearity for different values of the initial condition parameter A. An immediate question that arises after looking at these plots is: how does the distance between the extrema depend on the parameter A? The four curves, the solid, the dotted, the dashed and the dash-dotted, correspond to results for increasingly larger values of A. At first, as A increases the time difference between the minimum and maximum also increases. However, for A greater than a certain value, a significantly larger portion of the shallow profile grows rapidly because of the shape of the nonlinearity $f(u)$ (see Fig. 4.6). Therefore, the evolution of the initial condition gets substantially faster as A increases, and reduces the
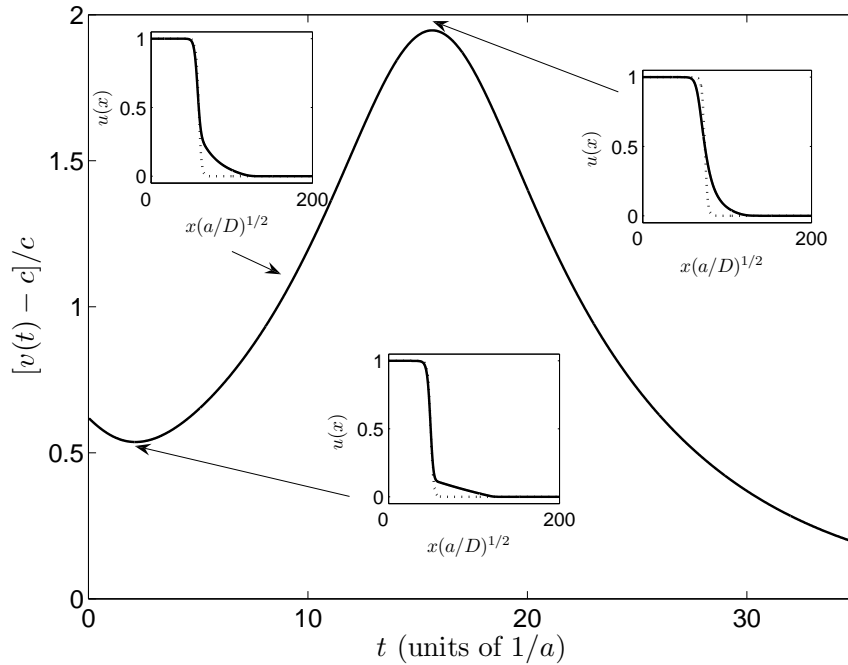
Figure 4.11: Excess speed as a function of time for the logarithmic nonlinearity with the kind of initial condition described in Sec. 4.4.3. The insets show the evolving solution of the R-D equation (solid curve) and the exact traveling front (dotted curve) at different times for comparison purposes. The exact traveling front is plotted by coinciding the two curves at $u = 1/2$.

time necessary for the profile to become shallow at all points in space. The last argument that we presented provides the reason for why the maximum of the dashed and dash-dotted curves shift to the left. The inset of the same figure shows the behavior of T_2, the time difference between the occurrence of the minimum and the maximum, as a function of A for each of the three nonlinearities. Note that the behavior of T_2 is significantly different for the cubic nonlinearity. This implies that the time difference T_2 depends heavily on the form of the nonlinearity around $u = 0$.
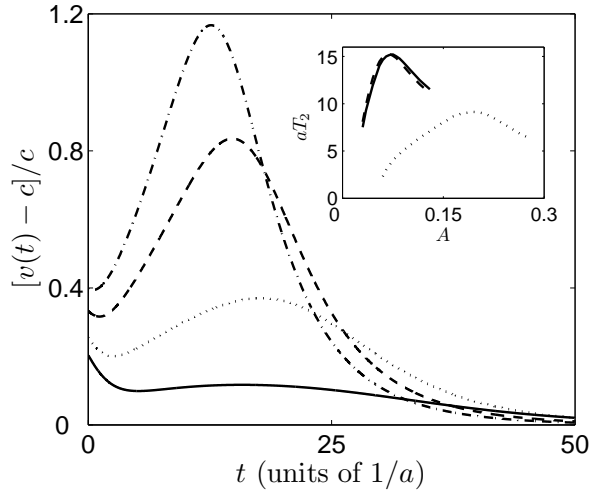
Figure 4.12: Excess speed as a function of time for the logarithmic nonlinearity for four initial conditions of the type mentioned in Sec. 4.4.3. The solid, dotted, dashed and dash-dotted curves correspond to $A = 0.04, 0.06, 0.1$ and 0.12, respectively. The inset shows how the dependence of T_2, the time difference between the minimum and the maximum, on A for the logarithmic(solid curve), quadratic(dashed curve), and the cubic(dotted curve) nonlinearities.

4.5   Linear stability of traveling fronts

4.5.1   The method

In this section, we follow the standard procedure [141, 106] to see if the traveling fronts discussed in this paper are stable against finite perturbations in the moving frame. Consider the diffusion reaction equation with a nonlinear term $f(u)$:

$$\frac{\partial u(x,t)}{\partial t} = \frac{\partial^2 u(x,t)}{\partial x^2} + f(u(x,t))$$

In the moving frame $(x,t) \rightarrow (z,t)$ where $z = x - ct$, the equation becomes

$$\left. \frac{\partial u(z,t)}{\partial t} \right|_z = c \left. \frac{\partial u(z,t)}{\partial z} \right|_t + \left. \frac{\partial^2 u(z,t)}{\partial z^2} \right|_t + f(u(z,t)) \tag{4.23}$$

Suppose that $u_0^c(z)$ is a traveling wave solution of (4.23). Lets introduce a finite perturbation $w(z, t)$ in the moving frame and write

$$u(z, t) = u_0^c(z) + \epsilon w(z, t) \tag{4.24}$$

Substituting (4.24) into (4.23) we get:

$$\epsilon \frac{\partial w}{\partial t} = c \frac{du_0^c}{dz} + \frac{d^2 u_0^c}{dz^2} + \epsilon c \frac{\partial w}{\partial z} + \epsilon \frac{\partial^2 w}{\partial z^2} + f(u_0^c + \epsilon w) \tag{4.25}$$

If we make a taylor series expansion of $f(u)$ around u_0^c and just keep the first order terms in ϵ we get

$$\frac{\partial w}{\partial t} = c \frac{\partial w}{\partial z} + \frac{\partial^2 w}{\partial z^2} + f'(u_0^c)w \tag{4.26}$$

If we assume that $w(z, t)$ is of the form $w(z, t) = \eta(z)e^{-\lambda t}$ and substitute this into Eq. (4.26). The result becomes

$$-\lambda \eta = c \frac{d\eta}{dz} + \frac{d^2 \eta}{dz^2} + f'(u_0^c)\eta \tag{4.27}$$

We can get rid of the first derivative in the equation above by making the transformation $\eta(z) = \xi(z)e^{-cz/2}$. Then Eq.(4.27) turns into

$$-\frac{d^2\xi}{dz^2} + \left(\frac{c^2}{4} - f'(u_0^c) \right) \xi = \lambda \xi$$

Now, if we define the operator $H_c = \left[-d^2/dz^2 + c^2/4 - f'(u_0^c(z)) \right]$, Eq. (4.27) can be expressed as

$$H_c \xi = \lambda \xi \tag{4.28}$$

In order that the traveling front solutions are stable, all λ's should be positive (the case $\lambda = 0$ is special and we will come to that) so that the perturbations $w(z, t)$ decay in time. This would be the case when H_c is a positive definite operator. Note that H_c is a self adjoint differential operator [142]. This makes Eq. (4.28) equivalent to the time independent Schrödinger equation with *potential energy* $V(z) = c^2/4 - f'(u_0^c(z))$ upto a constant in front

of the kinetic energy term but this is insignificant for our purposes. Using the analogy with the Schrödinger equation, we see that the energy eigenvalues, λ, are going to be greater than zero if the potential energy $V(z)$ is always greater than zero where $\xi(z)$ is non-zero (As the perturbations that we consider are finite, $\xi(z)$ should vanish outside of some interval (a, b) on z-axis). If the potential energy has negative values in (a, b) the traveling front may still be stable but then we need to prove that eigenvalues are greater than zero by making a different argument.

4.5.2 Linear stability of the fronts discussed in this chapter

In Fig.4.13 we plot $V(z)$ for each nonlinearity and find that for each case, it takes on negative values in some interval. So, if the fronts are stable, we should be able to show, by other means, that the eigenvalues are, in fact, positive . For this purpose, we are going to follow ref. [143] and find the eigenfunction of H_c that corresponds to $\lambda = 0$ and argue that the corresponding eigenvalue of H_c is the lowest.

Note that translated traveling wave solutions of the form $u_0^c(z + \epsilon)$ will still satisfy (2) because of the symmetry in the system. If we expand $u_0^c(z + \epsilon)$ around z, and keep the first order term in ϵ, we get

$$u_0^c(z + \epsilon) \approx u_0^c(z) + \epsilon \frac{du_0^c(z)}{dz}. \tag{4.29}$$

If we compare Eq. (4.29) with Eq. (4.24), we will see that when the perturbation $w(z, t)$ is equal to $du_0^c(z)/dz$ then the perturbed solution $u(z, t) = u_0^c(z) + \epsilon w(z, t)$ is just a translated traveling front as we showed above. Thus if the perturbation is in this form, then it will not grow or decay (as all it does is to shift the front along z) in time as the translated traveling front is also a solution of Eq. (4.23). We can find the eigenfunction corresponding to $\lambda = 0$, $\xi_0(z)$, by setting $\lambda = 0$ in $w(z, t) = \xi(z)e^{-cz/2}e^{-\lambda t}$ and equating this to $du_0^c(z)/dz$, as a
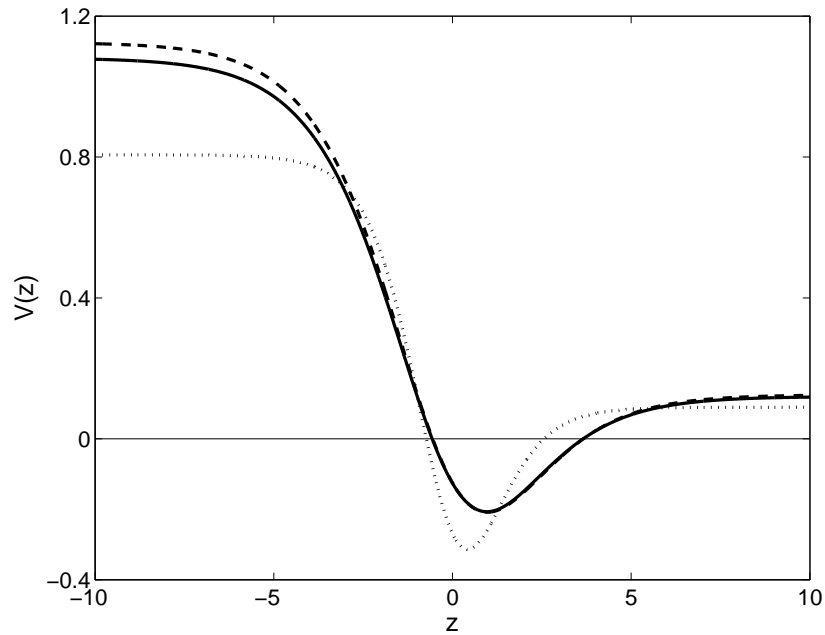
Figure 4.13: Plot of *potential energy vs z.* Solid, dashed and dotted lines correspond to logarithmic, quadratic and cubic nonlinearities respectively.

neither growing nor decaying perturbation should correspond to $\lambda = 0$. This gives

$$\xi_0(z) = e^{cz/2} \frac{du_0^c(z)}{dz}.$$

Now we will use another property of the solutions of the Schrödinger equation (4.28) to argue about the other eigenvalues of H_c. Note that $du_0^c(z)/dz$ is always negative for all nonlinearities we considered as the front shapes are monotonically decreasing functions of z. This means that $\xi_0(z)$ does not have any roots so the *wave function* corresponding to $\lambda = 0$ is nodeless. But it is well known in quantum mechanics that [144] the nodeless wave function would correspond to the ground state of the system with lowest λ. Therefore, all λ are greater or equal to zero for all nonlinearities we considered and $\lambda = 0$ simply means a translation of $u_0^c(z)$.

4.6 Pattern formation in an R-D system with spatially non -local interactions

As we mentioned in some detail in the introduction of this chapter, R-D systems display a wide range of phenomena including front propagation, oscillations, and chaotic behavior. One other interesting feature of these systems is that they can form patterns under certain circumstances when an instability in the system arises.

Formation of patterns in R-D systems have been extensively studied [145, 106, 146, 147, 148] after the pioneering work of Turing [19], who suggested the use of an R-D equation to study the formation of patterns in morphogenesis in biology. He showed that a system of chemical species that inhibit or activate each other and their own production in a simple way can lead to formation of patterns provided that an instability in the system arises as a consequence of such interactions.

In this section, we will study some aspects of pattern formation in an R-D system in which the mechanism that leads to the formation of structures in the system is quite different from what it is for Turing patterns. Recently it was shown by Fuentes, Kuperman, and Kenkre [114, 22] that R-D equations with spatially nonlocal interaction terms can lead to the formation of steady state patterns. The specific R-D equation they considered was an FKPP equation with a competition term that allows for non-local interactions between the constituents of the system. In this thesis, we are interested in studying the formation of patterns in a similar system. However, our special interest is for a transport mechanism that is not necessarily diffusive. We consider a more general R-D equation than the one mentioned in refs. [114, 22], by introducing a memory in the diffusion term. By choosing the memory appropriately, we can have super- or sub-diffusive transport of reactants in the system. Our main interest lies in investigating the conditions under which patterns can form as a function of the characteristic property of transport in the system, i.e. diffusive, super- or sub-diffusive.

In the next section we will briefly review the findings in ref. [22] about pattern formation in an FKPP equation with spatially non-local competition term, and then present our results for the case with memory.

4.6.1 Fisher equation with nonlocal competition term in the Markoffian limit

Fuentes, Kuperman, and Kenkre [114, 22] consider the following form of the FKPP equation with a modified competition term that allows nonlocal interactions

$$\frac{\partial u(x,t)}{\partial t} = D\frac{\partial^2 u(x,t)}{\partial x^2} + au(x,t) - bu(x,t)\int_\Omega dy f_\sigma(x,y)u(y,t), \tag{4.30}$$

where Ω is the extent of the system and $f_\sigma(x,y)$ is a function characterizing the influence of point y on point x. It is reasonable to think of $f_\sigma(x,y)$ as a function of $x - y$ in many situations. So we will assume $f_\sigma = f_\sigma(x - y)$ and that it is normalized on Ω such that

$$\int_\Omega dz f_\sigma(z) = 1. \tag{4.31}$$

If patterns do form as $t \to \infty$ then the homogeneous solution, $u_0 = a/b$, must be unstable [149, 147, 146]. Therefore, in order to obtain a condition for the existence of patterns, let us analyze the stability of the homogeneous solution. The rest of this section is a detailed review of the discussion in ref. [22] provided as an introduction to our study. Consider

$$u(x,t) = u_0 + \epsilon \cos kx e^{\varphi t}, \tag{4.32}$$

where ϵ is be taken as a perturbation parameter. Next, we substitute Eq. (4.32) in Eq. (4.30) to see under which conditions the perturbation grows or decays. We get

$$\varphi\epsilon \cos kx e^{\varphi t} = -Dk^2\epsilon \cos kx e^{\varphi t} + au_0 + a\epsilon \cos kx e^{\varphi t}$$
$$- b\left(u_0 + \epsilon \cos kx e^{\varphi t}\right)\int_\Omega dy f_\sigma(x,y)\left(u_0 + \epsilon \cos kx e^{\varphi t}\right). \tag{4.33}$$

Using the properties of $f_\sigma(x, y)$, we put Eq. (4.33) in the following form

$$0 = -\epsilon\left(\varphi + Dk^2 + a \int_\Omega dy f_\sigma(x - y)\frac{\cos ky}{\cos kx}\right) + O(\epsilon^2). \tag{4.34}$$

Neglecting the term that is second order in ϵ,

$$\varphi = -Dk^2 - a \int_\Omega dy f_\sigma(x - y)\frac{\cos ky}{\cos kx}. \tag{4.35}$$

Let us take Ω to be the interval $[-L/2, L/2]$ so that the size of the system is L. Then, the integration variable y takes values from $-L/2$ to $L/2$, and $z = x - y$ runs from $z = x + L/2$ to $z = x - L/2$. As we impose periodic boundary conditions on the system, z can be thought as a periodic variable, like an angle, with period L. This observation will be useful if we express the integral in Eq. (4.35) over z instead of y. After doing this, we get

$$\varphi = -Dk^2 - a \int_\Omega dy f_\sigma(x - y)\frac{\cos kx \cos kz + \sin kx \sin kz}{\cos kx}, \tag{4.36}$$

where we used $\cos(a + b) = \cos a \cos b - \sin a \sin b$. Expressing the integrals over z we get

$$\varphi = -Dk^2 - a\left(\int_{\Omega_+} dz f_\sigma(z) \cos kz + \tan kx \int_{\Omega_+} dz f_\sigma(z) \sin kz\right), \tag{4.37}$$

where Ω_+ means that z is increasing along the path of integration in Ω, and explains how we got rid of the minus sign introduced by the change of integration variable. Integrating throughout Ω, Eq. (4.37) becomes

$$\varphi = -Dk^2 - a\left(\int_{-L/2}^{L/2} dz f_\sigma(z) \cos kz + \tan kx \int_{-L/2}^{L/2} dz f_\sigma(z) \sin kz\right). \tag{4.38}$$

The second integral in Eq. (4.38) vanishes as the integrand is the product of an even and an odd function and we are left with

$$\varphi = -Dk^2 - a\mathscr{F}(k), \tag{4.39}$$

where

$$\mathscr{F}(k) = \int_{-L/2}^{L/2} dz f_\sigma(z) \cos kz,$$

is the Fourier cosine transform of the influence function. The perturbation will grow if φ given in Eq. (4.39) is positive and it will decay otherwise. As D, k, and a take positive values, the perturbation can grow only if $\mathscr{F}(k)$ is negative for at one of the k values and satisfies

$$\mathscr{F}(k) < -\frac{Dk^2}{a}.$$

The growth of perturbations is a necessary but not sufficient condition for pattern formation. If we take the influence function to be

$$f_\sigma(z) = \frac{1}{2\sigma} \left(\theta \left(\sigma - z \right) \theta \left(\sigma + z \right) \right),$$

where $\theta(x)$ is the Heaviside function

$$\theta(x) = \begin{cases} 1 & x \geq 0, \\ 0 & x < 0. \end{cases}$$

With this choice for the influence function, we have

$$\mathscr{F}(k) = \frac{\sin(k\sigma)}{k\sigma}. \tag{4.40}$$

A plot of the steady state patterns emerging in the R-D system characterized by Eq. (4.30) and the influence function given in Eq. (4.40) is shown in Fig. 4.14. Note that φ takes positive values for two intervals of k.

4.6.2   Our generalization with memory

The transport in the system governed by Eq. (4.30) is diffusive due to the term with the second space derivative. In order to allow for different transport types such as super- and sub-diffusion, we will modify this term by introducing a memory. If transport is coherent to some degree, then Eq. (4.30) can be replaced by

$$\frac{\partial u(x,t)}{\partial t} = D \int_0^t ds \phi(t-s) \frac{\partial^2 u(x,s)}{\partial x^2} + au(x,t) - bu(x,t) \int_\Omega dy f_\sigma(x,y) u(y,t), \tag{4.41}$$
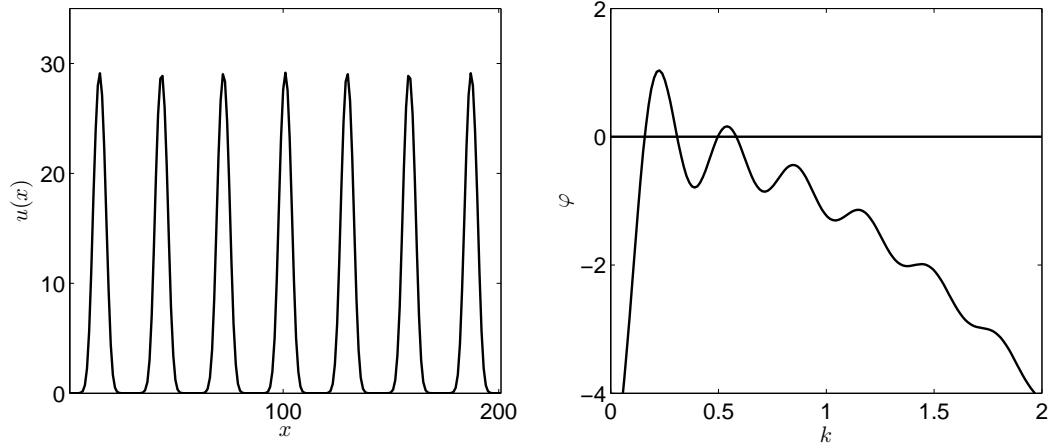
Figure 4.14: On the left, we plot the steady state patterns that appear in the R-D system described by Eqs. (4.30) and (4.40). On the right, the corresponding $\mathscr{F}(k)$ as a function of k is shown. The value of the dimensionless parameter $\sigma \sqrt{a/D}$ is equal to $20\sqrt{5}$.

See ref. [5] for a discussion on memory functions, generalized master equations, and coherent transport. In this case, we will employ a more general form of the perturbation given in Eq. (4.32), namely

$$u(x, t) = u_0 + \epsilon g(t) \cos kx. \tag{4.42}$$

substituting Eq. (4.42) in Eq. (4.41) and proceeding in the same way as in Sec. 4.6.1, we obtain

$$\frac{dg(t)}{dt} = -ag(t)\mathscr{F}(k) - Dk^2 \int_0^t ds\phi(t - s)g(s).$$

Taking the Laplace transform of the equation above and doing some algebra, we get

$$\widetilde{g}(\epsilon) = \frac{g(0)}{\epsilon + Dk^2\widetilde{\phi}(\epsilon) + a\mathscr{F}(k)}, \tag{4.43}$$

where tildes denotes Laplace transformed quantities and ϵ is the Laplace variable. Without loss of generality, we will take $g(0) = 1$ from now on. In the Markoffian limit, $\widetilde{\phi}(\epsilon) = 1$ and we have

$$\varphi = -Dk^2 - a\mathscr{F}(k),$$

133

given by Fuentes et al. [22].

In the following sections, we consider different memory functions and their effect on the stability of the homogeneous solution. The influence function we consider in all of the cases is given by

$$f_\sigma(z) = \frac{\theta(w - z)\theta(w + z)}{2w},$$ (4.44)

where $\theta(x)$ is the Heaviside function. Its Fourier cosine transform becomes

$$\mathscr{F}(k) = \frac{\sin kw}{kw}.$$ (4.45)

4.6.3   In discrete space

In the rest of this chapter, we will confine our interest to systems in discrete space. It is useful to obtain the results in discrete space especially when it comes to comparing analytical results with numerics. One of the discrete space analogs of Eq. (4.41) is

$$\frac{du_m}{dt} = h \int_0^t ds\phi(t - s) \left[u_{m+1} + u_{m-1} - 2u_m \right] + au_m - bu_m \sum_n F_n(w)u_{m-n},$$ (4.46)

where $F_n(w)$ is the influence function. In particular, we consider

$$F_n(w) = \frac{1}{2w + 1}\theta(w - n)\theta(w + n),$$ (4.47)

whose Fourier cosine transform is

$$\mathscr{F}(k) = \frac{1}{2w + 1} \left[\frac{\cos kw - \cos(k(w + 1))}{1 - \cos k} \right].$$

Again, we consider the evolution of the perturbed steady state $u = u_0 + \epsilon \cos(km)g(t)$, by substituting it in Eq. (4.46) and taking its Laplace transform, we get

$$\widetilde{g}(\epsilon) = \frac{1}{\epsilon + G(k)\widetilde{\phi}(\epsilon) + a\mathscr{F}(k)},$$ (4.48)

where

$$G(k) = 2h\left(1 - \cos k\right).$$

If the memory is a delta distribution, $\phi(t) = \delta(t - s)$,

$$\widetilde{g}(\epsilon) = \frac{1}{\epsilon + G(k) + a\mathscr{F}(k)},$$

therefore, $g(t)$ is given by

$$g(t) = e^{-(G(k)+a\mathscr{F}(k))t}, \tag{4.49}$$

and the perturbation would grow if

$$\mathscr{F}(k) < -\frac{G(k)}{a}. \tag{4.50}$$

The exponential time dependence is not surprising as we only kept terms that are linear in ϵ. If the memory is an exponentially decaying function, $\phi(t) = \alpha e^{-\beta t}$, $\widetilde{g}(\epsilon)$ becomes

$$\widetilde{g}(\epsilon) = \left[\frac{\epsilon + \xi}{(\epsilon + \xi)^2 - \eta} + \frac{\beta - \xi}{(\epsilon + \xi)^2 - \eta}\right],$$

where

$$\xi = \frac{\beta + a\mathscr{F}(k)}{2},$$

$$\eta = \frac{(\beta + a\mathscr{F}(k))^2}{4} - a\beta\mathscr{F}(k) - \alpha G(k),$$

and $g(t)$ is given by

$$g(t) = c_+ e^{-(\xi - \sqrt{\eta})t} + c_- e^{-(\xi + \sqrt{\eta})t},$$

$$c_\pm = \frac{1}{2}\left(1 \pm \frac{\beta - \xi}{\sqrt{\eta}}\right).$$

Let us take a closer look at the exponent

$$\xi \pm \sqrt{\eta} = \frac{\beta + a\mathscr{F}(k)}{2} \pm \frac{1}{2}\sqrt{(\beta + a\mathscr{F}(k))^2 - 4\left(a\beta\mathscr{F}(k) + \alpha G(k)\right)}.$$

Note that the exponent is positive only when

$$\mathscr{F}(k) < -\frac{\alpha}{\beta}\frac{G(k)}{a}.$$

The Markoffian limit corresponds to setting $\alpha = \beta$ and taking the limit $\beta \to \infty$. Let us rewrite the exponent as

$$\xi \pm \sqrt{\eta} = \frac{\beta + a\mathscr{F}(k)}{2} \pm \frac{\beta}{2}\sqrt{1 + \frac{4}{\beta}\left(-\frac{a\mathscr{F}(k)}{2} - \frac{\alpha}{\beta}G(k)\right) + \frac{1}{\beta^2}a^2\mathscr{F}^2(k)}.$$

As we are interested in the limit $\beta \to \infty$, the second term inside the square root sign is small compared to 1 so that we can make the approximation $\sqrt{1+x} \simeq 1 + x/2$, which leads to

$$\xi + \sqrt{\eta} = \beta - G(k),$$

$$\xi - \sqrt{\eta} = a\mathscr{F}(k) + G(k),$$

if we ignore the term which goes as β^{-2}. As β is large and positive, $e^{-(\xi+\sqrt{\eta})t}$ will vanish and $g(t)$ will be proportional to

$$g(t) \propto e^{-(\xi-\sqrt{\eta})t} = e^{-(a\mathscr{F}(k)+G(k))t},$$

which is the result we obtained in Markoffian limit earlier.

4.6.4 Slowly decaying memories

If the memory decays slowly, e.g. algebraically, then transport can be sub- or superdiffusive [5]. A $\phi(t)$ whose integral in $[0, \infty)$ is divergent will lead to superdiffusion. On the other hand, if the integral of $\phi(t)$ in the same interval vanishes and $\phi(t) \sim t^{-1-\gamma}$, where $0 < \gamma < 1$, then the transport will be subdiffusive.

$$\text{Superdiffusion: } \int_0^\infty ds\phi(s) \to \infty$$

$$\text{Subdiffusion: } \begin{cases} \int_0^\infty ds\phi(s) = 0 \\ \phi(t) \sim t^{-1-\gamma}, \ 0 < \gamma < 1 \end{cases}$$

In order to investigate superdiffusion, we consider memory functions of the form

$$\phi(t) = \alpha(\beta t + \gamma)^{\nu}, \quad -1 < \nu < 0, \tag{4.51}$$

whose first and second integrals are

$$\int_0^t ds\phi(s) = \frac{\alpha}{\beta(\nu + 1)} \left[(\beta t + \gamma)^{\nu+1} - \gamma^{\nu+1} \right],$$

$$\text{MSD} \propto \int_0^t ds \int_0^s ds'\phi(s') = \frac{\alpha}{\beta(\nu + 1)} \left[\frac{1}{\beta(\nu + 2)} \left[(\beta t + \gamma)^{\nu+2} - \gamma^{\nu+2} \right] - \gamma^{\nu+1} t \right] \sim t^{\nu+2},$$

where MSD stands for mean square displacement.

For subdiffusion, we take up

$$\phi(t) = \delta(t) + \alpha(\beta t + \gamma)^{\nu}, \quad -2 < \nu < -1, \tag{4.52}$$

with

$$\int_0^t ds\phi(s) = 1 + \frac{\alpha}{\beta(\nu + 1)} \left[(\beta t + \gamma)^{\nu+1} - \gamma^{\nu+1} \right],$$

$$\text{MSD} \propto \int_0^t ds \int_0^s ds'\phi(s') = \frac{1}{\beta(\nu + 2)\gamma^{\nu+1}} \left[(\beta t + \gamma)^{\nu+2} - \gamma^{\nu+2} \right] \sim t^{\nu+2}.$$

Observe that $\alpha/\beta = (\nu+1)/\gamma^{\nu+1}$ needs to hold in order that the integral $\int_0^\infty ds\phi(s)$ vanishes. Let us see what these basic properties imply about the time evolution of the perturbations when they decay. If the perturbations decay, then the integral $\int_0^\infty dtg(t) = \lim_{\epsilon\to 0}\widetilde{g}(\epsilon)$ will have a finite value. The value of this integral gives us an idea about the characteristic time associated with the decay of the perturbations, which is given by

$$\widetilde{g}(0) = \frac{1}{G(k)\widetilde{\phi}(0) + a\mathcal{F}(k)}. \tag{4.53}$$

The integral of the memory, $\widetilde{\phi}(0)$, is finite for exponential and δ-distribution memories as well as for the memory we considered in the subdiffusive case. Inverse of the characteristic time for each of these cases is given by

$$\tau_c^{-1} = \widetilde{g}(0) = \begin{cases} G(k) + a\mathcal{F}(k), & \phi(t) = \delta(t) \\ (\alpha/\beta)G(k) + a\mathcal{F}(k), & \phi(t) = \alpha e^{-\beta t} \\ a\mathcal{F}(k), & \phi = \delta(t) + \alpha(\beta t + \gamma)^{\nu} \end{cases}$$

Note that τ_c for the Markoffian limit is identical to the exponent we found in Eq. (4.49) and the expression for it is simplify modified by a factor of α/β if the memory is exponential. Obviously, the characteristic time of the decay for the subdiffusive case is meaningful only if $\mathscr{F}(k)$ is positive.

Our aim is to obtain a condition on the parameters of the memory function that determines whether the perturbation will grow or decay. We should not forget that the condition for the growth of the perturbation is not necessarily the same as the condition for pattern formation. Growth of the perturbation is necessary but not sufficient for the formation of patterns. In the rest of this section, we will discuss a way of obtaining the short time behavior of the function $g(t)$ for the super- and sub-diffusive cases. Let us consider the memory function

$$\phi(t) = \zeta\delta(t) + \alpha(\beta t + \gamma)^{\nu}. \tag{4.54}$$

If the parameter ζ is equal to 1, then Eq. (4.54) is the memory function we consider for the subdiffusive case, and if ζ is 0, it is identical to the memory in the superdiffusive case. The Laplace transform of Eq. (4.54) is given by

$$\widetilde{\phi}(\epsilon) = \zeta + \alpha \int_0^\infty dt\,(\beta t + \gamma)^{\nu}\, e^{-\epsilon t}. \tag{4.55}$$

Recall that the Laplace transform of the function $g(t)$ that describes the time evolution of the perturbation is given by

$$\widetilde{g}(\epsilon) = \frac{1}{\epsilon + G(k)\widetilde{\phi}(\epsilon) + a\mathscr{F}(k)}.$$

Our treatment of the evolution of the perturbation is valid only if the amplitude of the perturbation is small. Hence, we can rely on the expression for $g(t)$ only for short times. In the super- and sub- diffusive cases, it does not look like we can analytically take the Laplace transform of $\widetilde{g}(\epsilon)$ and obtain behavior of the perturbation as a function of time because of the complicated nature of $\widetilde{g}(\epsilon)$. Because we are necessarily interested in the short time behavior of $g(t)$, we can focus our interest on approximating it. In order to do

this, we notice that the behavior of a function $f(t)$ at short times is related to its Laplace transform at large values of the Laplace variable. For the limiting behavior of $f(t)$, we have the well known result [59]

$$\lim_{t \to 0} f(t) = \lim_{\epsilon \to \infty} \epsilon \widetilde{f}(\epsilon). \tag{4.56}$$

As we are interested in the values of $g(t)$ for small values of t different from 0, we can take the inverse Laplace transform of the approximate form of $\widetilde{g}(\epsilon)$ for large values of ϵ. If we make the change of variables $\tau = \beta t + \gamma$, then Eq. (4.55) can be written as

$$\widetilde{\phi}(\epsilon) = \zeta + \frac{\alpha}{\beta}I,$$

where

$$I = \int_{\gamma}^{\infty} d\tau \tau^{\nu} e^{-\frac{\epsilon}{\beta}(\tau - \gamma)}.$$

Performing integration by parts twice on the integral, we obtain

$$I = \frac{\gamma^{\nu}}{\epsilon/\beta} + \frac{\nu}{\epsilon/\beta} \left[\frac{\gamma^{\nu-1}}{\epsilon/\beta} + \frac{\nu - 1}{\epsilon/\beta} \int_{\gamma}^{\infty} d\tau \tau^{\nu-2} e^{-\frac{\epsilon}{\beta}(\tau - \gamma)} \right].$$

We realize that if we perform n integration by parts, we will get the following result

$$I_n = \sum_{m=0}^{n-1} \gamma^{\nu-m} \frac{\nu!}{(\nu - m)!} \frac{1}{(\epsilon/\beta)^{m+1}} + \frac{\nu!}{(\nu - n)!} \frac{1}{(\epsilon/\beta)^n} \int_{\gamma}^{\infty} d\tau \tau^{\nu-n} e^{-\frac{\epsilon}{\beta}(\tau - \gamma)}, \tag{4.57}$$

where the subscript n on I denotes the number of times we used integration by parts. Up to this point, the expressions we have worked with are exact. In order to be able to continue with analytical calculations, we now make an approximation which is exact for $\epsilon \to \infty$. Note that the exponential under the integral sign in I would be vanishingly small for the large values of ϵ which we are interested in calculating $\widetilde{g}(\epsilon)$ at. Therefore, we make the following approximation

$$(\epsilon/\beta) e^{\frac{\epsilon}{\beta}(\tau - \gamma)} \approx \delta(\tau - \gamma),$$

that leads to

$$\int_\gamma^\infty d\tau \tau^{\nu-n} e^{-\frac{\epsilon}{\beta}(\tau-\gamma)} \approx \frac{\gamma^{\nu-n}}{\epsilon/\beta},$$

which is exact when $\epsilon/\beta \to \infty$. It is worthwhile to note that approximation of the integral in I would get better and better with increasing values of n, as $\tau^{\nu-n}$ gets weaker for large values of τ, with increasing n. Using this approximation we can express $\widetilde{g}(\epsilon)$ as

$$\widetilde{g}(\epsilon) = \frac{P(\epsilon)}{Q(\epsilon)}, \tag{4.58}$$

where $P(\epsilon)$ and $Q(\epsilon)$ are polynomials in ϵ. Hence, taking the inverse Laplace transform of $\widetilde{g}(\epsilon)$ reduces to the problem of finding the roots of the polynomial $Q(\epsilon)$ and then calculating the residues of $\widetilde{g}(\epsilon)$ at these roots.

One can go through this procedure and get approximate forms for $g(t)$, but for our purpose it is not essential to do so. We would like to know whether the perturbation is going to grow or decay. In other words, we are interested in finding how $g(t)$ changes for small t. By using the following theorem for Laplace transforms [59]

$$\mathcal{L}\left\{\frac{df(t)}{dt}\right\} = \epsilon \widetilde{f}(\epsilon) - f(0),$$

and Eq. (4.56), we can write

$$\lim_{t\to 0} \frac{dg(t)}{dt} = \lim_{\epsilon\to\infty} \left[\frac{\epsilon^2}{\epsilon + G(k)\widetilde{\phi}(\epsilon) + a\mathscr{F}(k)} - \epsilon\right].$$

In the limit $\epsilon \to \infty$, we can replace $\widetilde{\phi}(\epsilon)$ by $\gamma^\nu/(\epsilon/\beta)$ due to the discussion above. After doing this, we get

$$\lim_{t\to 0} \frac{dg(t)}{dt} = -\left[G(k)\zeta + a\mathscr{F}(k)\right].$$

Therefore, the necessary conditions for the perturbations to grow in the super- and sub-diffusive cases are

$$\lim_{t\to 0} \frac{dg(t)}{dt} > 0 \text{ if } \begin{cases} a\mathscr{F}(k) < 0 & \text{super-diffusive case,} \\ [G(k) + a\mathscr{F}(k)] < 0 & \text{sub-diffusive case.} \end{cases} \tag{4.59}$$

Note that the growth rate of the perturbation at $t = 0$ for the sub-diffusive case is identical to that in the Markoffian limit given by Eq. (4.50). For super-diffusion, we see that the growth rate at $t = 0$ is independent from the $G(k)$ which is the term that involves h, the analog of the diffusion coefficient in discrete space.

As we have seen above, we can calculate the first derivative of $g(t)$ exactly at $t = 0$. In fact we can do the same for all higher derivatives of $g(t)$ by using the following property of the Laplace transforms

$$\mathcal{L}\left\{\frac{d^n f(t)}{dt^n}\right\} = \epsilon^n \widetilde{f}(\epsilon) - \epsilon^{n-1} f(0) - \ldots - \left.\frac{d^{n-1} f(t)}{dt^{n-1}}\right|_{t=0}.$$

Using this and Eq. (4.56), we can calculate $d^n g(t)/dt^n$ and expand $g(t)$ in a Taylor series around $t = 0$. We find that the the first four terms in the Taylor expansion are

$$g(t) \approx 1 - a\mathscr{F}(k)t + \left[-\alpha\gamma^\nu G(k) + a^2\mathscr{F}^2(k)\right]\frac{t^2}{2}$$
$$- a\mathscr{F}(k)\left[-2\alpha\gamma^\nu G(k) + a^2\mathscr{F}^2(k)\right]\frac{t^3}{6}, \tag{4.60}$$

for the super-diffusive case, and

$$g(t) \approx 1 - (G(k) + a\mathscr{F}(k))\, t + \left[-\frac{\nu+1}{\gamma}G(k) + (G(k) + a\mathscr{F}(k))^2\right]\frac{t^2}{2}$$
$$- (G(k) + a\mathscr{F}(k))\left[-2\frac{\nu+1}{\gamma}G(k) + (G(k) + a\mathscr{F}(k))^2\right]\frac{t^3}{6} \tag{4.61}$$

for the sub-diffusive case. Therefore, Eqs. (4.60) and (4.61) provide an alternative for finding an approximate form for $g(t)$ by inverting the Laplace transform in Eq. (4.58).

4.7 Numerical solution of the integro-differential equation and results of our analysis

In this section we will go over the method we employed to solve the system of integro-differential equations (4.46) numerically. Eq. (4.46) is a Volterra integro-differential equation with a convolution kernel, which appears in many dynamical systems (see ref. [150]

and references therein). Numerical solution of systems of Volterra integro-differential equations is costly, especially when the one discretizes a partial differentiation operator and uses small step sizes to obtain reasonable accuracy. The fact that we restrict our attention to a discrete R-D system rather than considering Eq. (4.41) helps us go around this problem of having to choose small step sizes in discretizing the space variable. Below, we give an algorithm that approximates the solution of a system of Volterra integro-differential equations using embedded Runge-Kutta methods, found in Hoppensteadt and others [150] and follows from the results obtained in refs. [151, 152, 153, 154].

Consider the system of equations

$$\frac{du(t)}{dt} = \mathcal{G}\left(t, u(t), \int_0^t ds k(t-s) f(s, x(s))\right), \tag{4.62}$$

with the initial condition $u(0) = u_0$, where $u(t)$ is a vector and $\mathcal{G}$ is a vector valued function of its arguments that can be nonlinear. Discretizing the time interval $[0, t]$ such that $t_{n+1} = t_n + h_n$, the 5$^\text{th}$ order Runge-Kutta approximation to solution of Eq. (4.62) at the $n + 1^\text{st}$ timestep is found to be [150]

$$u_{n+1} = u_n + h_n \sum_{j=1}^{s} b_j \mathcal{G}\left(t_n + c_j h_n, X_{j,n}, F_n^*\left(t_n + c_j h_n\right) + Z_{j,n}\right), \tag{4.63}$$

where

$$X_{i,n} = x_n + h_n \sum_{j=1}^{i-1} a_{ij} \mathcal{G}\left(t_n + c_j h_n, X_{j,n}, F_n^*\left(t_n + c_j h_n\right) + Z_{j,n}\right),$$

$$Z_{j,n} = h_n \sum_{l=1}^{j-1} a_{jl} k\left((c_j - c_l) h_n\right) f\left(t_n + c_l h_n, X_{l,n}\right),$$

$F_n^*(t)$ is the approximation for the integral

$$F_n(t) = \int_0^{t_n} ds k(t-s) f(s, x(s)) \approx F_n^*(t)$$

$$= \sum_{l=1}^{n-1} h_l \sum_{j=1}^{s} b_j k\left(t - t_l - c_j h_l\right) f\left(t_l + c_j h_l, X_{j,l}\right),$$

u_1 is taken to be the same as the initial condition, and the indices i and n run from 1 to s and N, respectively. The values of a_{ij}, b_i, and c_i depend on the order of the Runge-Kutta method used. For a 5$^{\text{th}}$ order approximation we have (see Eq. (1.4) of ref. [150])

$$
a = \begin{bmatrix}
0 & 0 & 0 & 0 & 0 & 0 & 0 \\
\frac{1}{5} & 0 & 0 & 0 & 0 & 0 & 0 \\
\frac{3}{40} & \frac{9}{40} & 0 & 0 & 0 & 0 & 0 \\
\frac{44}{45} & -\frac{56}{15} & \frac{32}{9} & 0 & 0 & 0 & 0 \\
\frac{19372}{6561} & -\frac{25360}{2187} & \frac{64448}{6561} & -\frac{212}{729} & 0 & 0 & 0 \\
\frac{9017}{3168} & -\frac{355}{33} & \frac{46732}{5247} & \frac{49}{176} & -\frac{5103}{18656} & 0 & 0 \\
\frac{35}{384} & 0 & \frac{500}{1113} & \frac{125}{192} & -\frac{2187}{6784} & \frac{11}{84} & 0
\end{bmatrix},
$$

$$
b = \begin{bmatrix} 35/384 & 0 & 500/1113 & 125/192 & -2187/6784 & 11/84 & 0 \end{bmatrix},
$$

and

$$
c = \begin{bmatrix} 0 & 1/5 & 3/10 & 4/5 & 8/9 & 1 & 1 \end{bmatrix}.
$$

These values for a, b, and c describe the method proposed by Dormand and Prince [154]. Now we will display the results obtained by numerically solving Eq. (4.46) using the algorithm described above.

When the transport in the system is sub-diffusive such that the memory is given by Eq. (4.52), we find that the system still forms patterns. The nature of the patterns seem to be very similar to those that arise in the Markoffian limit. Moreover, the condition for the growth of perturbations, as given in Eq. (4.59) is the same as it is in the Markoffian limit. Obviously, the time evolution in the sub-diffusive case is much slower than it is in the Markoffian limit. In Fig. 4.15, we display the patterns that form for a particular choice of parameters along with the function $\Omega(k) = -(G(k) + a\mathscr{F}(k))$, which shows the growth rate of the kth Fourier mode of the perturbation. The parameter values for these plots can be found in the figure captions.
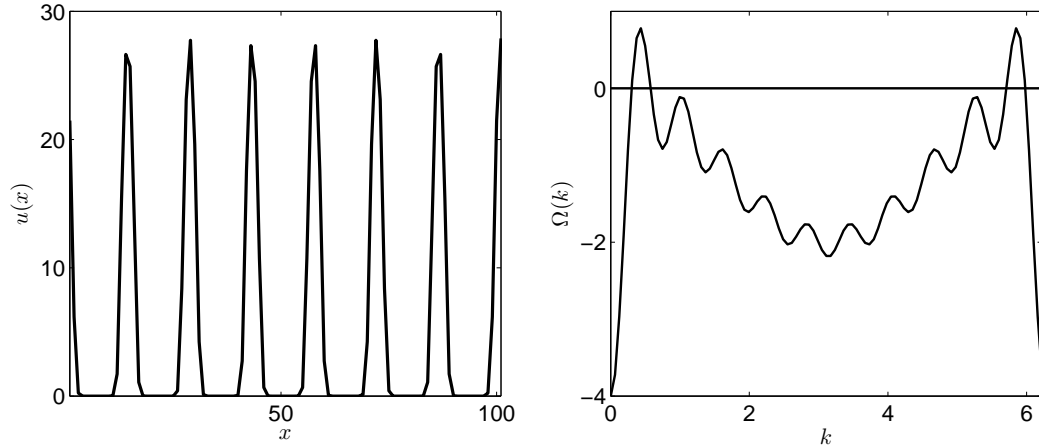
Figure 4.15: On the left, we display the steady state patterns observed in the R-D system given in Eq. (4.46) with parameter values $h = 0.5$, $a = 4$, $b = 1$, $\gamma = 0.1$, $w = 10$, $\beta = 1$, $v = -3/2$. The discrete system consists of 101 lattice points, and periodic boundary conditions are imposed (this explains the split peaks in the pattern structure around $x = 0$ and 100). The stepsize used in the integration is $\Delta t = 0.2$. The shape of the patterns that arise in this case seem to be identical to those in the Markoffian limit. On the right, the quantity $\Omega(k) = -(G(k) + a\mathscr{F}(k))$ is plotted as a function of k. As explained in the text, if $\Omega(k)$ is greater than 0, then the corresponding Fourier mode grows in time and if it is less than 0, then the Fourier mode decays. Bear in mind that these statements are valid only for short times as our calculations are for small amplitudes of the perturbation. If $\Omega(k)$ is less than 0 for all k, then small perturbations will not lead to the formation of patterns.

In Fig. 4.16, both numerical findings and theoretical results for the time evolution of the amplitude of the perturbation, $g(t)$, is plotted. The initial condition we consider in this case is of the following form

$$u_m = u_0 + \omega g(t) \cos Km, \tag{4.64}$$

where K is a particular value of the Fourier variable k, u_0 is the steady state solution of Eq. (4.46), and ω is the amplitude of the perturbation. In our analysis we set $u_0 = 4$ and $\omega = 0.1$. The plots show the Kth Fourier mode of the numerical solution of Eq. (4.46) as a function of time. The left plot in Fig. 4.16 corresponds to $K = 0.4355$ (the k value at the first peak), and the Fourier mode grows. On the right, we plot the time evolution of the Fourier mode with $K = 0.7465$ (corresponding to the first dip after the first peak) which

decays, in accordance with the theoretical predictions. In both of these plots, open circles correspond to numerical findings with the parameter values given in the figure caption, solid lines represent theoretically obtained $g(t)$ curves given in Eq. (4.61), and the dashed lines represent the approximation to $g(t)$ calculated by taking the inverse Laplace transform of Eq. (4.58), which is

$$g'(t) = e^{-\xi t/2} \left[\cosh\left(\sqrt{\xi^2 - 4\eta} t/2 \right) - \frac{\xi \sinh\left(\sqrt{\xi^2 - 4\eta} t/2 \right)}{\sqrt{\xi^2 - 4\eta}} \right], \tag{4.65}$$

where

$$\xi = \zeta G(k) + a\mathcal{F}(k),$$

$$\eta = \left[\left(\frac{\nu + 1}{\gamma^{\nu+1}} \right) \zeta + \alpha \left(1 - \zeta \right) \right] \gamma^{\nu} G(k)$$

Eq. (4.65) is obtained by keeping just a few of the terms in Eq. (4.58) that vanish in the limit $\epsilon \to \infty$ and thus, only approximates $g(t)$ crudely.

For the super-diffusive case, steady state patterns do not form. In this case, our numerical findings indicate that when perturbations grow, patterns that oscillate in time evolve. Therefore, the super-diffusive case requires a different treatment in which one takes the effects of the full nonlinearity into account.

4.8 Concluding remarks

Results on two different aspects of R-D systems, front propagation and pattern formation, was studied in the first and second parts of this chapter respectively. The research we presented on front propagation differs from most of the work that has been done in the literature as it focuses on the transient dynamics in the system rather than on the steady state behavior. Exploring the transient dynamics in systems which obey nonlinear evolution equations is a difficult task and can seldom be done exactly. In our case, it also was
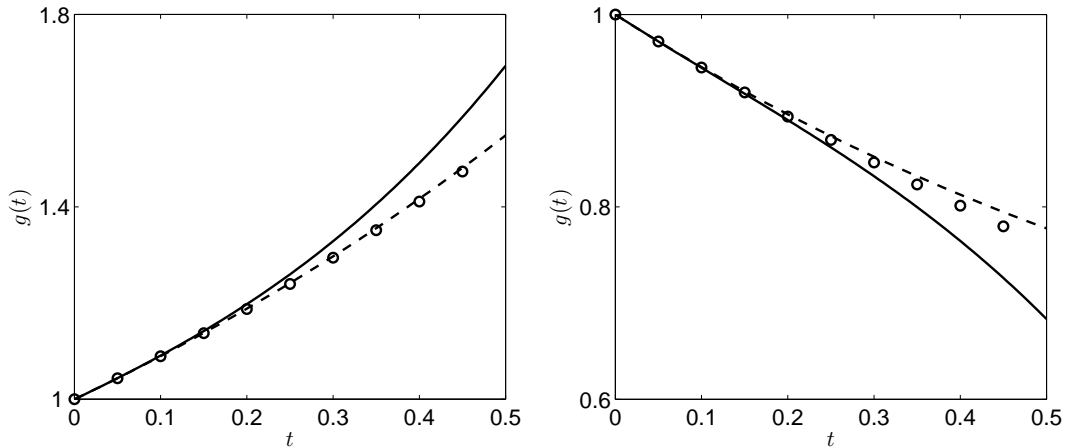
Figure 4.16: Here we plot the short time behavior of the solution of Eq. (4.46) with the initial condition being the perturbation given in Eq. (4.64), for two values of K. The parameter values are $h = 0.1$, $a = 4$, $b = 1$, $\gamma = 0.1$, $w = 10$, $\beta = 1$, $\nu = -3/2$ and the system consist of 101 lattice points. The integration in time is performed by using a stepsize of $\Delta t = 0.005$. On the left, $K = 0.4355$ which corresponds to the value of k at the first peak of the curve in Fig. 4.15 (right). For this K value, the perturbation grows in time. On the right $K = 0.7465$, corresponding to the first dip in Fig. 4.15 (right). In this case the perturbation decays. The solid and dashed lines represent the theoretical, approximate, predictions for the time evolution of the perturbation, given by Eqs. (4.61) and (4.65), respectively.

not possible to solve the evolution equation exactly, therefore we resorted to a numerical analysis. However, we carefully selected our R-D equation so that we can obtain their traveling front solutions analytically, which provided us a well defined method of analyzing transient dynamics, as explained in Sec. 4.4. We reviewed the concept of linear stability of traveling fronts and applied it to our traveling front solutions. Our results are displayed in Figs. 4.8, 4.9, 4.10, 4.11, 4.12 and show aspects of the relaxation behavior of the different initial conditions we consider. As we mentioned in the introduction, the type of R-D systems we considered here are relevant in real world problems such as flame propagation and population dynamics. The results we obtained would be relevant in studying the response of these kind of systems when their steady states are perturbed in the ways that we describe in Fig. 4.7.

The aim of the second part of this chapter is to explore the effects of anomalous diffusion on the formation of patterns in an R-D system. The specific R-D system we considered here is described by the FKPP equation with a modified nonlinear term that allows spatially non-local interactions. Based on the analysis of Fuentes, Kuperman, and Kenkre [114, 22] regarding the emergence of patterns in this R-D system, we derived necessary conditions for the formation of patterns under more general transport types. The necessary condition for pattern formation is the growth of perturbations in the steady state, or the steady state becoming unstable, can depend on the transport mechanism in the system. In order to explore this, we generalized the equation used by Fuentes et al. [22] to include a memory, that can be specified appropriately to attain diffusive, super- or sub-diffusive transport in the system. When the memory is a $\delta-$distribution, we recover the results obtained in ref. [22]. For different types of memories, including exponentially and algebraically decaying forms, we found that the rate of change of the perturbations in the diffusive and sub-diffusive cases are the same as $t \rightarrow 0$ as seen in Eqs. (4.49) and (4.59), whereas in the super-diffusive case, it has a different value given by Eq. (4.59). For $t > 0$, the evolution of the perturbations is found to be different in each case. It is not possible to solve the R-D equation we consider exactly, therefore, analyzed the problem by doing numerical simulations. In our simulations, we found that if the perturbations grow in the diffusive and sub-diffusive cases, the system forms steady state patterns, although we did not establish a sufficient condition for the formation of patterns. For the super-diffusive case, we noticed that when the perturbations grow, steady state patterns do not form, instead, oscillating structures appear. As yet, we have not fully pursued the properties of these oscillations mainly due to the well known difficulties of numerically solving integro-differential equations for extended periods of time. Therefore, a clear future direction of the research we presented here is studying the dynamics in the system for super-diffusive transport. A question that needs to be answered is whether the oscillations arise because of the particular memory function we considered for the super-diffusive case, or is it a general feature of super-diffusive transport.

Chapter 5

Cluster size distribution in an addition-deletion network

5.1 Introduction

The work described in this chapter was done while the author was working at the Los Alamos National Laboratory as a summer student in collaboration with Eli Ben-Naim of the theoretical division of the Los Alamos National Laboratory. It is loosely connected with the rest of the thesis. It deals with a problem in complex networks, the latter providing the connection with the rest of the thesis.

Studying the properties of networks has attracted an enormous amount of attention over the past 10 years [30, 28, 29, 31]. The main reason is the usefulness of networks in representing complex systems of many different kinds, seemingly as disparate as food webs [155], semantic networks [156], and Bose-Einstein condensates [28]. Networks, or graphs in the terminology of applied mathematics, have been studied by using both numerical and analytical techniques. The vast majority of the results obtained in the literature pertain to static properties of networks, and not as much have been done about studying network

structures that evolve, at least in terms of obtaining exact results. See Dorogovstev and Mendes [29] on a relatively early review on evolving networks.

Here, we are interested in studying an addition-deletion network in which nodes, the basic elements of the network, are added and removed in a random fashion as a function of time. See refs. [23, 24, 25, 27, 26] for examples of addition-deletion networks. These types of networks are potentially useful in modeling a wide range of systems, including the world wide web [27]. Many properties of these networks have been studied, such as the degree distribution [23, 24, 25, 27, 26], the in-component distribution [26], the height distribution [26], and the effects of preferential attachment [27]. In our study, we consider random recursive trees, which are perhaps the simplest of all network structures. For a detailed discussion on trees and many other graph structures, see, for instance, ref. [157]. Our goal is to study the distribution of cluster sizes in a random recursive tree, in which nodes are randomly removed as well as added in the course of time. Below, we will give the necessary properties of the network structures we study, along with the explanation of the terminology, without going into much detail.

This chapter is organized as follows: in Sec. 5.2, we give the definition of some of the commonly used terms in the study of networks, and present a description of the problem we are interested in. In Secs. 5.3 and 5.4, we describe the methods we use to approach the problem and give our numerical findings. Some of the results that we obtained analytically, concerning a simpler version of the quite general problem we began with, is given in Sec. 5.5. In Sec. 5.6, we make concluding remarks.

5.2   Some basic definitions and description of the problem

The basic elements of a network, or a graph, are nodes and links. A network is characterized by a set of nodes, that may or may not be connected to each other with links. In

general, links can point in a particular direction but our study focuses on a network with undirected links. If each of the two connected nodes are also connected to a third node a cycle appears. Cycles of larger sizes can appear with the involvement of more than three connected nodes. The degree of a given node is defined as the number of links that it has, thus it is equal to the number of nodes to which it is connected. These concepts are illustrated in Fig. 5.1 for a randomly constructed network. The structure of the addition-deletion network we consider is similar to that of a randomly grown recursive tree. One can generate a random recursive tree by starting with one node at $t = 0$ and subsequently introducing new nodes. The newly introduced node is attached to a randomly selected existing node, which we will call the parent node. Therefore, each new node starts with a degree equal to 1. Note that a network that grows according to this rule cannot have cycles (hence, the name tree is used to described these kinds of structures). If the parent node has a degree of k, it will have a degree of $k + 1$ after the addition of the new node. Therefore, it is straightforward to write a Master equation for the evolution of the number of nodes with degree k, denoted by n_k, as

$$\frac{dn_k}{dt} = \frac{1}{N}(n_{k-1} - n_k) + \delta_{k,1},$$

where N is the total number of nodes in the system at time t, and for convenience we set the rate at which new nodes come about to 1. This equation can easily be solved for n_k in the long-time limit, giving $n_k = N2^{-k}$ so that the probability of finding a node with degree k is $p_k = 2^{-k}$. Therefore, the average degree of a node is given by $\langle k \rangle = 2$. Many exact results like these are known about more general types of evolving graphs (for a few examples, see refs. [158, 159, 160, 161, 26]).

The dynamics of the network that we are interested in studying differs from what we described above in the way that nodes can also be deleted at a certain rate. Hence, the term addition-deletion network is used to describe these structures. Networks with such dynamics were studied in the past by several authors [23, 24, 25, 27, 26]. A schematic illustration showing the evolution of the addition-deletion network we study is given in
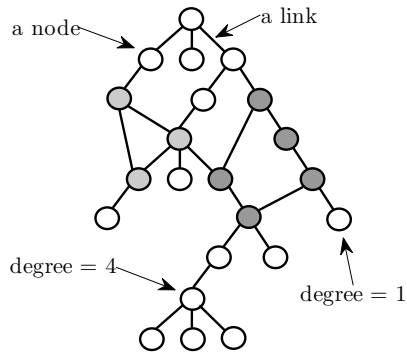
Figure 5.1: A general network structure employed to illustrate the concepts we mention in the text. The colored nodes are part of cycles of length 3 and 5. One of the properties of recursive trees, which we are interested in studying throughout this chapter, is that they do not have cycles.

Fig. 5.2. Note that as a result of the deletion events, the network is partitioned into smaller segments, which are also trees, that we will call clusters. Our aim is to gain an understanding of the distribution of cluster sizes in this network.
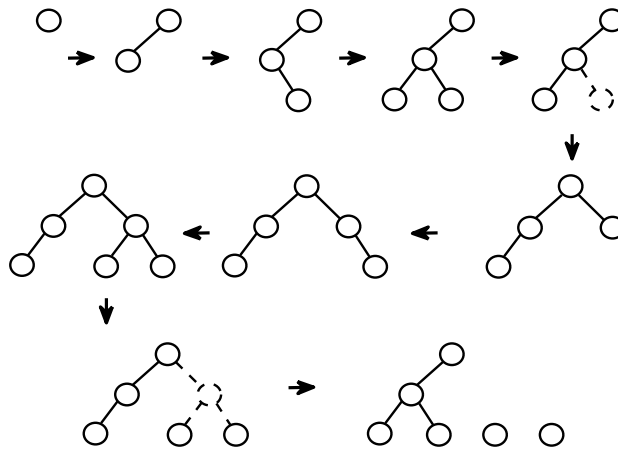
Figure 5.2: A schematic illustration of the evolution of the addition-deletion network. At $t = 0$ there is only one node, the root. Arrows point to the next state of the network after each time step in the simulations. Links and nodes with dashed lines correspond to deletion events, and they are removed from the network. In the last step of the evolution, the deletion of a node along with all its link lead to the formation of three clusters one of which has size 3, while the other two consist of disconnected nodes.

5.3   Methods of study

Firstly, we perform Monte Carlo simulations of the addition-deletion network and explore the properties of the numerically obtained distribution of cluster sizes. We will describe the simulation methods and give the results in Sec. 5.4 below. The original aim of this investigation was to obtain an exact expression for the distribution of cluster sizes, or for its the asymptotic behavior. As yet, we have not succeeded in accomplishing that task. It turns out that writing a closed equation for the evolution of cluster sizes in the form of a Master equation is not straightforward. However, we succeed in obtaining exact expressions for the distribution of branch sizes of a given node, which we think is an important step in solving the original problem. The calculations and results pertaining to the distribution of branch sizes will be presented in Sec. 5.5. In the rest of this section, we briefly describe our strategy in solving this problem aside from doing simulations.

In the opinion of the author, there are two different approaches that one can take in an attempt to make progress in determining how cluster sizes are distributed. One of them is concerned with finding out the specific ways in which trees of different sizes give rise to new clusters when they are fractured(because of the random removal of a node). This could give us an idea about how the rate of appearance of new clusters with different sizes behave as a function of the size of the cluster being fractured. We call this approach *microscopic* as it is all about unraveling patterns in randomly growing trees of different sizes. The second approach treats the number of clusters of size s, n_s, as a random variable and tries to figure out the stochastic process that describes this random variable. As no reference to the underlying structure of the network is made here, we call this approach *macroscopic*.

For networks that grow without the removal of nodes, it is easier to write down closed equations for various quantities like the degree distribution. When a node is removed from a network, along with all the links associated with it, multiple events occur at one time

step. The removal of a node produces clusters of many different sizes. If one adopts the microscopic approach, in order to give an account on how the number of clusters of a certain size evolve, one needs to find out about the details of this process. To do this, we do simulations in which a random recursive tree is grown until it has $N + 1$ nodes, without any removal of nodes, and then one node is removed from it at random. As a result, the original tree breaks up into disconnected components. Then we calculate the probability of finding a component of size s along with the probability of finding n of these components of size s. We find that the function that relates the size $N + 1$ of the original tree and the size distribution of the subsequent components scale as

$$f(N, s) = \frac{1}{(N + 1)^2} f\left(\frac{s}{N + 1}\right).$$

The derivation of the exact form of the size distribution of these components, or branches, will be given in Sec. 5.5 in detail.

If we look at the problem from the point of view of the macroscopic approach, we may proceed in the following way. Let $n_s(t_i)$ be a random variable that corresponds to the number of clusters with size s. Let $F(n_s, \Delta t)$, $\Delta t = t_{i+1} - t_i$, be a stochastic process that governs the evolution of n_s. Then,

$$n_s(t_{i+1}) = n_s(t_i) + F(n_s, \Delta t). \tag{5.1}$$

If we can gain some insight into whar the functional form of the process F is by doing simulations, we may be able to analytically express the number of clusters of size s as $t \to \infty$. The author has not pursued this method.

5.4 Simulation of the addition-deletion network

We perform Monte Carlo simulations of the addition-deletion network we study, in trying to explore the cluster size distribution. During a time step of the Monte Carlo simulation,

a new node is added to an existing node with probability

$$p_{\text{add}} = \frac{r}{r+1},$$

and an existing node is deleted with probability

$$p_{\text{del}} = \frac{1}{r+1}.$$

Typically, we run the simulation until the total number of nodes in the network reach $10^7 \sim 10^8$. We repeat this procedure a few thousand times and ensemble average over the findings to obtain the final results. While constructing the network in this way, we calculate various quantities like the frequency of observing clusters of different sizes.

The main result obtained from the simulations is the cluster size distribution $P(s)$. In Fig. 5.3, we plot $P(s)$ as a function of the cluster size s, for various values of r. The functional form of $P(s)$ for large values of s is well approximated by a stretched exponential,

$$P(s) \simeq e^{-s^\gamma}.$$

In order to estimate the parameter γ, $\ln(-\ln(P(s)))$ found numerically and is plotted against $\ln(s)$. A linear fit is performed by considering the points with $s > s_0$ for some s_0. Fig. 5.4 shows the behavior of $\ln(-\ln(P(s)))$ as a function of $\ln(s)$. Furthermore, In Fig. 5.5 we plot $\ln(P(s))$ against s^γ with the γ values obtained by the procedure described above, to see if the relationship is linear, which would provide more reason for us to think that $P(s)$ behaves like a stretched exponential for large s values.

It is also worth mentioning that the simulation described above is repeated for a special case of random recursive trees for which the maximum degree is two, i.e. only two nodes can be attached to a given node, one being its parent, and the other its child. For a chain like network like this, we find that the cluster size distribution falls off exponentially.

Another interesting quantity we explore in the simulations is the number and size of the clusters that result from removing a node from a random recursive tree with $N + 1$ nodes.

Understanding this simple problem may help us in developing a theory for the cluster size distribution. Note that this is related to the microscopic approach we mentioned earlier. We observe numerically that the size distribution of the clusters obtained by removing one node from a network of $N + 1$ nodes is a function of the form

$$f(N, s) = 1/(N + 1)^2 f(1/(N + 1), s).$$

Also, the number of clusters of a certain size obtained in this way seems to follow an exponential distribution. In this, case the simulation is performed in the following way. A recursive tree is grown until it reaches a size of $N + 1$ by constantly, and randomly, adding new nodes to the existing nodes in a uniform fashion. Then a randomly selected node is removed from the tree. The resulting structure is a collection of disconnected trees (or a tree with N nodes if the node chosen for removal is a leaf, which is a node of degree 1), which we call clusters. We are interested in obtaining the probability of finding a cluster of size s after the removal of a node from a tree of size $N + 1$. This quantity is denoted by $P_s(N)$ and is numerically calculated as follows: during each run of the simulation a random tree of size $N + 1$ is grown and one randomly chosen node is removed. Then the number and size of the resulting clusters are found and $P_s^i(N)$ is updated to give

$$P_s^{i+1}(N) = \frac{P_s^i(N) + n_s^i/S^i}{i + 1} \tag{5.2}$$

where the index i pertains to the ensemble averaging carried out, making $P_s^i(N)$ the probability of finding a cluster of size s when a node is randomly removed from a tree of size $N + 1$ averaged over $i + 1$ different realizations. Here, n_s^i is the number of clusters of size s and S^i the total number of clusters found after the ith run of the simulation ($P_s^0(N) = 0$). With this definition of $P_s(N)$ we obviously have the normalization condition

$$\sum_s P_s(N) = 1.$$

The average degree of a node in a growing network of this kind is 2, in the limit $N \to \infty$, as we mentioned earlier. Therefore, on average, one should expect to find two clusters as

a result of removing a node at random. This is indeed what we see in the simulations. The simulation results that pertain to this case is presented in Sec. 5.5, along with the exact expressions.
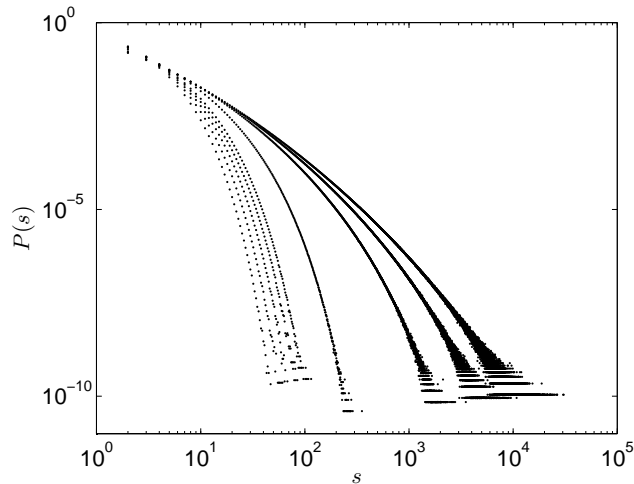
Figure 5.3: The cluster size distribution $P(s)$ as a function of s on log-log scale, for various values of the parameter r. The value of r determines the probabilities of addition and deletion of a node at each simulation step. From left to right, the data sets correspond to $r = 1.1, 1.3, 1.5, 1.7, 1.9, 3, 6, 8$, and 10. Note that for large values of r, which correspond to fewer deletion events, big clusters appear with more probability, as expected. In order to obtain each data set, the network is allowed to evolve until it contains $10^7 \sim 10^8$ nodes. This procedure is repeated a few thousand times and the results are averaged to obtain the displayed values of $P(s)$.

We also calculate the probability that the number of clusters with a given size s changes by n during one time step. Knowing this probability distribution would provide one with the details of the stochastic process by which the random variable n_s, number of clusters with size s, evolves. We did not pursue research along these lines further, as we mentioned in passing while discussing the macroscopic approach above.
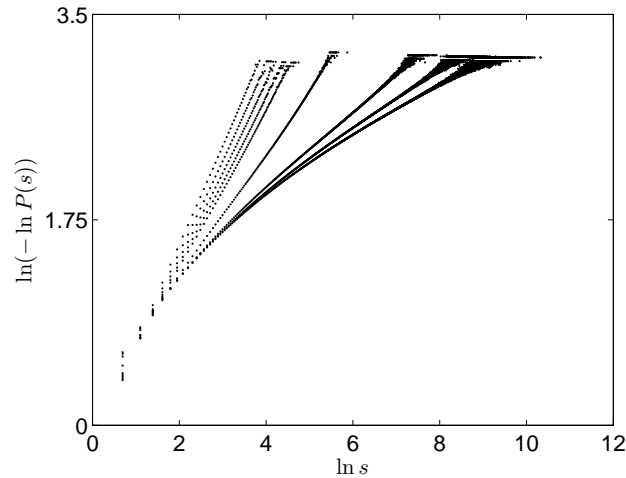
Figure 5.4: We suggest that the cluster size distribution behaves like a stretched exponential, e^{-s^γ}, for large values of s. If it is so, then plots of $\ln(-\ln P(s))$ against $\ln s$ should be well approximated by straight lines. Here, we display such plots corresponding to $r = 1.1, 1.3, 1.5, 1.7, 1.9, 3, 6, 8,$ and 10 from left to right. Note that for small values of r, $\ln(-\ln P(s))$ seems to vary linearly with $\ln s$.

5.5 Exact results for the distribution of branch sizes

In this section we study the distribution of the branch sizes of a randomly selected node, which is equivalent to the distribution of the size of the clusters that appear as a result of removing a randomly chosen node of a tree. Note that the clusters thus formed would themselves be trees as shown in Fig. 5.6. Therefore, a branch is a tree whose root is connected to the node that is intended to be removed. Accordingly, the number of branches that form after the removal is equal to the degree of the node being removed. As the average degree for a random recursive tree is equal to 2, on average, one would expect to see two clusters forming after a removal event. Two of the most abundant type of nodes in a random recursive tree are leaves that have degree equal to 1, and the nodes that are connected to leaves. This means that most of the time the removal of a node will partition the network into one piece with one less node than the original tree or into two parts with a disconnected node and all the rest.
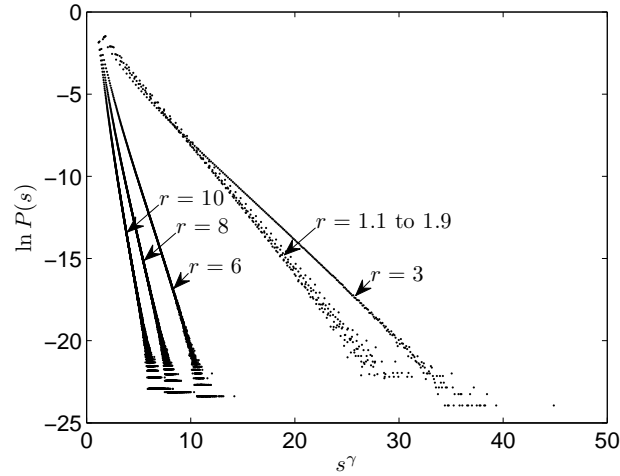
Figure 5.5: Plotted is $\ln P(s)$ as a function of s^γ, where the γ values are found by fitting lines to the plots in Fig. 5.4. Each data set corresponds to a different value of r, as indicated on the figure. The data sets that correspond to r values that lie between 1.1 and 1.9 are practically indistinguishable. Looking at these plots, we see that it is reasonable to approximate them with straight lines. This provides further support for our suggestion thar $P(s)$ behaves like a stretched exponential for large values of s. Supposing that $P(s)$ is truly a stretched exponential distribution for large s values, the slopes of the lines in these plots would correspond to the constant α in $P(s) \simeq e^{-\alpha s^\gamma}$. Note that α seems to depend on r in a non-monotonic fashion.

In order to write a closed equation for a quantity related to the distribution of branch sizes, we first define a parameter τ associated with each node. The value of τ for a given node indicated the time at which it was introduced to the network. Thus, the root has $\tau = 0$ and all other nodes have $\tau > 0$. Then we define the average number of branches of a node, introduced at $t = \tau$, at time t as $P_s(t, \tau)$. Examining the network structure shown in Fig. 5.6 helps us realize that $P_s(t, \tau)$ obeys the recursion relation

$$P_s(t + 1, \tau) = P_s(t, \tau) + \frac{(s - 1)P_{s-1}(t, \tau) - sP_s(t, \tau) + \delta_{s,1}}{t + 1}, \tag{5.3}$$

where $t + 1$ is equal to the total number of nodes in the system at time t.

The last three terms in Eq. (5.3) represent the change in $P_s(t, \tau)$ when a newly arriving node attaches itself to one of the branches of the node characterized with τ. Among these terms, the first, the second, and the third correspond to the newly added node attaching
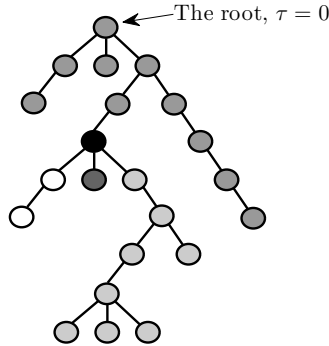
Figure 5.6: An illustration showing the branches of a given node in a random realization of the addition-deletion network we consider. The black colored node has 4 branches of size 1, 2, 6, and 10, each represented by coloring the nodes in the same branch with different shades of grey. Note that each branch is itself a tree.

itself to a branch of size $s - 1$, s, and to the node itself. The minus sign in the second term simply indicates that when the new node is attached to a branch of size s, the number of branches with size s decreases. Note that a node that is added to the network at $t = \tau$ satisfies the intial condition

$$P_s(\tau, \tau) = \delta_{s,\tau},\tag{5.4}$$

which says the the new node only has a single branch of size s. Finally, the average size of a branch in a tree of size $N + 1$ can be obtained by averaging $P_s(t, \tau)$ as follows

$$P_s(N) = \frac{1}{N + 1} \sum_{\tau=0}^{N} P_s(N, \tau).\tag{5.5}$$

The branch size distribution satisfies the normalization

$$N = \sum_{s} sP_s(N).\tag{5.6}$$

In the rest of this section, we will be concerned with the details of calculating the distribution $P_s(N)$. Using the above recursion relations we can find the average size of a branch

for small N.

$$P_s(1) = \delta_{s,1}$$

$$P_s(2) = \frac{2}{3}(\delta_{s,1} + \delta_{s,2})$$

$$P_s(3) = \frac{1}{12}(7\delta_{s,1} + 4\delta_{s,2} + 7\delta_{s,3}).$$

5.5.1   Solving the recursion relation for $P_s(t, \tau)$

Let us write down the equation for $P_1(\tau + 1, \tau)$ by substituting $t = \tau$ in Eq. (5.3),

$$P_1(\tau + 1, \tau) = \frac{1}{\tau + 1}\left[1 + \tau\delta_{1,\tau}\right], \tag{5.7}$$

where we used $P_s(\tau, \tau) = \delta_{s,\tau}$. Now that we have $P_1(\tau + 1, \tau)$, we can substitute it into Eq. (5.3) to get $P_1(\tau + 2, \tau)$. Repeating this for n times we find that

$$P_1(\tau + n, \tau) = \frac{1}{\tau + n}\left[n + \tau\delta_{1,\tau}\right]. \tag{5.8}$$

Going over this procedure for different values of s, we find that $P_s(\tau+n, \tau)$ for small values of s are given by

$$P_2(\tau + n, \tau) = \frac{1}{(\tau + n)(\tau + n - 1)}\left[\frac{n(n-1)}{2} + n\tau\delta_{1,\tau} + \tau(\tau - 1)\delta_{2,\tau}\right] \tag{5.9}$$

$$P_3(\tau + n, \tau) = \frac{1}{(\tau + n)(\tau + n - 1)(\tau + n - 2)}\left[\frac{n(n-1)(n-2)}{3}\right.$$
$$\left. + n(n-1)\tau\delta_{1,\tau} + 2n\tau(\tau - 1)\delta_{2,\tau} + \tau(\tau - 1)(\tau - 2)\delta_{3,\tau}\right] \tag{5.10}$$

$$P_4(\tau + n, \tau) = \frac{1}{(\tau + n)(\tau + n - 1)(\tau + n - 2)(\tau + n - 3)}\left[\frac{n(n-1)(n-2)(n-3)}{4}\right.$$
$$+ n(n-1)(n-2)\tau\delta_{1,\tau} + 3n(n-1)\tau(\tau - 1)\delta_{2,\tau}$$
$$\left. + 3n\tau(\tau - 1)(\tau - 2)\delta_{3,\tau} + \tau(\tau - 1)(\tau - 2)(\tau - 3)\delta_{4,\tau}\right] \tag{5.11}$$

$$P_5(\tau + n, \tau) = \frac{1}{(\tau + n)(\tau + n - 1)(\tau + n - 2)(\tau + n - 3)(\tau + n - 4)}$$
$$\times \left[\frac{n(n-1)(n-2)(n-3)(n-4)}{5} + n(n-1)(n-2)(n-3)\tau\delta_{1,\tau} \right.$$
$$+ 4n(n-1)(n-2)\tau(\tau-1)\delta_{2,\tau} + 6n(n-1)\tau(\tau-1)(\tau-2)\delta_{3,\tau}$$
$$\left. + 4n\tau(\tau-1)(\tau-2)(\tau-3)\delta_{4,\tau} + \tau(\tau-1)(\tau-2)(\tau-3)(\tau-4)\delta_{5,\tau} \right]$$

$$(5.12)$$

Observe that in all of these terms, the term that multiplies everything in the square brackets has the form

$$\frac{(\tau + n - s)!}{(\tau + n)!}. \tag{5.13}$$

The first term that appears in the square brackets has the form

$$\frac{1}{s} \prod_{i=0}^{s-1} (n - i), \tag{5.14}$$

and the rest of the terms in the square brackets can be represented by

$$\sum_{j=1}^{s-1} \left(\prod_{k=0}^{j-1} (\tau - k) \right) \left(\prod_{l=0}^{s-j-1} (n - l) \right) \binom{s-1}{j-1} \delta_{j,\tau} + \prod_{m=0}^{s-1} (\tau - m)\, \delta_{s,\tau}, \tag{5.15}$$

where the summation in the first term is defined to be zero for $s = 1$. Therefore, it looks like we have

$$P_s(\tau + n, \tau) = \frac{(\tau + n - s)!}{(\tau + n)!} \left[\sum_{j=1}^{s-1} \left(\prod_{k=0}^{j-1} (\tau - k) \right) \left(\prod_{l=0}^{s-j-1} (n - l) \right) \binom{s-1}{j-1} \delta_{j,\tau} \right.$$
$$\left. + \prod_{m=0}^{s-1} (\tau - m)\, \delta_{s,\tau} + \frac{1}{s} \prod_{p=0}^{s-1} (n - p) \right]. \tag{5.16}$$

Eq. (5.16) can also be expressed as

$$P_s(t, \tau) = \frac{(t - s)!}{t!} \left[\frac{1}{s} \prod_{i=0}^{s-1} (t - \tau - i) + \tau \frac{(t - \tau)!(s - 1)!}{(t - s)!(s - \tau)!} \sum_{j=1}^{s} \delta_{j,\tau} \right]. \tag{5.17}$$

where $t = \tau + n$ and $t \geq s$. For $t \geq s + \tau$, the product in Eq. (5.17) can be replaced by a ratio of factorials and we have

$$P_s(t \geq s + \tau, \tau) = \frac{1}{s} \frac{(t - \tau)!}{t!} \left(\frac{(t - s)!}{(t - s - \tau)!} + \frac{\tau s!}{(s - \tau)!} \sum_{j=1}^{s} \delta_{j,\tau} \right). \tag{5.18}$$

We need to verify that Eq. (5.17) is a solution of Eq. (5.3). For $s = 1$, Eq. (5.3) reads

$$P_1(t + 1, \tau) = P_1(t, \tau) - \frac{P_1(t, \tau)}{t + 1} \tag{5.19}$$

Substituting $s = 1$ in Eq. (5.17) gives

$$P_1(t, \tau) = \frac{1}{t} (t - \tau + \tau \delta_{1,\tau}). \tag{5.20}$$

By substituting this into Eq. (5.3), we clearly see that it is the correct solution. In order to verify the solution for all $s \neq 1$, we substitute Eq. (5.17) into Eq. (5.3). With simple algebraic manipulations, we make the limits of the sums and products the same all through the equation. Then it is found that the coefficients of the sums and products at each side of the equality are the same, implying that Eq. (5.17) is the solution of Eq. (5.3).

For the first few values of τ, Eq. (5.17) gives

$$P_s(t, 0) = P_s(t, 1) = \frac{1}{s},$$
$$P_s(t, 2) = \frac{1}{s} + \frac{3s - (1 + 2t)}{t(t - 1)},$$
$$P_s(t, 3) = \frac{1}{s} + \frac{2s^2 - 3(4 - t)s + 4 + 6t - 3t^2}{t(t - 1)(t - 2)}. \tag{5.21}$$

Observe that $P_s(t, \tau)$ is independent from t for the root and the first node. In the limit $t \to \infty$ (but finite τ), Eq. (5.18) becomes

$$\lim_{t \to \infty} P_s(t \geq s + \tau, \tau) = \frac{1}{s} \tag{5.22}$$

as

$$\lim_{t \to \infty} \left(\frac{(t - \tau)!}{t!} \frac{(t - s)!}{(t - s - \tau)!} \right) = 1$$
$$\lim_{t \to \infty} \left(\frac{(t - \tau)!}{t!} \frac{\tau s!}{(s - \tau)!} \right) = 0. \tag{5.23}$$

We can express the average number of branches of size s of randomly chosen node in a tree with $N + 1$ nodes as

$$P_s(N) = \frac{1}{N+1} \sum_{\tau=0}^{N} P_s(N, \tau). \tag{5.24}$$

which can be found by using Eq. (5.17) to be

$$P_s(N) = \frac{1}{s(s+1)} + \frac{(s-1)!}{(N+1)!} \sum_{n=1}^{s} \frac{(N-n)!}{(s-n)!} n, \tag{5.25}$$

or equivalently

$$P_s(N) = \frac{1}{s(s+1)} + \frac{1}{(N+1)} \sum_{n=1}^{s} \frac{\binom{s-1}{n-1}}{\binom{N}{n}}. \tag{5.26}$$

It is instructive to examine the first few values of $P_s(N)$

$$P_1(N) = \frac{1}{2} + \frac{1}{(N+1)N} \tag{5.27}$$

$$P_2(N) = \frac{1}{6} + \frac{1}{(N+1)N} + \frac{2}{(N+1)N(N-1)} \tag{5.28}$$

$$P_3(N) = \frac{1}{12} + \frac{1}{(N+1)N} + \frac{4}{(N+1)N(N-1)} + \frac{6}{(N+1)N(N-1)(N-2)} \tag{5.29}$$

Note that $P_1(3) = P_3(3)$ and $P_1(2) = P_2(2)$, this suggests that $P_s(N)$ has a symmetric form. Examining Eqs. (5.27-5.29) closely, it is evident that $P_s(N)$ has the following simple form

$$P_s(N) = \frac{1}{s(s+1)} + \frac{1}{(N+2-s)(N+1-s)}, \tag{5.30}$$

and the symmetry in the expression is now clear

$$P_s(N) = P_{N+1-s}(N). \tag{5.31}$$

We can easily calculate the first few moments of $P_s(N)$,

$$M_0[P_s(N)] = \sum_{s=1}^{N} P_s(N) = 2\frac{N}{N+1}, \tag{5.32}$$

$$M_1[P_s(N)] = \sum_{s=1}^{N} sP_s(N) = N, \tag{5.33}$$

$$M_2[P_s(N)] = \sum_{s=1}^{N} s^2 P_s(N) = N(N+3) - 2(N+2)\sum_{k=1}^{N}\frac{1}{k+1}$$

$$= (N+4)(N+1) - 2(N+2)H_{N+1}. \tag{5.34}$$

where $H_N = \sum_{i=1}^{N} 1/i$ which is asymptotically equal to $H_N \simeq \ln(N) + \gamma$, γ being the Euler constant, and we used $\sum_{i=1}^{n} 1/(i(i+1)) = n/(n+1)$. In general

$$M_n[P_s(N)] = \sum_{s=1}^{N} s^n P_s(N) = \sum_{k=1}^{N}\left[\frac{k^n + (N+1-k)^n}{k(k+1)}\right], \tag{5.35}$$

$$= \sum_{k=1}^{N}\left[\frac{k^{n-1}(1+(-1)^n)}{k+1} + \frac{1}{k}\sum_{m=0}^{n-1}\binom{n}{m}(N+1)^{n-m}(-1)^m\frac{k^m}{k+1}\right], \tag{5.36}$$

$$= \sum_{k=1}^{N}\left[(1+(-1)^n)\left(\sum_{l=0}^{n-2}(-1)^l k^{n-l-2} + \frac{(-1)^{n-1}}{k+1}\right)\right.$$

$$\left.+ \frac{1}{k}\sum_{m=0}^{n-1}\binom{n}{m}(N+1)^{n-m}(-1)^m\left(\sum_{l=0}^{m-1}(-1)^l k^{m-l-1} + \frac{(-1)^m}{k+1}\right)\right], \tag{5.37}$$

where in (5.35), we made the change of variable $k = N + 1 - s$ and used the fact that it also runs from 1 to N, in (5.36) the binomial theorem is used and in (5.37) we employed

$$\frac{k^m}{k+1} = \sum_{n=0}^{m-1}(-1)^n k^{m-n-1} + \frac{(-1)^m}{k+1}. \tag{5.38}$$

Although Eq. (5.37) looks complicated, one only needs to evaluate sums of powers of integers, which may be represented by closed forms when the powers are fixed, and sum over finite harmonic sequences.

Note that, in Eq. (5.37), the term with the largest power of N is produced by the second term in the brackets with $m = 0$, except for $n = 0$, which is

$$\binom{n}{0}N(N+1)^{n-1}. \tag{5.39}$$

Therefore, as $N \to \infty$ we have

$$M_0[P_s(N)] \simeq 2,$$

$$M_{n>0}[P_s(N)] \simeq N^n.$$

5.5.2 The $N \to \infty$ limit

In the $N \to \infty$ limit, the degree distribution Q_k is exponential $Q_k = 2^{-k}$. Consequently the average degree equals 2. The average degree equals the average number of branches and therefore,

$$2 = \lim_{N \to \infty} \sum_s P_s(N). \tag{5.40}$$

It is possible to show this by using our solution for $P_s(N)$. In the limit $N \to \infty$, Eq. (5.32) becomes

$$\lim_{N \to \infty} \sum_s P_s(N) = \lim_{N \to \infty} 2\frac{N}{N+1} = 2. \tag{5.41}$$

Furthermore, the probability that a node is a leaf is $1/2$ and therefore we should expect,

$$\frac{1}{2} = \lim_{N \to \infty} P_N(N). \tag{5.42}$$

Because of the symmetry, we have $P_1(N) = P_N(N)$. The expression for $P_1(N)$ should reduce to $1/2$ in the limit $N \to \infty$, and it indeed does

$$\lim_{N \to \infty} P_N(N) = \lim_{N \to \infty} P_1(N) = \lim_{N \to \infty} \left(\frac{1}{2} + \frac{1}{N(N+1)} \right) = \frac{1}{2}. \tag{5.43}$$

Lastly, we would like to consider how $P_s(N)$ scales with tree size. Note that Eq. (5.30) can be written in the following form

$$P_s(N) = \frac{1}{(N+1)^2} \left[\frac{1}{\left(\frac{s}{N+1} \right)\left(\frac{1}{N+1} + \frac{s}{N+1} \right)} + \frac{1}{\left(1 + \frac{1}{N+1} - \frac{s}{N+1} \right)\left(1 + \frac{2}{N+1} - \frac{s}{N+1} \right)} \right]. \tag{5.44}$$

For large values of N, Eq. (5.44) becomes

$$P_s(N \gg 1) = \frac{1}{(N+1)^2} \left[\frac{1}{\left(\frac{s}{N+1}\right)^2} + \frac{1}{\left(1 - \frac{s}{N+1}\right)^2} \right].$$ (5.45)

Therefore, $P_s(N)$ has the scaling form

$$P_s(N) = \frac{1}{(N+1)^2} F\left(\frac{s}{N+1}\right)$$ (5.46)

$$F(x) = \frac{1}{x^2} + \frac{1}{(1-x)^2}$$ (5.47)

$$F(x) = F(1-x)$$
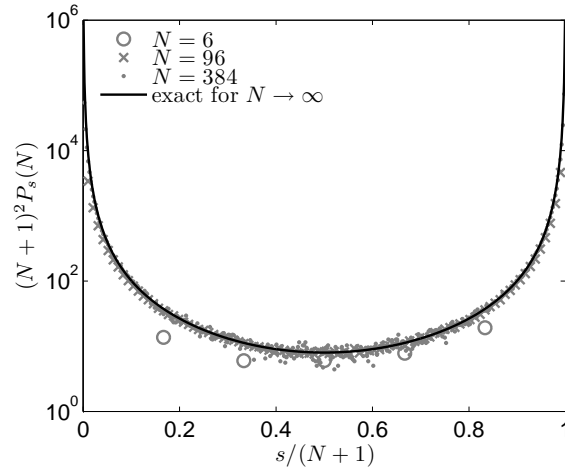
Figure 5.7: $(N+1)^2 P_s(N)$ vs $s/(N+1)$ for $N =6$(open circles), 96(crosses), and 384(dots) corresponding to the results of the Monte Carlo simulations. The solid line shows the behavior of the scaling function $F(x)$ in $x \in (0, 1)$.

5.6 Concluding remarks

The main goal of the research described in this chapter is to reveal a previously unexplored aspect of addition-deletion networks, which is calculating the cluster size distribution. In

order to solve this problem, we did Monte Carlo simulations of the addition-deletion network we consider, and as a result, suggested that the distribution of cluster sizes asymptotically behaves like a stretched exponential. Figs. 5.3, 5.4, and 5.5 in Sec. 5.4 show the results of our analysis. Although we could not arrive at an analytical expression for the cluster size distribution or the evolution equation for it, we managed to gain some insight into the quantities we are interested in through simulations. However, we managed to find the exact solution of a simplified version of the general problem, which is the cluster size distribution after a single deletion event, for any network size. We believe that solving the simpler problem was an important step in making progress towards solving our original problem, as it captures the essential features of the dynamics of the system. To our knowledge, the exact result we obtained for the cluster size distribution after a one deletion event, given in Eq. (5.44) in Sec. 5.5, was not known in the literature.

We believe that the findings of this research project will help us reach the solution of our original problem in the near future.

Chapter 6

> Knowledge so conceived is not a series of self-consistent theories that converges towards an ideal view; it is not a gradual approach to the truth. It is rather an ever increasing ocean of mutually incompatible alternatives, each single theory, each fairy-tale, each myth that is part of the collection forcing the others into greater articulation and all of them contributing, via this process of competition, to the development of our consciousness. Nothing is ever settled, no view can ever be omitted from a comprehensive account.
>
> *Paul K. Feyerabend, "Against Method"*

Conclusion

The results obtained in this thesis can be concisely stated as follows. In Chapter 2, it is shown by comparison with experimental data that a simple mathematical model that describes the motion of a random walker moving in the presence of permeable barriers can adequately predict the observed diffusion properties of molecules in cell membrane. Furthermore a generalized mathematical model that allows one to account for the possible effects of structural disorder in the system is provided. In Chapter 3, extensions are presented of the well-known effective medium theory of transport in disordered lattices to predict the time dependence of transport quantities as well as their asymptotic values. Some other interesting aspects of the results provided by effective medium theory are also discussed such as the appearance of a percolation threshold for finite systems, significance of long-range memory functions and the effects of correlations in the disordered lattice. Our findings appear to indicate that the type of correlated disorder we consider does not modify the long-time diffusion coefficient in the system. In the next chapter, where the focus is on the analysis of R-D systems, results are presented on the transient dynamics in front propagation and conditions for pattern formation. Because of the difficulties involved in the analysis, our results for the transient dynamics in front propagation are only of qualitative, rather than quantitative, nature. Exact results are presented for necessary

conditions for pattern formation in a generalized R-D equation, with different, and gener-alized, transport modes. Chapter 5, the last chapter of this thesis, is about an exploratory investigation of the cluster size distribution in addition-deletion networks. Results of our simulations and exact analysis are presented there, it is suggested that the cluster size dis-tribution is well approximated by a stretched exponential for large values of the cluster size, and an analytical expression on the distribution of branch sizes is provided.

As a result of having worked on all these research projects in the last four years, par-ticipating in numerous research meetings, and being a graduate student in physics as well as taking part in a biology-inspired interdisciplinary program, the authors views about sci-ence have changed considerably. The interdisciplinary program exposed me to research done by scientists from many different backgrounds, ranging from anthropology to com-puter science. I believe that this was a unique experience and it gave me a good idea about how different scientists from other disciplines tend to think and approach their own, as well as others, problems. I had the opportunity to observe when a physicists approach to a given problem of general nature is favorable, and when it is not. In the future, I would like to keep learning and practicing physics, but at the same time work with groups of scientists with from different backgrounds. I think this is an excellent way of developing oneself as a scientist and an intellectual in general.

References

[1] A. Kusumi, C. Nakada, K. Ritchie, K. Murase, K. Suzuki, H. Murakoshi, R.S. Kasai, J. Kondo, and T. Fujiwara. *Annu. Rev. Biophys. Biomol. Struct.*, 34:351, 2005.

[2] S.J. Singer and G.L. Nicholson. *Science*, 175:720, 1972.

[3] G.J. Powles, M.J.D. Mallett, G. Rickayzen, and W.A.B. Evans. *Proc. Roy. Soc. London A*, 436:391, 1992.

[4] O.K. Dudko, A.M. Berezhkovskii, and G.H. Weiss. *J. Chem. Phys.*, 121:11283, 2004.

[5] V. M. Kenkre. Exciton dynamics in molecular crystals and aggregates: the master equation approach. In G. Hoehler, editor, *Springer Tracts in Modern Physics, Vol. 94*. Springer, Berlin, Germany, 1982.

[6] D.A.G. Bruggeman. *Ann. Phys. (Leipzig)*, 24:636, 1935.

[7] T. Odagaki and M. Lax. *Phys. Rev. B*, 24:5284, 1981.

[8] Lax M. and Odagaki T. Hopping conduction from multiple scattering theory and continuous time random walk to the coherent medium approximation. In M.F. Schlesinger and B.J. West, editors, *Random Walks and Their Applications in the Physical and Biological Sciences: AIP Conference Proceedings No. 109*, pages 133–154. AIP, New York, NY, 1984.

[9] J.W. Haus, K.W. Kehr, and K. Kitahara. *Phys. Rev. B*, 36:5639, 1987.

[10] B. D. Hughes. *Random Walks and Random Environments*, volume 1-2. Oxford University Press, New York, NY, 1995.

[11] S. Kirkpatrick. *Rev. Mod. Phys.*, 45:574, 1973.

References

[12] P.E. Parris. *Phys. Rev. B*, 36:5437, 1987.

[13] P.E. Parris. *Phys. Rev. B*, 39:9343, 1989.

[14] P.E. Parris and B.D. Bookout. *Phys. Rev. B*, 53:629, 1996.

[15] V. M. Kenkre. *Granular Matter*, 3:23, 2001.

[16] V.M. Kenkre, Z. Kalay P.E., and Parris. *Phys. Rev. E*, 79:011114, 2009.

[17] R.A. Fisher. *Ann. Eugen.*, 7:355, 1937.

[18] A. Kolmogorov, I. Petrovsky, and N. Piskunov. *Bull. Univ. Moskou Ser. Internat. Sec. A*, 1:1, 1937.

[19] A. M. Turing. *Philos. Trans. R. Soc. London, Ser. B*, 327:37, 1952.

[20] B. P. Belousov. *Compilation of Abstracts on Radiation Medicine*, 147:145, 1959.

[21] A. M. Zhabotinsky. *Biofizika*, 9:306, 1964.

[22] M.A. Fuentes, M.N. Kuperman, and V.M. Kenkre. *J. Phys. Chem. B*, 108:10505, 2004.

[23] N. Sarshar and V. Roychowdhury. *Phys. Rev. E*, 69:026101, 2004.

[24] F. Chung and L. Lu. *Internet Mathematics*, 1:409, 2004.

[25] C. Cooper, A. Frieze, and J. Vera. *Internet Mathematics*, 1:463, 2004.

[26] E. Ben-Naim and P.L. Krapivsky. *J. Phys. A: Math. Theor.*, 40:8607, 2007.

[27] C. Moore, G. Ghoshal, and M.E.J. Newman. *Phys. Rev. E.*, 74:036121, 2006.

[28] R. Albert and A.L. Barabasi. *Rev. Mod. Phys.*, 74:47, 2002.

[29] S.N. Dorogovtsev and J.F.F. Mendes. *Adv. Phys.*, 51:1079, 2002.

[30] D.J. Watts and S.H. Strogatz. *Nature*, 393:440, 1998.

[31] M.E.J. Newman, A.-L. Barabasi, and D.J. Watts. *The Structure and Dynamics of Networks*. Princeton University Press, Princeton, NJ, 2006.

[32] C. Boyer and U. Merzbach. *A History of Mathematics*. Wiley, New York, NY, 2nd edition, 1989.

[33] P. Erdős and A. Rényi. *Publicationes Mathematicae*, 6:290, 1959.

References

[34] H.T. McMahon and J.L. Gallop. *Science*, 438:590, 2005.

[35] T. Higashi, K. Suzuki, , and N. Otsuji. *J. of Bacteriology*, 146:1117, 1981.

[36] G. Krauss. *Biochemistry of Signal Transduction and Regulation*. John Wiley & Sons, Darmstadt, Germany, 2nd edition, 2001.

[37] F.R. Maxfield and I. Tabas. *Science*, 438:612, 2005.

[38] V. M. Kenkre, L. Giuggioli, and Z. Kalay. *Phys. Rev. E*, 77:051907, 2008.

[39] Z. Kalay, P. E. Parris, and V. M. Kenkre. *J. Phys.: Condens. Mat.*, 20:245105, 2008.

[40] Gorter E. and F. Grendel. *The Journal of Experimental Medicine*, 41:439, 1925.

[41] J.F. Danielli and H. Davson. *J. Cell Comp. Physiol.*, 5:495, 1935.

[42] M. Edidin, S.C. Kuo, and M.P. Sheetz. *Science*, 254:1379, 1991.

[43] M. Edidin, M.C. Zuniga, and M.P. Sheetz. *Proc. Natl. Acad. Sci. USA*, 91:3378, 1994.

[44] Y. Sako, A. Nagafuchi, S. Tsukita, M. Takeichi, and A. Kusumi. *J. Cell Biol.*, 140:1227, 1998.

[45] M. Tomishige, Y. Sako, and A. Kusumi. *J. Cell Biol.*, 142:989, 1998.

[46] R. Simson, B. Yang, S.E. Moore, P. Doherty, F.S. Walsh, and K.A. Jacobson. *Biophys. J.*, 74:297, 1998.

[47] G.G. Capps, S. Pine, M. Edidin, and M.C. Zuniga. *Biophys. J.*, 86:2896, 2004.

[48] D.M. Engelman. *Science*, 438:578, 2005.

[49] R. Iino, I. Koyama, and A. Kusumi. *Biophys. J.*, 80:2667, 2001.

[50] P.G. Saffman and M. Delbruck. *Proc. Natl. Acad. Sci. USA*, 72:3111, 1975.

[51] W.L. Vaz, M. Criado, V.M. Madeira, G. Schoellmann, and T.M. Jovin. *Biochemistry*, 21:5608, 1982.

[52] D. Axelrod, P. Ravdin, D.E. Koppel, J. Schlessinger, W.W. Webb, E.L. Elson, and T.R. Podleski. *Proc. Natl. Acad. Sci. USA*, 73:4594, 1976.

[53] C. Dietrich, Z.N. Volovyk, M. Levi, N.L. Thompson, and K. Jacobson. *Proc. Natl. Acad. Sci. USA*, 98:10642, 2001.

References

[54] E.D. Sheets, G.M. Lee, R. Simson, and K. Jacobson. *Biochemistry*, 36:12449, 1997.

[55] K. Ritchie, X.-Y. Shan, J. Kondo, K. Iwasawa, T. Fujiwara, and A. Kusumi. *Biophys. J.*, 88:2266, 2005.

[56] K. Murase, T. Fujiwara, Y. Umemura, K. Suzuki, R. Iino, H. Yamashita, M. Saito, H. Murakoshi, K. Ritchie, and A. Kusumi. *Biophys. J.*, 86:4075, 2004.

[57] T. Fujiwara, K. Ritchie, H. Murakoshi, K. Jacobson, and A. Kusumi. *J. Cell Biology*, 157:1071, 2002.

[58] N. Morone, T. Fujiwara, K. Murase, R.S. Kasai, H. Ike, S. Yuasa, J. Usukura, and A. Kusumi. *J. Cell Biol.*, 174:851, 2006.

[59] G.E. Roberts and H. Kaufman. *Table of Laplace Transforms*. W.B. Saunders, Philadelphia, PA, 1966.

[60] J. Candia, P.E. Parris, and V.M. Kenkre. *J. Stat. Phys.*, 129:323, 2007.

[61] G. Doetsch. *Introduction to the Theory and Application of the Laplace Transformation*. Springer-Verlag, New York, NY, 1974.

[62] K. Suzuki, K. Ritchie, E. Kajikawa, T. Fujiwara, and A. Kusumi. *Biophys. J.*, 88:3659, 2005.

[63] I.S. Gradsteyn and I.M. Rizhik. *Tables of Integrals, Series and Products*. Academic Press, San Diego, CA, 6th edition, 2000.

[64] M.A. Pope and C. Swenberg. *Electronic Processes in Organic Crystals and Polymers*. Oxford Univ. Press, New York, NY, 1999.

[65] E.A. Silinsh and V. Capek. *Organic Molecular Crystals: Interaction, Localization, and Transport Phenomena*. AIP, New York, NY, 1994.

[66] M. Dresden M. *Rev. Mod. Phys.*, 33:265, 1961.

[67] J. Rammer. *Rev. Mod. Phys.*, 63:781, 1991.

[68] S. Alexander, J. Bernasconi, W.R. Schneider, and R. Orbach. *Rev. Mod. Phys.*, 53:175, 1981.

[69] M.J. Saxton. *Biophys. J.*, 55:21, 1989.

[70] M.J. Saxton. *Biophys. J.*, 57:1167, 1990.

[71] D. Bedeaux, K. Lakatos-Lindenberg, and K. Shuler. *J. Math. Phys.*, 12:2116, 1971.

References

[72] I. Oppenheim, K.E., Shuler, and G.H.Weiss. *Stochastic Processes in Chemical Physics: The Master Equation*. MIT Press, Cambridge, MA, 1977.

[73] N.G. van Kampen. *Stochastic Processes in Physics and Chemistry*. Elsevier North-Holland, New York, NY, 1981.

[74] V.M. Kenkre. Mathematical methods for the description of energy transfer. In B. DiBartolo, editor, *Proceedings of the NATO Advanced Study Institute on Energy Transfer, Erice, Italy*, page 205. Plenum, New York, NY, 1984.

[75] R. Zwanzig. *J. Stat. Phys.*, 28:127, 1981.

[76] K. Kawazu and H. Kesten. *J. Stat. Phys.*, 37:561, 1984.

[77] B. Derrida and J. M. Luck. *Phys. Rev. B*, 28:7183, 1983.

[78] J. Machta. *Phys. Rev. B*, 24:5260, 1981.

[79] J.C. Dyre and T.B. Schroder. *Rev. Mod. Phys.*, 72:873, 2000.

[80] J.W. Haus, K.W. Kehr, and K. Kitahara. *Phys. Rev. B*, 25:4918, 1982.

[81] J.W. Haus, K.W. Kehr, and K. Kitahara. *Phys. Rev. B*, 28:3573, 1983.

[82] P.E. Parris. *J. Chem. Phys.*, 90:2486, 1989.

[83] V. M. Kenkre. The generalized master equation and its applications. In U. Landman, editor, *Statistical Mechanics and Statistical Methods in Theory and Application*. Plenum, New York, NY, 1977.

[84] V.M. Kenkre and R.S Knox. *Phys. Rev. B*, 9:5279, 1974.

[85] H. Scher and M. Lax. *Phys. Rev. B*, 7:4491, 1973.

[86] R.W. Zwanzig. In W.E. Downs and J. Down, editors, *Lectures in Theoretical Physics, Vol. 3*. Interscience, New York, NY, 1961.

[87] S. Nakajima. *Prog. Theor. Phys.*, 20:948, 1958.

[88] R. Zwanzig. *J. Chem. Phys.*, 33:1338, 1960.

[89] V.M. Kenkre and M. Dresden. *Phys. Rev. Lett.*, 27:9, 1971.

[90] V.M. Kenkre. *Phys. Rev. A*, 4:2327, 1971.

[91] A. Muriel and M. Dresden. *Physica*, 43:424, 1969.

References

[92] L. van Hove. *Physica*, 21:517, 1955.

[93] L. van Hove. *Physica*, 25:268, 1959.

[94] R. Zwanzig. *J. Stat. Phys.*, 28:127, 1982.

[95] J. Abate and W. Whitt. *Queueing Systems*, 10:5, 1992.

[96] A. Talbot. *J. Inst. Maths. Applics.*, 23:97, 1979.

[97] T. Weeks. *J. ACM*, 13:419, 1986.

[98] D. P. Gaver. *Operations Research*, 14:444, 1966.

[99] H. Stehfest. *Commun. ACM*, 13:47, 1976.

[100] J. Abate and W. Whitt. *INFORMS J. on Computing*, 18:4, 2006.

[101] J. Abate. *ORSA J. on Computing*, 7:36, 1995.

[102] S. H. Strogatz. *Nonlinear Dynamics and Chaos*. Westview Press, Cambridge, MA, 1994.

[103] P.E. Parris, M. Kus, D.H. Dunlap, and V.M. Kenkre. *Phys. Rev. E*, 56:5295, 1997.

[104] S.K. Scott. *Oscillations, Waves and Chaos in Chemical Kinetics*. Oxford University Press, Oxford, UK, 1994.

[105] Y. Kuramoto. *Chemical Oscillations, Waves, and Turbulence*. Springer-Verlag, Berlin, Germany, 1984.

[106] J.D. Murray. *Mathematical Biology*, chapter 13. Springer, New York, NY, 3rd edition, 2001.

[107] A. Okubo and S. Levin. *Diffusion and Ecological Problems: Modern Perspectives*. Springer-Verlag, Berlin, 2nd edition, 2001.

[108] V.M. Kenkre. *Physica A*, 356:121, 2005.

[109] V. M. Kenkre, L. Giuggioli, G. Abramson, and G. Camelo-Neto. *Eur. Phys. J. B*, 55:461, 2007.

[110] M.A. Aguirre, G. Abramson, A.R. Bishop, and V.M. Kenkre. *Phys. Rev. E*, 66:041908, 2002.

[111] L. Giuggioli and V. M. Kenkre. *Physica D*, 183:245, 2003.

References

[112] V.M. Kenkre and M. Kuperman. *Phys. Rev. E*, 67:051921, 2003.

[113] D.R. MacInnis. *Applications of Nonlinear Science and Kinetic Equations to the Spread of Epidemics*. Doctoral dissertation, University of New Mexico, Albuquerque, NM, May 2007.

[114] M.A. Fuentes, M.N. Kuperman, and V.M. Kenkre. *Phys. Rev. Lett.*, 91:158104, 2003.

[115] M.G. Clerc, D. Escaff, and V.M. Kenkre. *Phys. Rev. E*, 72:056217, 2005.

[116] Ya. B. Zel'dovich and G.I. Barenblatt. *Combust. Flame*, 3:61, 1959.

[117] P. Clavin. *Ann. Rev. Fluid Mech.*, 26:321, 1994.

[118] A.C. Scott. *Rev. Mod. Phys.*, 47:487, 1975.

[119] A.C. Scott. *Neurophysics*. Wiley, New York, NY, 1977.

[120] G. Parisi and Y.C. Zhang. *J. Stat. Phys.*, 41:1, 1985.

[121] B. Shraiman D. Bensimon and L.P. Kadanoff. In F. Family and D.P. Landau, editors, *Kinetics of Aggregation and Gelation*, chapter 3, page 75. Elsevier-North Holland, Amsterdam, Netherlands, 1984.

[122] L. Giuggioli and V.M. Kenkre. *Physica D*, 183:245, 2004.

[123] I.D. Peixoto, L. Giuggioli, and V.M. Kenkre. *Physica D*, 72:041902, 2005.

[124] K.K. Manne, A.J. Hurd, and V.M. Kenkre. *Phys. Rev. E*, 61:4177, 2000.

[125] G. Abramson, A.R. Bishop, and V.M. Kenkre. *Phys. Rev. E*, 66:66615, 2001.

[126] L. Giuggioli, Z. Kalay, and V.M. Kenkre. *Eur. Phys. J. B*, 62:341, 2008.

[127] W. van Saarloos. *Phys. Rev. A*, 37:211, 1988.

[128] W. van Saarloos. *Phys. Rev. A*, 39:6367, 1989.

[129] U. Ebert and W. van Saarloos. *Physica D*, 146:1, 2000.

[130] D.G. Aronson and H.F. Weinberger. *Adv. Math.*, 30:33, 1978.

[131] M. Bransom. *Mem. Am. Math. Soc.*, 285:1, 1983.

[132] M. Cencini, C. Lopez, and D. Vegni. *Lect. Notes Phys.*, 636:187, 2003.

[133] U. Ebert and W. van Saarloos. *Phys. Rev. Lett.*, 80:1650, 1998.

References

[134] D. Panja and W. van Saarloos. *Phys. Rev. E*, 65:057202, 2002.

[135] M.J. Metcalf, J.H. Merkin, and S.K. Scott. *Proc. R. Soc. Lond. A*, 447:155, 1994.

[136] P. Tracqui, A.M. Perault-Staub, G. Milhaud, and J.F. Staub. *Proc. R. Soc. Lond. A*, 49:597, 1987.

[137] M.-H. Wang, M. Kot, and M.G. Neubert. *J. Math. Biol.*, 44:150, 2002.

[138] M.-H. Wang and M. Kot. *Math. Biosciences*, 171:83, 2001.

[139] Ya.B. Zel'dovich and D.A. Frank-Kamenetsky. *Doklady Akademii Nauk. SSSR*, 19:693, 1938.

[140] W. van Saarloos, M. van Hecke, and R. Holyst. *Phys. Rev. E*, 52:1773, 1995.

[141] U. Ebert and W. van Saarloos. *Physica D*, 146:1, 2000.

[142] P. Morse and H. Feshbach. *Methods of Theoretical Physics Part I*, chapter 5, sec. 2. McGraw Hill, New York, NY, 1953.

[143] D. Panja and W. van Saarloos. *Phys. Rev. Lett.*, 65:057202, 2002.

[144] A. Messiah. *Quantum Mechanics*, chapter 3, sec. 5. Dover, New York, NY, 1999.

[145] M.C. Cross and P.C. Hohenberg. *Rev. Mod. Phys.*, 65:851, 1993.

[146] A.C. Newell. The dynamics and analysis of patterns. In H.F. Nijhout, L. Nadel, and D.L. Stein, editors, *Lecture Notes of the Santa Fe Institute Vol. V.: Pattern Formation in the Physical and Biological Sciences*. Addison-Wesley, Reading, MA, 1997.

[147] M.I. Rabinovich, A.B. Ezersky, and P.D. Weidman. *The Dynamics of Patterns*. World Scientific, London, UK, 2000.

[148] V. M. Kenkre. Memory formalism, nonlinear techniques, and kinetic equation approaches. In V.M. Kenkre and K. Lindenberg, editors, *Proceedings of the PASI on Modern Challenges in Statistical Mechanics: Patterns, Noise, and the Interplay of Nonlinearity and Complexity*. AIP, New York, NY, 2003.

[149] G. Nicolis. *Introduction to Nonlinear Science*. Cambridge University Press, Cambridge, UK, 1995.

[150] F.C. Hoppensteadt, Z. Jackiewicz, and B. Zubik-Kowal. *BIT Numerical Mathematics*, 47:325, 2008.

References

[151] C. Lubich. *Numer. Math.*, 40:119, 1982.

[152] P. Pouzet. *Rev. Française Traitement Information Chiffres*, 6:79, 1963.

[153] H. Brunner and P.J. van der Houwen. *The Numerical Solution of Volterra Integral Equations*. North-Holland, Amsterdam-New York, 1986.

[154] J.R. Dormand and P.J. Prince. *J. Comput. Appl. Math.*, 6:19, 1980.

[155] R.J. Williams, E.L. Berlow, J.A Dunne, A.L. Barabasi, and N.D. Martinez. *Proc. Natl. Acad. Sci. USA*, 99:12913, 2002.

[156] J.F. Sowa, editor. *Principles of Semantic Networks: Explorations in the Representation of Knowledge*. Morgan Kaufmann Publishers, San Mateo, CA, 1991.

[157] J.L. Gross and J. Yellen, editors. *Handbook of graph theory*. CRC Press, Boca Raton, 2004.

[158] J.F.F Mendes S.N. Dorogovtsev and A.N. Samukhin. arXiv:cond-mat/0011077, 2000.

[159] S.N. Dorogovtsev, J.F.F. Mendes, and A.N. Samukhin. *Phys. Rev. Lett.*, 85:4633, 2000.

[160] P.L. Krapivsky and S. Redner. Statistical mechanics of complex networks. In R. Pastor-Satorras, M. Rubi, and A. Diaz-Guilera, editors, *Lecture notes in physics, Vol. 625*, pages 3–22. Springer, Berlin, Germany, 2003.

[161] E. Ben-Naim and P.L. Krapivsky. *Phys. Rev. E*, 71:026129, 2005.